Chapter 5
Thermal Properties of Solids and the Size Effect

One of the thrust areas of research in micro/nanoscale heat transfer is related to properties and transport processes in solid materials and devices. In the early 1990s, much research was conducted to identify the regimes when the microscale effect must be considered in dealing with problems occurring at small length and/or timescales [1, 2]. Significant progress has been made in the past decades on understanding the fundamental thermal transport properties of solids and nanostructures. Cahill et al. [3, 4] provided comprehensive surveys on the thermal phenomena and measurement techniques associated with solid-state devices across the nano-, micro-, and macro-length scales and in a large temperature range. The critical dimensions of integrated circuits have continued to shrink during the past few decades, and feature sizes smaller than 10 nm have been reached in recent years. Overheating caused by thermal energy generation is a major source of device failure, and it often occurs in very small regions, known as hot spots. A remarkable number of micro/nanostructured materials and systems have temperature-dependent figures of merit. Therefore, understanding the thermophysical properties, thermal transport physics, and thermal metrology from the micrometer down to the nanometer length scales is critically important for the future development of microelectronic devices and nanobiotechnology.

This chapter focuses on simple phonon theory and electronic theory of the specific heat, thermal conductivity, and thermoelectricity of metals and insulators. The Boltzmann transport equation (BTE) has been used to facilitate the understanding of microscopic behavior, together with the quantum statistics of phonons and electrons. The quantum size effect on phonon specific heat is extensively covered. Examples are given to analyze direct thermoelectric conversion for temperature measurement, power generation, and refrigeration. Furthermore, a detailed treatment of classical size effect on thermal conductivity is presented. Finally, the concepts of quantum electrical conductance and thermal conductance are introduced.

Z. M. Zhang, *Nano/Microscale Heat Transfer*, Mechanical Engineering Series,
https://doi.org/10.1007/978-3-030-45039-7_5

5.1 Specific Heat of Solids

In this section, simple models of the specific heat of bulk solids are described considering the contribution of lattice vibrations as well as free electrons in metals. The purpose is to understand macroscopic behavior from a microscopic point of view and to prepare students for further study on the quantum size effect to be discussed in subsequent sections.

5.1.1 Lattice Vibration in Solids: The Phonon Gas

The atoms in solids are close to each other, and interatomic forces keep them in position. Atoms cannot move around except for vibrations near their equilibrium positions. In crystalline solids, atoms are organized into periodic arrays, and each identical structural unit is called a lattice. Lattice vibrations contribute to thermal energy storage and heat conduction. In metals, electrons are responsible for electrical transport and heat conduction but are less important for storing thermal energy except at very low temperatures.

The simple oscillator model treats each atom as a harmonic oscillator, which vibrates along all three axes as shown in Fig. 5.1. If the vibrational degrees of freedom were completely excited, we would expect the high-temperature limit of the specific heat of elementary (monatomic) solids to be

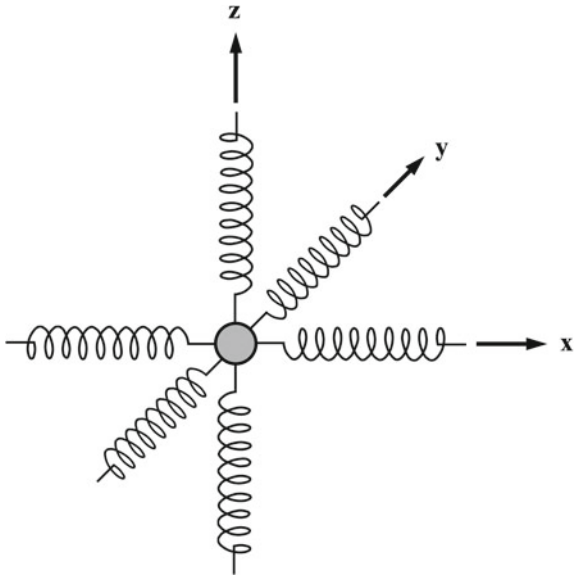

Fig. 5.1 The harmonic oscillator model of an atom in a solid

$$\bar{c}_v = 3\bar{R} \tag{5.1}$$

This is called the Dulong–Petit law, named after Pierre-Louis Dulong and Alexis-Thérèse Petit in 1819. The Dulong–Petit law can be understood in terms of the equipartition principle in classical statistics. However, it cannot predict low-temperature behavior; even above room temperature, the model significantly overpredicts the specific heats for diamond, graphite, and boron.

Einstein in 1907 proposed a simple harmonic oscillator model and its quantized energy levels $(i + \frac{1}{2})h\nu$, $i = 1, 2, \ldots$, to obtain the specific heat as a function of temperature. Here, the frequency ν is a characteristic vibration frequency of the solid material. The procedure is similar to the analysis of vibration energies for diatomic gas molecules, e.g., Eqs. (3.59)–(3.62). The resulting specific heat for a monatomic solid is

$$\bar{c}_v(T) = 3\bar{R}\frac{\Theta_\mathrm{E}^2}{T^2}\frac{\mathrm{e}^{\Theta_\mathrm{E}/T}}{\left(\mathrm{e}^{\Theta_\mathrm{E}/T} - 1\right)^2} \tag{5.2}$$

where the factor 3 accounts for oscillation in all three directions and $\Theta_\mathrm{E} = h\nu/k_\mathrm{B}$ is called the Einstein temperature [5, 6]. It can be shown that $\bar{c}_v \to 0$ as $T \to 0$ and $\bar{c}_v \to 3\bar{R}$ at $T \gg \Theta_\mathrm{E}$. In the intermediate temperature range, however, the Einstein specific heat is significantly lower than the experimental data. This can be seen from Fig. 5.2, where the experimental results of the constant-pressure specific heat are taken from Ashcroft and Mermin [6]. It should be noted that $c_p = c_v$ for a solid under the incompressible assumption. The reduced temperature is the ratio of the temperature to the characteristic temperature (either the Einstein temperature or Debye temperature depending on the model). The experimental data were plotted using the Debye temperature given in Table 5.1. The reason that the specific heat of diamond is far from $3\bar{R}$ near room temperature is because of its

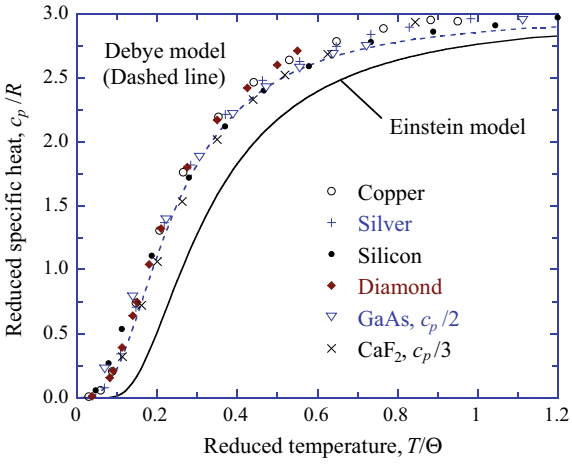

Fig. 5.2 Comparison of model predictions with experimental data of the specific heat for several crystalline solids

Table 5.1 The Debye temperature, melting temperature, and other properties for selected solids. The data are mainly taken from Kittel [5] and Ashcroft and Mermin [6]. The reported densities are for 22 °C except for Ar

Element or compound	Symbol or formula	M (kg/kmol)	Θ_D (K)	T_{melt} (K)	n_a (10^{28} m^{-3})	ρ (10^3 kg/m^3)
Argon	Ar	40	92	84	2.66 (4 K)	1.77 (4 K)
Mercury	Hg	200.6	72	234	4.26	14.26
Sodium	Na	23	158	371	2.65	1.013
Lithium	Li	6.9	344	454	4.7	0.542
Lead	Pb	207	105	601	3.3	11.34
Zinc	Zn	65.4	327	692	6.55	7.13
Magnesium	Mg	24.3	400	922	4.30	1.74
Aluminum	Al	27	428	934	6.03	2.7
Calcium	Ca	40	230	1113	2.30	1.53
Silver	Ag	108	225	1235	5.85	10.5
Copper	Cu	63.5	340	1358	8.45	8.93
Gold	Au	197	165	1338	5.90	19.3
Iron	Fe	56	470	1811	8.50	7.87
Silicon	Si	28	645	1687	5.0	2.33
Diamond	C	12	2000	3620	17.6	3.52
Potassium bromide	KBr	119	177	1007		2.75
Sodium chloride	NaCl	58.5	281	1074		2.17
Gallium arsenide	GaAs	144.6	360	1511		5.32
Calcium fluoride	CaF_2	78	474	1696		3.18

very high characteristic temperature (or frequency of vibration) compared to other materials as shown in Table 5.1.

In the Einstein model, each atom is treated as an independent oscillator and all atoms are assumed to vibrate at the same frequency. In 1912, Max Born and Theodore von Kármán first realized that the bonding in a solid prevents independent vibrations. Therefore, a collection of vibrations must be considered under the force–spring interactions of the nearby atoms. To avoid the complicated calculations, Peter Debye in 1912 simplified the model by assuming that the velocity of sound is the same in all crystalline directions and for all frequencies. In addition, there is a high-frequency cutoff, and no vibration can occur beyond this frequency. As to be seen from subsequent sections, the Debye model is a great success and has prevailed even though more advanced and realistic theories have been developed.

5.1.2 The Debye Specific Heat Model

The Debye model for the specific heat of solids includes a large number of closely spaced modes (or vibration frequencies) up to a certain upper bound ν_{m}, which is determined by the total number of vibration modes $3N$, where N is the number of atoms. The high-frequency limit is indeed plausible because the shortest wavelength of the lattice wave should be on the order of the interatomic distances, or the lattice constants. Rather than treating each atom as an individual oscillator, the Debye model assumes that vibrations are inside the whole crystal just like standing waves. For elastic vibrations, there are longitudinal waves (e.g., sound waves) and transverse waves (with two polarizations) in a crystal. In analogy to electromagnetic waves and photons, the quanta of lattice waves are called *phonons*. The energy of a phonon is $\varepsilon = h\nu$, where ν is the vibration frequency. The momentum of a phonon is $p = h\nu/v_{\mathrm{p}} = h/\lambda$, where ν is the frequency, λ is the wavelength, and $v_{\mathrm{p}} = \lambda\nu$ is the speed of propagation (or phase speed) for the given phonon mode. It should be noticed that the propagation speeds of longitudinal and transverse acoustic waves are different. So far, we have related lattice vibrations to lattice waves and to the translational movement of the phonon gas, which follows the Bose–Einstein statistics. However, the total number of phonons is not conserved since it depends on temperature. Thus, we do not need to apply the constraint given in Eq. (3.2) and can simply set $\alpha = 0$ in Eq. (3.16). The result is

$$\frac{N_i}{g_i} = \frac{1}{\mathrm{e}^{\varepsilon_i/k_{\mathrm{B}}T} - 1} \tag{5.3}$$

Suppose the energy levels are closely spaced; we can write Eq. (5.3) in terms of a continuous function called the Bose–Einstein distribution function at a given temperature T as

$$f_{\mathrm{BE}}(\nu) = \frac{\mathrm{d}N}{\mathrm{d}g} = \frac{1}{\mathrm{e}^{h\nu/k_{\mathrm{B}}T} - 1} \tag{5.4}$$

The *degeneracy* for phonons is the number of quantum states per unit volume in the phase space. For a given volume V and within a spherical shell in the momentum space (from p to $p + \mathrm{d}p$), we have from Eq. (3.87) that $\mathrm{d}g = 4\pi V p^2 \mathrm{d}p/h^3 = 4\pi V \nu^2 \mathrm{d}\nu/v_{\mathrm{p}}^3$. Hence,

$$\frac{\mathrm{d}g}{V} = \frac{g(\nu)\mathrm{d}\nu}{V} = D(\nu)\mathrm{d}\nu = \frac{4\pi\nu^2}{v_{\mathrm{p}}^3}\mathrm{d}\nu \tag{5.5}$$

Here, we have introduced the *density of states* (DOS) of phonons, $D(\nu)$, which is the number of quantum states per unit volume per unit frequency or energy ($h\nu$)

interval. Equation (5.4) gives the *mean occupation number*, i.e., the average number of bosons per quantum state at frequency ν. The phonon number density in terms of the DOS can be expressed as

$$n = \int_0^\infty f_{\mathrm{BE}}(\nu) D(\nu) \mathrm{d}\nu \tag{5.6}$$

Because there exist one longitudinal and two transverse waves, the phonon DOS in a large spherical shell of the momentum space can be written as

$$D(\nu) = 4\pi \nu^2 \left(\frac{1}{v_l^3} + \frac{2}{v_t^3} \right) = \frac{12\pi \nu^2}{v_\mathrm{a}^3} \tag{5.7}$$

where v_l is the speed of the longitudinal wave, v_t is the speed of the transverse wave, and v_a is a weighted average defined in the above equation. The total number of quantum states must be equal to $3N$, since each quantum state corresponds to a harmonic oscillator. Using integration in place of summation, we have

$$\frac{3N}{V} = \int_0^\infty D(\nu) \mathrm{d}\nu = \int_0^{\nu_\mathrm{m}} \frac{12\pi \nu^2}{v_\mathrm{a}^3} \mathrm{d}\nu \tag{5.8}$$

where ν_m is an upper limit of the frequency that can be obtained from Eq. (5.8) as

$$\nu_\mathrm{m} = \left(\frac{3n_\mathrm{a}}{4\pi} \right)^{1/3} v_\mathrm{a} \tag{5.9}$$

Here, $n_\mathrm{a} = N/V$ is the number density of atoms.

The Debye temperature is defined as

$$\Theta_\mathrm{D} = \frac{h\nu_\mathrm{m}}{k_\mathrm{B}} = \frac{h}{k_\mathrm{B}} \left(\frac{3n_\mathrm{a}}{4\pi} \right)^{1/3} v_\mathrm{a} \tag{5.10}$$

The Debye temperature and the number density for various solids are listed in Table 5.1 together with some other properties. The listed values of the Debye temperature were based on the experimentally measured specific heat at very low temperatures, rather than that calculated from the speed of sound. The result of the Debye specific heat theory agrees fairly well with the experimental data for several crystalline solids in a large temperature range, as can be seen from Fig. 5.2. The high-temperature limit of the specific heat is $6\bar{R}$ for GaAs and $9\bar{R}$ for CaF_2, because the number of atoms in a unit cell of the lattice is 2 and 3, respectively.

Example 5.1 The average speed of the longitudinal waves is $v_l = 8970\,\text{m/s}$ and that of the transverse waves is $v_t = 5400\,\text{m/s}$ in silicon. Find the average propagation speed, the maximum frequency, the Debye temperature, and the minimum wavelength $\lambda_{\min}$. How does $\lambda_{\min}$ compare with the average distance between atoms?

Solution Since $v_a^3 = 3/(v_l^{-3} + 2v_t^{-3})$, we have $v_a = 5972\,\text{m/s}$. Given $n_a = 5.0 \times 10^{28}\,\text{m}^{-3}$, we obtain $\nu_m = 1.36 \times 10^{13}\,\text{Hz} = 13.6\,\text{THz}$ from Eq. (5.9) and $\Theta_D = 655\,\text{K}$ from Eq. (5.10), which is a little bit higher than the experimental value of 645 K listed in Table 5.1. The experimental value was obtained by fitting the low-temperature specific heat with the Debye model. The minimum wavelength is estimated by $\lambda_{\min} = v_a/\nu_m = 0.44\,\text{nm} = 4.4\,\text{Å}$. The average spacing between atoms can be estimated by $L_0 = n_a^{-1/3} = 0.27\,\text{nm}$ or 2.7 Å, suggesting that $\lambda_{\min} \approx 2L_0$. The maximum wavelength of the lattice wave will be twice the extension of the solid. For a cubic solid with each side L, we have $\lambda_{\max} \approx 2L$. The lattice waves are illustrated in Fig. 5.3 in a 1D case.

The distribution function for phonons can now be written as

$$f(\nu) = \frac{1}{V}\frac{\mathrm{d}N}{\mathrm{d}\nu} = D(\nu) f_{\text{BE}}(\nu) = \frac{12\pi\nu^2}{v_a^3(e^{h\nu/k_B T} - 1)} = \frac{9n_a\nu^2}{\nu_m^3(e^{h\nu/k_B T} - 1)}, \nu \le \nu_m \tag{5.11}$$

The vibration contribution to the internal energy can be written as

$$U - U_0 = \int_0^\infty f(\nu) h\nu \mathrm{d}\nu \tag{5.12a}$$

where U_0 is the internal energy at 0 K when no vibration modes are excited. The result after some manipulation becomes

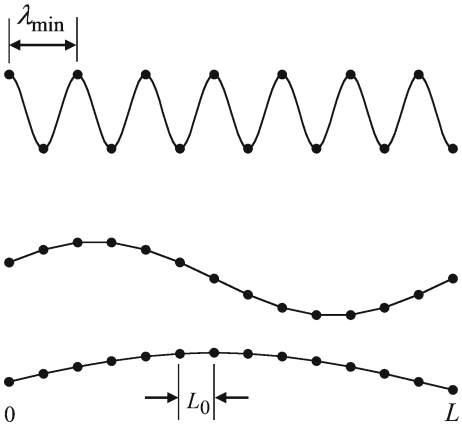

Fig. 5.3 Illustration of the minimum wavelength $\lambda_{\min} = 2L_0$ and the maximum wavelength $\lambda_{\max} = 2L$ associated with lattice vibrations in a solid with a dimension L and with a periodic array of atoms (dots)

$$U - U_0 = 9Nk_B T\left(\frac{T}{\Theta_D}\right)^3 \int_0^{x_D} \frac{x^3}{e^x - 1} dx \tag{5.12b}$$

where $x_D = \Theta_D/T$. The molar specific heat is then

$$\bar{c}_v(T) = \left(\frac{\partial \bar{u}}{\partial T}\right)_V = 9\bar{R}\left(\frac{T}{\Theta_D}\right)^3 \int_0^{x_D} \frac{x^4 e^x}{(e^x - 1)^2} dx \tag{5.13}$$

The specific heat predicted by the Debye theory agrees very well with experimental data of many solids, as shown in Fig. 5.2. Notice that $\int_0^{x_D} x^4 e^x (e^x - 1)^{-2} dx = 4\int_0^{x_D} x^3 (e^x - 1)^{-1} dx - x_D^4/(e^{x_D} - 1)$. When $T \gg \Theta_D$, $x_D \to 0$ and $e^x - 1 \approx x$. Thus, $\int_0^{x_D} x^3 (e^x - 1)^{-1} dx \to x_D^3/3$, and the Debye specific heat approaches $3\bar{R}$ in the high-temperature limit. The relative difference is about 5% at $T = \Theta_D$. Using Eq. (B.9), it can be shown that at $T \ll \Theta_D$, Eq. (5.13) can be approximated by

$$\bar{c}_v(T) = \frac{12\pi^4}{5}\bar{R}\left(\frac{T}{\Theta_D}\right)^3 \propto T^3 \tag{5.14}$$

which is known as the T^3 law, and it agrees with experiments for many solid materials within a few percent for $T/\Theta_D < 0.1$ [7].

In essence, the Einstein specific heat theory assumed that all oscillations are at the same frequency, and it implied that the DOS has a sharp peak at that frequency and is zero at all other frequencies. On the other hand, the Debye theory is based on a parabolic function, $D(\nu) \propto \nu^2$. More detailed studies have revealed that the actual phonon density of states is a complicated function of the frequency [6, 8], as illustrated in Fig. 5.4 for aluminum and copper according to neutron scattering measurements. There are different phonon branches in a real crystal that affect the DOS in different frequency regions. A detailed discussion will be deferred to Chap. 6 when we take

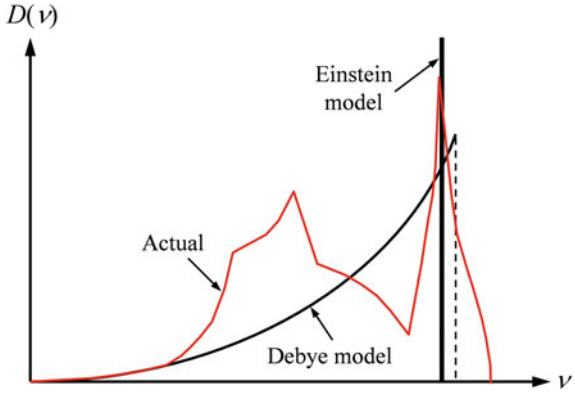

Fig. 5.4 Illustration of the phonon density of states in the Einstein model and the Debye model as compared with the actual behavior of metals

a deeper look into the crystalline structures and phonon dispersion relations. In general, the Debye theory predicts correctly the low-temperature behavior when only the low-frequency phonon modes are excited; this is probably the most significant contribution of the Debye model. At higher temperatures, the Debye model can be considered as a first-order approximation, as shown in Fig. 5.2.

5.1.3 *Free-Electron Gas in Metals*

The translational motion of free electrons within metals is largely responsible for their electrical and thermal conductivities. Sometimes, the free electrons are called electron gas, drawing an analogy between electrons and monatomic molecules. However, there are distinct differences between electrons in a solid and molecules in an ideal gas. The number of free electrons is on the order of the number of atoms. For Au, Cu, and Ag, we shall assume there is one (1) free electron per atom, but there are three (3) electrons per atom for Al and four (4) electrons per atom for Pb (see Table 5.2). Electrons obey the Fermi–Dirac distribution given in Eq. (3.24). A continuous function called the *Fermi function* can be defined as

$$f_{\mathrm{FD}}(\varepsilon) = \frac{\mathrm{d}N}{\mathrm{d}g} = \frac{1}{\mathrm{e}^{(\varepsilon-\mu)/k_{\mathrm{B}}T} + 1} \tag{5.15}$$

The Fermi function is plotted in Fig. 5.5a, where $\mu_{\mathrm{F}} = \mu$ at $T = 0$ K is called the *Fermi energy* (or Fermi level). It will be shown later that μ changes little when the temperature is not very high. At the absolute temperature of 0 K, $f_{\mathrm{FD}} = 1$ when $\varepsilon < \mu_{\mathrm{F}}$, and $f_{\mathrm{FD}} = 0$ when $\varepsilon > \mu_{\mathrm{F}}$. This suggests that each quantum state whose energy is below the Fermi energy is occupied by one electron. All quantum states whose energies exceed the Fermi energy are not occupied. As the temperature increases, the function falls less sharply. Hence, the quantum states slightly below the Fermi level are still filled, and those slightly above the Fermi level remain empty. However, the quantum states are only partially filled around the Fermi level.

The degeneracy for electrons is further increased by 2, due to the existence of positive and negative spins. In a volume V of a spherical shell in the momentum space, we have $\mathrm{d}g = 8\pi V(m_{\mathrm{e}}/h)^3 v^2 \mathrm{d}v$ from Eq. (3.86) by considering the spin degeneracy. Hence, the distribution function in terms of the electron speed is

$$f(v) = \frac{1}{V}\frac{\mathrm{d}N}{\mathrm{d}v} = 8\pi\left(\frac{m_{\mathrm{e}}}{h}\right)^3 \frac{v^2}{\mathrm{e}^{(\varepsilon-\mu)/k_{\mathrm{B}}T} + 1} \tag{5.16}$$

Using $f(v)\mathrm{d}v = f(\varepsilon)\mathrm{d}\varepsilon$ and $\varepsilon = m_{\mathrm{e}}v^2/2$, we obtain the distribution function in terms of the kinetic energy of electrons as

$$f(\varepsilon) = \frac{1}{V}\frac{\mathrm{d}N}{\mathrm{d}\varepsilon} = 4\pi\left(\frac{2m_{\mathrm{e}}}{h^2}\right)^{3/2} \frac{\sqrt{\varepsilon}}{\mathrm{e}^{(\varepsilon-\mu)/k_{\mathrm{B}}T} + 1} \tag{5.17}$$

Table 5.2 Electronic properties of selected metals; data mainly from Kittel [5]

	Li	Na	K	Cu	Ag	Au	Mg	Ca	Zn	Al	Pb
μ_F (eV)	4.72	3.23	2.12	7.0	5.51	5.5	7.13	4.68	9.39	11.6	9.37
$n_e(10^{28}\ m^{-3})$ Valence electrons	4.7 (1)	2.65 (1)	1.4 (1)	8.45 (1)	5.85 (1)	5.90 (1)	8.60 (2)	4.60 (2)	13.1 (2)	18.1 (3)	13.2 (4)
$r_e(\mu\Omega\,cm)$ at 22 °C	9.32	4.75	7.19	1.70	1.61	2.20	4.30	3.60	5.92	2.74	21.0

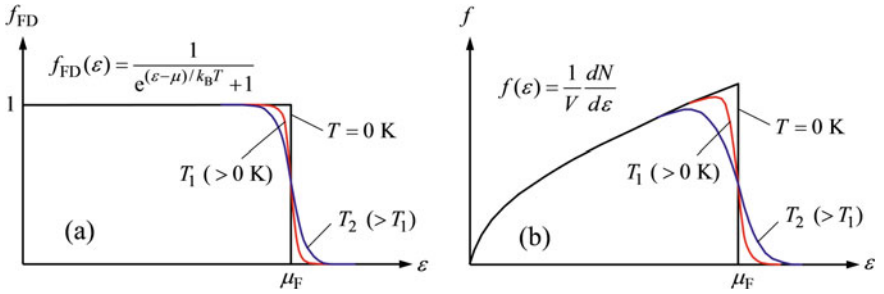

Fig. 5.5 **a** The Fermi function and **b** the distribution function of free electrons in a metal

This equation is plotted in Fig. 5.5b. Note that $f(\varepsilon) = f_{FD}(\varepsilon)D(\varepsilon)$, where $D(\varepsilon)$ is the density of states for free electrons and is expressed as

$$D(\varepsilon) = 4\pi\left(\frac{2m_e}{h^2}\right)^{3/2}\sqrt{\varepsilon} \tag{5.18}$$

Now, we are ready to evaluate the Fermi energy μ_F. At $T \to 0$, the number density of electrons becomes

$$n_e = \frac{N_e}{V} = \lim_{T\to 0}\int_0^{\mu} 4\pi\left(\frac{2m_e}{h^2}\right)^{3/2}\frac{\sqrt{\varepsilon}}{e^{(\varepsilon-\mu)/k_B T}+1}\mathrm{d}\varepsilon \tag{5.19}$$

which gives

$$\mu_F = \frac{h^2}{8m_e}\left(\frac{3n_e}{\pi}\right)^{2/3} \tag{5.20}$$

Typical values of μ_F range from 2 to 12 eV. Table 5.2 lists the Fermi energy, the electron number density, the number of electrons per atom, and the electrical resistivity of various metals. The temperature dependence of μ for electrons is given by the Sommerfeld expansion [6]:

$$\mu(T) = \mu_F\left[1 - \frac{1}{3}\left(\frac{\pi k_B T}{2\mu_F}\right)^2 + \cdots\right] \tag{5.21a}$$

It can be seen that $\mu(T) \approx \mu_F$ at moderate temperatures. Arnold Sommerfeld (1868–1951) was a German physicist and one of the founders of quantum mechanics. As a professor at the University of Munich, he advised a large number of doctorate students who became famous in their own right, including Peter Debye, Wolfgang Pauli, and Werner Heisenberg, among others. Sommerfeld applied the FD statistics to study free electrons in metals and resolved the difficulty in the classical theory for

electron specific heat. The Sommerfeld expansion for the integration involving the FD function is derived in Appendix B.8. As discussed in Chap. 3, electrons tend to fill all the quantum states up to a certain energy level. In many texts, $\mu(T)$ is called the Fermi level or the Fermi energy, which is temperature dependent. As the temperature increases, only those electrons near the Fermi level will be redistributed. By noticing that the difference between $\mu(T)$ and μ_F is small, we can use Eqs. (B.74) and (B.78) to express the electron number density as follows:

$$n_e = \int_0^\infty D(\varepsilon) f_{FD}(\varepsilon, T) d\varepsilon \approx \int_0^{\mu_F} D(\varepsilon) d\varepsilon + (\mu - \mu_F) D(\mu_F) + \frac{\pi^2 (k_B T)^2}{6} D'(\mu_F)$$

where the first term is the same as the right-hand side of Eq. (5.19). Since the number density is independent of temperature, we must have

$$(\mu - \mu_F) D(\mu_F) + \frac{\pi^2 (k_B T)^2}{6} D'(\mu_F) = 0 \tag{5.21b}$$

which proves Eq. (5.21a) since $D(\varepsilon)/D'(\varepsilon) = 2\varepsilon$.

Example 5.2 Calculate μ at 300 and 10,000 K for copper using $\mu_F = 7\,\text{eV}$. Find the maximum speed (Fermi velocity) and the average speed of electrons for copper at 0 K. How will the Fermi velocity change if the temperature is changed to $T =$ 300 K?

Solution Note that $k_B = 1.381 \times 10^{-23}/1.602 \times 10^{-19} = 8.62 \times 10^{-5}\,\text{eV/K}$. Let us calculate the relative changes of μ at a given temperature T. From Eq. (5.21a), we have

$$\frac{\mu(T) - \mu_F}{\mu_F} \approx -\frac{1}{3}\left(\frac{\pi k_B T}{2\mu_F}\right)^2 = -1.24 \times 10^{-10} T^2$$

which is about 0.0011% at 300 K and 1.2% at 10,000 K. The change in μ is indeed very small. At $T = 0$, $\mu_F = \frac{1}{2} m_e v_{max}^2 = \frac{1}{2} m_e v_F^2$. Hence,

$$v_{max} = v_F = \sqrt{2\mu_F / m_e} \tag{5.22a}$$

$$\bar{\varepsilon} = \frac{1}{2} m_e \overline{v^2} = \frac{U}{N} = \int_0^{\mu_F} f(\varepsilon) \varepsilon d\varepsilon \Big/ \int_0^{\mu_F} f(\varepsilon) d\varepsilon = \frac{3}{5}\mu_F \tag{5.22b}$$

$$v_{rms} = \sqrt{\frac{2\bar{\varepsilon}}{m_e}} = \sqrt{\frac{6\mu_F}{5m_e}} \tag{5.22c}$$

Electrons are constantly moving even at absolute zero temperature. For copper, we get $v_F = 1.57 \times 10^6$ m/s and $v_{rms} = 1.22 \times 10^6$ m/s, which is about three-quarters

of v_F. The classical model based on the equipartition principle or the Maxwell–Boltzmann distribution would give $\frac{3}{2}k_BT = \frac{1}{2}m_e\overline{v^2}$ or $v_{rms} = \sqrt{3k_BT/m_e} = 0$ at absolute zero temperature. Because μ changes little from 0 to 300 K, the Fermi velocity at 300 K is essentially the same as that obtained at 0 K.

Discussion: If we use the rms velocity to calculate the de Broglie wavelength as in Example 3.2, we obtain $\lambda_{DB} = 0.6$ nm. If an electron is accelerated in vacuum to 50 keV, the velocity will be greater than one-third of that of light, and the de Broglie wavelength will be extremely small ($\lambda_{DB} \approx 0.0066$ nm). The resolutions in conventional optical microscopy and photolithography are usually limited by $\lambda/2$ (the diffraction limit), which is on the order of 200 nm for visible light. Electron microscopy can have a much higher resolution (~0.1 nm), and e-beam nanolithography allows the manufacturing of features just a few nanometers.

In order to find out the specific heat of electrons, we first calculate the internal energy:

$$U = V\int_0^\infty \varepsilon f_{FD}(\varepsilon)D(\varepsilon)\mathrm{d}\varepsilon \tag{5.23a}$$

Because the distribution function does not vary significantly except near $\varepsilon = \mu$, the Sommerfeld expansion can be used to express the integration [see Eq. (B.78) in Appendix B]. Hence,

$$\frac{U}{V} \approx \int_0^{\mu_F} \varepsilon D(\varepsilon)\mathrm{d}\varepsilon + \mu_F(\mu - \mu_F)D(\mu_F) + \frac{(\pi k_BT)^2}{6}[\mu_F D'(\mu_F) + D(\mu_F)]$$

One can see from Eq. (5.21b) that the two middle terms on the right side cancel out. It should also be noted that $D(\mu_F) = 3n_e/2\mu_F$. Therefore,

$$U \approx \frac{3}{5}N\mu_F\left[1 + \frac{5\pi^2}{12}\left(\frac{k_BT}{\mu_F}\right)^2 + \cdots\right] \tag{5.23b}$$

The specific heat of free electrons can then be obtained as

$$\bar{c}_{v,e} = \left(\frac{\partial \bar{u}}{\partial T}\right)_V = \frac{\pi^2 k_BT}{2\mu_F}\bar{R} \tag{5.24}$$

which is much smaller than $\frac{3}{2}\bar{R}$ as we would obtain if electrons were behaving as an ideal monatomic molecular gas. Another way of obtaining Eq. (5.24) is to use integration, which is left as an exercise (see Problem 5.6). Electronic contribution to the specific heat of solids is negligible except at very low temperatures (a few kelvins or less). The specific heat of metals at very low temperatures can thus be expressed as

$$c_v(T) = \gamma T + BT^3 \tag{5.25}$$

where the linear term is the electronic contribution and the cubic term is the lattice contribution for which B can be obtained from Eq. (5.14). The coefficient γ is known as the *Sommerfeld constant*. The experimental values of γ generally agree with those predicted by the free-electron model given in Eq. (5.25) for most alkali metals (e.g., Na, K) and noble metals (e.g., Cu, Ag, Au). For transition metals with magnetic properties, such as Fe and Mn, the measured γ value can be an order of magnitude greater than the predicted. On the other hand, for semimetals like Bi, the measured γ value can be an order of magnitude smaller than the predicted. Further discussions can be found from the text of Ashcroft and Mermin [6].

Example 5.3 Calculate and plot the specific heat of copper, and compare with the data in Touloukian and Buyco [7]. Discuss the contribution of electrons and lattice vibrations.

Solution From Table 5.1, the Debye temperature for Cu is $\Theta_D = 340\,\text{K}$. At $T < 30$ K, we can apply the T^3 law given in Eq. (5.14) to find the coefficient B in Eq. (5.25) to be $5.95 \times 10^{-6}\,\bar{R}\,[\text{K}^{-3}]$. Using $\mu_F = 7\,\text{eV}$ from Table 5.2, the Sommerfeld coefficient can be calculated from Eq. (5.24) as $\gamma = 6.08 \times 10^{-5}\,\bar{R}\,[\text{K}^{-1}]$. Therefore, the two contributions will be equal at $T = 3.2$ K. The results are plotted in Fig. 5.6a at temperatures below 10 K. At higher temperatures, as shown in Fig. 5.6b, the electronic contribution is much smaller compared with the lattice specific heat: about 0.3% at 100 K, 0.6% at 300 K, and 2% at 1000 K. The data show much higher specific heat values than those predicted by the Debye model. The addition of the electronic contributions cannot fully account for the difference. Noting that $R = \bar{R}/M = 130.9\,\text{J/kg K}$ at 1000 K, the specific heat calculated from the Debye model of $c_v = 390.6\,\text{J/kg K}$ is 99.5% of $3R$ given by the Dulong–Petit law. There are several reasons that may be responsible for the deviation between the Debye model

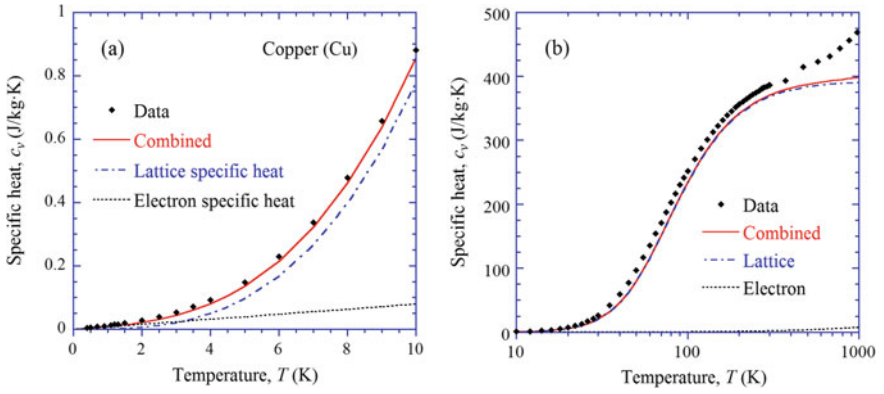

Fig. 5.6 Electron and lattice contributions to the specific heat of Cu **a** at low temperatures and **b** from 10 to 1000 K

and measurements at high temperatures. The first is the anharmonic vibration that was not considered in the simple models with harmonic vibrations. The contribution of anharmonic vibrations becomes more important at higher temperatures since the amplitude of vibration increases with temperature. Secondly, thermal expansion cannot be ignored at high temperatures. The variation of the distance between atoms may change the potential function and thus increase the specific heat. Additionally, when thermal expansion is not negligibly small, the specific heat at constant pressure (that is measured) may be greater than that at constant volume (that is predicted). Interested readers are referred to the literature for further discussions [9, 10].

5.2 Quantum Size Effect on Specific Heat

The above discussion assumes that the physical dimensions are much larger than the lattice constant. In nanoscale devices and structures, such as 2D thin films or superlattices, 1D nanowires or nanotubes, or 0D quantum dots or nanocrystals, substitution of summation by integration is no longer appropriate. Note that a 2D thin film is confined in one dimension, a 1D wire is confined in two dimensions, and a 0D quantum dot is confined in all three dimensions. In nanostructures, it is necessary to consider quantization of the energy levels. The specific heat becomes a function of the actual dimensions. Experimental demonstrations of quantum size effect on specific heat have been made on Pb particles [11], carbon nanotubes [12], and titanium dioxide nanotubes [13], to name a few. To analyze the quantum size effect on the lattice specific heat, we begin with a wavelike treatment of the vibrational modes in this section.

5.2.1 Periodic Boundary Conditions

Consider a 1D chain of $N + 1$ atoms as sketched in Fig. 5.3, where the end nodes are fixed in position. The solution should be a standing wave with the following eigenfunctions:

$$\sin\left(\frac{\pi x}{L}\right), \quad \sin\left(\frac{2\pi x}{L}\right), \quad \sin\left(\frac{3\pi x}{L}\right), \ldots, \quad \sin\left(\frac{\pi x}{L_0}\right) \tag{5.26}$$

where $L/L_0 = N$, which is the total number of vibration modes within a length of L. Another approach is based on the Born–von Kármán periodic boundary conditions [6]. Instead of treating the solid as a bounded specimen whose atoms are fixed at each boundary, the Born–von Kármán lattice model takes the medium as an infinite extension with periodic boundary conditions. For a solid whose dimensions are L_x, L_y, L_z in the Cartesian coordinates, the standing wave solutions are

$$\exp(\mathrm{i}k_x x), \quad \exp\left(\mathrm{i}k_y y\right), \quad \exp(\mathrm{i}k_z z) \tag{5.27}$$

where $\mathbf{k} = (k_x, k_y, k_z)$ is called the *lattice wavevector* with $k^2 = k_x^2 + k_y^2 + k_z^2$. The allowed discretized values are

$$k_x = 0, \quad \pm\frac{2\pi}{L_x}, \quad \pm\frac{4\pi}{L_x}, \quad \pm\frac{6\pi}{L_x}, \ldots, \quad \pm\frac{(N_x-1)\pi}{L_x}, \quad +\frac{N_x\pi}{L_x} \tag{5.28a}$$

$$k_y = 0, \quad \pm\frac{2\pi}{L_y}, \quad \pm\frac{4\pi}{L_y}, \quad \pm\frac{6\pi}{L_y}, \ldots, \quad \pm\frac{(N_y-1)\pi}{L_y}, \quad +\frac{N_y\pi}{L_y} \tag{5.28b}$$

$$k_z = 0, \quad \pm\frac{2\pi}{L_z}, \quad \pm\frac{4\pi}{L_z}, \quad \pm\frac{6\pi}{L_z}, \ldots, \quad \pm\frac{(N_z-1)\pi}{L_z}, \quad +\frac{N_z\pi}{L_z} \tag{5.28c}$$

where the last term only has "+" term and should only be included if the number of atoms along each direction N_x, N_y, or N_z is an even number. The central distance between adjacent atoms is L_x/N_x, L_y/N_y, or L_z/N_z in the given direction. The individual components of the lattice wavevector may be negative or zero in this case. In the 1D case, it can be seen that the total number of modes is the same as the total number of atoms along the 1D chain. However, the infinite medium representation with periodic boundary conditions is advantageous not only in mathematical derivations but also for the physical interpretation of lattice dynamics.

5.2.2 General Expressions of Lattice Specific Heat

The general expression of the lattice vibrational energy in a solid is given as

$$u(T) = u_0 + \sum_P \sum_K \hbar\omega \left(\frac{1}{\mathrm{e}^{\hbar\omega/k_\mathrm{B}T} - 1} + \frac{1}{2} \right) \tag{5.29}$$

where u_0 accounts for the static energy at absolute zero temperature, the first term in the parenthesis is the Bose–Einstein distribution $f_\mathrm{BE}(\omega, T)$ given in Eq. (5.4), and the second term in the parenthesis corresponds to the *zero-point energy* that is associated with the $\frac{1}{2}h\nu$, due to *quantum fluctuation* or *vacuum fluctuation,* in the vibrational energy levels. We use $h\nu$ and $\hbar\omega$ interchangeably whichever is more convenient. The summation is over all phonon branches in terms of the wavevector index K and the polarization index P. A phonon branch (sometimes also called a phonon mode) describes the behavior of a type of phonons with a continuous frequency rather than a discrete frequency. The concept of phonon branches will be presented in detail in the subsequent chapter. The lattice specific heat can be expressed as [5]

$$c_v(T) = \sum_P \sum_K \hbar\omega \frac{\partial f_\mathrm{BE}(\omega, T)}{\partial T} \tag{5.30}$$

Upon introducing the DOS, we can replace the summation over k-space with an integration as follows:

$$c_v(T) = \sum_P \int_0^\infty \hbar\omega \frac{\partial f_{\mathrm{BE}}}{\partial T} D(\omega)\mathrm{d}\omega$$
$$= k_\mathrm{B} \sum_P \int_0^\infty \left(\frac{\hbar\omega}{k_\mathrm{B}T}\right)^2 \frac{\mathrm{e}^{\hbar\omega/k_\mathrm{B}T}}{(\mathrm{e}^{\hbar\omega/k_\mathrm{B}T}-1)^2} D(\omega)\mathrm{d}\omega \tag{5.31}$$

Since the DOS is expressed as the number of modes per unit volume, Eq. (5.31) gives the specific heat per unit volume. Neutral scattering and Raman scattering are common ways of determining the DOS from the relationship between ω and the lattice wavevector $\mathbf{k}$ along selected crystal directions. The function $\omega = \omega(\mathbf{k})$ is called a *dispersion relation.* If discretized values are expressed using the Delta functions in the expression of $D(\omega)$, Eq. (5.31) is equivalent to Eq. (5.30), and both the equations can be considered as the general expressions of the specific heat due to lattice vibrations. For a nanostructure with very few atoms in a particular direction, Eq. (5.30) may be more convenient to use. On the other hand, in directions with a large number of atoms, Eq. (5.31) would be the preferable choice.

5.2.3 Dimensionality

The method of periodic boundary conditions allows one to determine the density of states for simple dispersion relations easily. Figure 5.7 shows the k-space, or the *reciprocal lattice space,* in the 2D case. Each individual block of area $4\pi^2/(L_x L_y)$

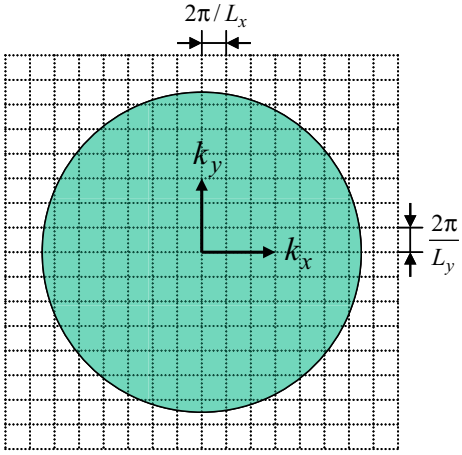

Fig. 5.7 Schematic of the reciprocal lattice space, or k-space

represents a mode, and the number of modes up to a certain value of k is equal to the total number of blocks inside the circle. One can also use this graph to visualize the 3D case. Each box of volume $8\pi^3/(L_xL_yL_z)$ represents a mode. The number of modes for a given upper limit k is equal to the total number of boxes within a sphere of radius k, hence,

$$N = \frac{4\pi k^3}{3}\frac{L_xL_yL_z}{8\pi^3} = \frac{Vk^3}{6\pi^2} \tag{5.32}$$

When the dimensions are large enough, the DOS can be expressed as

$$D(\omega) = \frac{1}{V}\frac{\mathrm{d}N}{\mathrm{d}\omega} = \frac{k^2}{2\pi^2}\frac{\mathrm{d}k}{\mathrm{d}\omega} \tag{5.33}$$

Assume the dispersion relation is linear, then

$$\omega = v_\mathrm{a}k \tag{5.34}$$

where v_a is the average speed of the longitudinal and transverse waves as in Eq. (5.7). We can rewrite Eq. (5.33) as

$$D(\omega) = \frac{\omega^2}{2\pi^2 v_\mathrm{a}^3} \tag{5.35}$$

This expression is equivalent to Eq. (5.7) for a single polarization. Equations (5.32) and (5.34) can be combined to obtain the high-frequency limit by setting N equal to the number of atoms. The result is the same as Eq. (5.9). When Eq. (5.35) is substituted into Eq. (5.31), the Debye expression of the specific heat given in Eq. (5.13) is readily obtained.

If the number of atoms is very small in a particular direction, there will only be a few values for the particular wavevector component. The dimensionality will be reduced, and the wavevector component can be assumed as zero in that direction. For a 2D solid (such as a thin film or a quantum well), the DOS is defined as the number of quantum states per unit area. By assuming a linear dispersion relation, we obtain

$$N = \frac{\pi k^2}{4\pi^2/(L_xL_y)} = \frac{Ak^2}{4\pi} \tag{5.36}$$

and

$$D(\omega) = \frac{1}{A}\frac{\mathrm{d}N}{\mathrm{d}\omega} = \frac{k}{2\pi}\frac{\mathrm{d}k}{\mathrm{d}\omega} = \frac{\omega}{2\pi v_\mathrm{a}^2} \tag{5.37}$$

For a 1D solid (such as a nanowire or a nanotube), by noting that $N = 2k\big/(2\pi/L_x) = Lk/\pi$, we find the DOS to be

$$D(\omega) = 1/(\pi v_a) \tag{5.38}$$

which is independent of the frequency. It can be shown that, in the low-temperature limit, the specific heat for a 2D solid is proportional to T^2 and that for a 1D solid is proportional to T [14, 15]. Experimental evidence of the dimensionality change has been known for a long time in graphite, which has a layered lattice structure with a strong bonding between atoms within each layer and a weak interactive force between layers. The specific heat of graphite is approximately proportional to T^2 at low temperatures [16]. On the other hand, the linear temperature dependence of specific heat has been observed in carbon nanotubes [12].

It can be seen from Eq. (5.31) that when $\hbar\omega \gg k_B T$, the integrand approaches zero. Therefore, the contribution to the specific heat is negligibly small when the phonon energy is much higher than $k_B T$. The speed of lattice waves ranges from 1000 to 10,000 m/s, and the phonon wavelength corresponding to $k_B T$ is called *thermal phonon wavelength,* which can be calculated from $\lambda_{th} = v_a h/k_B T$. At room temperature, λ_{th} is approximately 0.3 nm for $v_a = 2000\,\text{m/s}$ and 1 nm for $v_a = 6000\,\text{m/s}$. At 10 K, $\lambda_{th} \approx 10\,\text{nm}$ for $v_a = 2000\,\text{m/s}$, and $\lambda_{th} \approx 30\,\text{nm}$ for $v_a = 6000\,\text{m/s}$. It is expected that the quantum size effect will become more significant at low temperatures, because the thermal phonon wavelength may be greater than the smallest physical length, such as the thickness of the film and the diameter of the wire.

5.2.4 Thin Films and Nanowires

Thin films, or quantum wells, are important components for microelectronic and photonic devices. We will use the following example to elucidate the effect of film thickness and temperature on the specific heat of thin films.

Example 5.4 Evaluate the low-temperature behavior of the specific heat of a thin film made of a monatomic solid. Assume that the film thickness is L, which has q monatomic layers, i.e., $L = qL_0$. The average acoustic speed v_a may be assumed to be independent of temperature. Values of silicon given in Example 5.2 may be used in the numerical evaluation.

Solution The molar specific heat can be expressed as

$$\bar{c}_v(T) = \frac{3V\bar{R}}{Nk_B} \sum_{k_x,k_y,k_z} \hbar\omega \frac{\partial f_{BE}}{\partial T} \tag{5.39}$$

where the number 3 accounts for the three phonon polarizations. Assume the dimension perpendicular to the film is the z-direction. The allowable modes in the z-direction are given by $k_z = 0, \pm 2\pi/L, \pm 4\pi/L, \ldots$ In order for the total number of

modes in the z-direction to be equal to q for all q values, we shall use the following limits:

$$k_z = \begin{cases} 0, \pm\frac{2\pi}{L}, \pm\frac{4\pi}{L}, \ldots \pm\frac{(q-1)\pi}{L}, & \text{for } q = 1, 3, 5 \ldots \\ 0, \pm\frac{2\pi}{L}, \ldots \pm\frac{(q-2)\pi}{L}, +\frac{q\pi}{L}, & \text{for } q = 2, 4, 6 \ldots \end{cases} \tag{5.40}$$

Assume that the lattice is infinitely extended in the directions parallel to the film. We can substitute the summation with integration in the parallel directions using cylindrical coordinates. Therefore,

$$\bar{c}_v(T) = \frac{3V\bar{R}}{(2\pi)^3 N k_\mathrm{B}} \sum_{k_z} \left(\int_0^{\beta_\mathrm{D}} \hbar\omega \frac{\partial f_\mathrm{BE}}{\partial T} 2\pi\beta \mathrm{d}\beta \right) \Delta k_z \tag{5.41}$$

where $\beta^2 = k_x^2 + k_y^2$, $\Delta k_z = 2\pi/L$, and $\beta_\mathrm{D} = \sqrt{k_\mathrm{D}^2 - k_z^2}$. The cutoff value k_D is determined by setting the total number of modes equal to the number of atoms per unit area. Equation (5.36) can be used to evaluate the number of modes for each k_z and then summed up over all k_z values. Hence,

$$\frac{N}{A} = \sum_{k_z} \frac{\beta_\mathrm{D}^2}{4\pi} = \sum_{k_z} \frac{k_\mathrm{D}^2 - k_z^2}{4\pi} \tag{5.42a}$$

Note that $N = AL/L_0^3 = Aq/L_0^2$ and there are q terms in the summation according to the k_z values given in Eq. (5.40). We can solve Eq. (5.42a) to obtain

$$k_\mathrm{D} = \sqrt{\frac{4\pi}{L_0^2} + \sum_{k_z} \frac{k_z^2}{q}} \tag{5.42b}$$

In the limit of a single atomic layer, $k_\mathrm{D} = 2\sqrt{\pi}/L_0 \approx 3.54 L_0^{-1}$; when $q \to \infty$, $k_\mathrm{D} \approx 3.98 L_0^{-1}$, which is very close to the 3D value of $k_\mathrm{D} = (6\pi^2)^{1/3}/L_0 \approx 3.90 L_0^{-1}$. Note that the value of k_D normalizes the specific heat so that c_v approaches to the high-temperature limit of $3R$. At low temperatures, when the quantum size effect is significant, a slight difference in k_D does not alter the results much.

Using the linear dispersion relation, $\omega = v_\mathrm{a} k = v_\mathrm{a}\sqrt{\beta^2 + k_z^2}$, we see that $2\beta\mathrm{d}\beta = k\mathrm{d}k$ for fixed k_z. Therefore, Eq. (5.41) can be recast to the following:

$$\bar{c}_v(T) = \frac{3\bar{R}}{2\pi N/A} \left(\frac{k_\mathrm{B} T}{\hbar v_\mathrm{a}} \right)^2 \sum_{k_z} \int_{x_z}^{x_\mathrm{D}} \frac{x^3 \mathrm{e}^x}{(\mathrm{e}^x - 1)^2} \mathrm{d}x \tag{5.43}$$

where $x = \frac{\hbar v_\mathrm{a} k}{k_\mathrm{B} T}$, $x_\mathrm{D} = \frac{\hbar v_\mathrm{a} k_\mathrm{D}}{k_\mathrm{B} T}$, and $x_z = \frac{\hbar v_\mathrm{a} |k_z|}{k_\mathrm{B} T}$. The T^2 dependence at low temperatures is evident when $q = 1$ or $k_z = 0$ only. The modes associated with $k_z = 0$ are

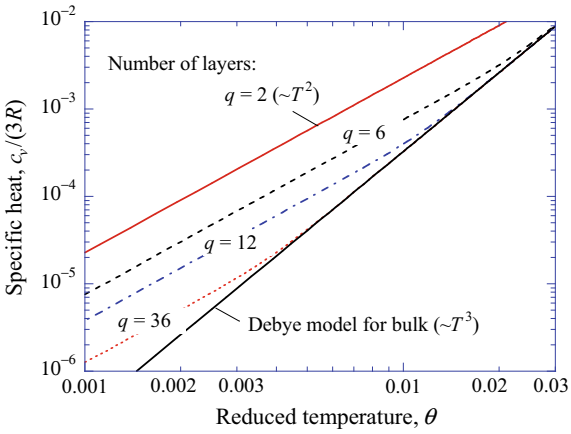

Fig. 5.8 Quantum size effect on the specific heat of thin films, where the reduced temperature is defined as $\theta = Tk_B L_0/hv_a$

parallel to the interface and are called *planar modes*. We have carried out a numerical evaluation of Eqs. (5.42) and (5.43) for different values of N to see when the departure from bulk behavior will occur. The results are plotted in Fig. 5.8 as a function of the reduced temperature, defined as $\theta = Tk_B L_0/hv_a = L_0/\lambda_{th}$. It can be shown that $hv_a/k_B L_0 \approx 1.61\Theta_D$, where Θ_D is the Debye temperature. When q and T are sufficiently large, the result from Eq. (5.43) is the same as that predicted by the Debye model for bulk materials. The departure occurs at low temperatures and especially for small q values.

As mentioned earlier, due to the layerlike structure of graphite, its specific heat exhibits 2D solid behavior at low temperatures [16]. The procedure used for this example is essentially the same as that used by Prasher and Phelan [17], except that we have considered the planar modes ($k_z = 0$) in evaluating Eq. (5.43). The result is an increase in the specific heat in the microscopic regime, as discussed in detail in Ref. [15]. Hence, planar modes are critically important when the thickness is small, especially at low temperatures.

A similar formulation can be derived for a nanowire with a square or rectangular cross section [15, 16]. When axial modes are allowed for a wire parallel to the z-axis, $k_x = k_y = 0$, the specific heat of this single mode dominates all other modes at sufficiently low temperatures and varies linearly with the temperature T [15]. Another way to show the linear temperature dependence is to combine the DOS given in Eq. (5.38) with Eq. (5.31) as mentioned previously [14]. Note that the discussion here assumes that the linear dispersion relation, Eq. (5.34), holds for the average phonon speed with only three phonon modes. The actual phonon modes and dispersion relations can be rather complicated, and rather sophisticated tools are required to model the thermal properties of nanostructured materials. Several studies have been conducted for silicon nanowires [18–20].

5.2.5 *Nanoparticles or Nanocrystals*

For 3D confinement or 0D structures, consider cuboidal nanoparticles of dimensions (L_x, L_y, L_z) with the number of atoms in each direction as (N_x, N_y, N_z). The molar specific heat can be written as a summation using Eq. (5.30) as follows:

$$\bar{c}_v(\theta) = \frac{3\bar{R}}{N_x N_y N_z} \sum_{j,m,n} \frac{\eta^2 e^\eta}{(e^\eta - 1)^2} \tag{5.44}$$

where

$$\eta = \frac{1}{\theta}\left(\frac{j^2}{N_x^2} + \frac{m^2}{N_y^2} + \frac{n^2}{N_z^2}\right)^{1/2} \text{with}\, \theta = \frac{T k_B L_0}{h v_a} \tag{5.45}$$

Note that the summation indices are based on the wavevector values given in Eq. (5.28). For nanoparticles, the aspect ratio and shape can affect the specific heat characteristics. Therefore, T^n (where $1 < n < 3$) behavior may occur for cuboids below the Debye temperature but not at very low temperatures [15].

When the temperature is very low, only the mode(s) with the lowest frequency can be excited and a *second quantum size effect* will occur. Consider a cubic nanocrystal with q atoms in each dimension. Among the q^3 total modes, we are left with only six axial modes, which are $\mathbf{k} = (\pm 2\pi/L, 0, 0)$, $(0, \pm 2\pi/L, 0)$, and $(0, 0, \pm 2\pi/L)$. These modes have the longest phonon wavelength. From Eq. (5.44), the specific heat can be expressed as

$$c_v(T \to 0) = \frac{a}{T^2} \exp\left(-\frac{b}{T}\right) \tag{5.46}$$

where a and b are positive constants. Because Eq. (5.46) converges to zero faster than T^3, the second quantum size effect will reduce the specific heat at extremely low temperatures [21, 22]. Experiments were made in the early 1970s on lead particles as small as 2.2-nm diameter [11]. At temperatures below 15 K, the specific heat of these particles is much greater than that for the bulk material. However, as the temperature is reduced to about 2 K, the difference diminishes. Below 2 K, the specific heat of the nanoparticles decreases much rapidly than that of the bulk. Note that Eq. (5.46) only applies to the 3D confined case because for 1D or 2D confined cases, the wavevector in the unconfined direction is not restricted.

For bulk solids, as discussed previously, the Born–von Kármán periodic boundary condition is equivalent to the Dirichlet or Neumann boundary conditions [6]. However, for nanocrystals, the applied boundary conditions can affect the model predictions significantly [15, 22]. Let us consider cuboidal nanoparticles. The Dirichlet boundary condition fixes the value at the boundary and is called a clamped

boundary condition. The eigenfunctions are given in Eq. (5.26), allowing only positive wavevectors. The specific heat may still be computed using Eq. (5.44), while Eq. (5.45) is modified as

$$\eta = \frac{1}{2\theta}\left(\frac{j^2}{N_x^2} + \frac{m^2}{N_y^2} + \frac{n^2}{N_z^2}\right)^{1/2}, \quad j = 1, 2, \ldots, N_x; \; m = 1, 2, \ldots, N_y; \; n = 1, 2, \ldots, N_z \tag{5.47a}$$

For a cubic nanoparticle with $N_x = N_y = N_z = q$, the lowest phonon mode corresponds to $(j, m, n) = (1, 1, 1)$ or $k_x = k_y = k_z = \pi/L$. The result is a minimum wavevector $k_{\min} = \sqrt{3}\pi/L$ and $\eta_{\min} = \sqrt{3}/(2\theta q)$. For the periodic boundary conditions as discussed before, $k_{\min} = 2\pi/L$ and $\eta_{\min} = (\theta q)^{-1}$. While the minimum wavevector is slightly smaller, the resulting $\eta_{\min}$ for the lowest phonon mode is greater with Dirichlet boundary conditions. Hence, the predicted specific heat using the Dirichlet boundary conditions is always lower than that of the corresponding bulk material which is independent of the boundary conditions. This is also true for spherical particles using spherical Bessel functions [22].

On the other hand, when Neumann free-surface boundary conditions are applied, the eigenfunctions are cosine functions and the indices in Eq. (5.47a) should be modified to allow zero indices as long as at least one of them is nonzero, that is

$$j = 0, 1, \ldots, (q_x - 1); \; m = 0, 1, \ldots, (q_y - 1); \; n = 0, 1, \ldots, (q_z - 1) \tag{5.47b}$$

where $j, m,$ and n cannot be simultaneous zero. In this case, we see from Eq. (5.47a) that $k_{\min} = \pi/L$ and $\eta_{\min} = (2\theta q)^{-1}$. Therefore, the phonon frequency of the lowest mode is half of that in the case of periodic boundary conditions. The reduction of phonon frequency toward low temperatures is called *phonon softening*. Phonon softening results in an enhancement of the specific heat of nanoparticles at low temperatures until the temperature becomes sufficiently low when the second quantum size effect described by Eq. (5.46) will dominate the specific heat behavior. The result for cubic nanoparticles is in general consistent with that of spherical nanoparticles based on the Neumann boundary conditions [15, 22].

5.2.6 Graphite, Graphene, and Carbon Nanotubes

Unlike diamond, which contains 3D tetrahedral structures, graphite crystallizes in the hexagonal system with sheetlike structures. While diamond and graphite are each a polymorph of the element carbon, they exhibit dramatically different properties due to their different crystalline structures. Diamond is hard, transparent, and an electrical insulator. On the contrary, graphite is quite soft, opaque, and a good electrical conductor. Graphene is a single atomic layer of carbon atoms packed into a periodic benzene-ring structure. Carbon nanotubes may be considered as rolled from

a graphene sheet into a hollow cylinder, with one or both of its ends capped with half a fullerene molecule. The discovery of C_{60} and other fullerenes by Robert Curl, Harold Kroto, and Richard Smalley was recognized through the 1996 Nobel Prize in Chemistry conferred on them. The diameter of single-walled carbon nanotubes (SWNTs) can be as small as 0.4 nm with a typical diameter 1–2 nm and as long as 100 μm or so. Multi-walled carbon nanotubes (MWNTs) and nanotube ropes can have a diameter from 10 to 200 nm.

As mentioned earlier, graphite has a 2D structure and exhibits T^2 dependence at low temperatures [16]. For an isolated graphene sheet, the in-plane or parallel transverse acoustic phonon mode or branch has a velocity of $v_{\mathrm{TA-p}} = 15,000\,\mathrm{m/s}$ and the longitudinal acoustic phonon mode has a velocity of $v_{\mathrm{LA}} = 24,000\,\mathrm{m/s}$. On the other hand, the out-of-plane or perpendicular transverse phonon branch is described by a quadratic dispersion relation, $\omega \propto k^2$, which is the dominant mode for the specific heat at low temperatures. Considering the dimensionality and the dispersion relation, the specific heat of a graphene sheet depends almost linearly on T at lower temperatures (see Problem 5.11) and on T^2 as the temperature is raised above 100 K or so.

The four acoustic phonon modes or branches are expected to be the dominant contributions to the specific heat of isolated SWNTs at low temperatures. These include two (degenerate) transverse modes, one longitudinal mode, and a twisting mode or torsional mode associated with the rigid rotation around the nanotube axis. The dispersion relation is linear for all four modes at low frequencies [23]. Therefore, because of the 1D structure, the specific heat is expected to be linearly dependent on temperature. As the temperature is raised, however, higher frequency modes are excited and the 2D characteristics of carbon nanotubes come into play. Watt de Heer has written an elegant article on this topic [24]. There are significant differences between SWNTs, MWNTs, and nanotube ropes or bundles; the actual temperature dependence can be more complicated and dependent on the diameter [12, 23–25].

In nanostructures, the electron DOS is also subject to quantization. The theory for the electronic contribution to the specific heat is more complicated. The electron–electron and electron–phonon interactions as well as the distribution of energy levels and the Fermi energy need to be considered in a detailed model [26, 27]. The electronic specific heat of small particles is still a linear function of temperature. Generally speaking, the electronic contribution to the specific heat is negligibly small unless the temperature is below about 1 K. Therefore, we will not discuss the electronic size effect on the specific heat any further.

5.3 Electrical and Thermal Conductivities of Solids

In this section, we use kinetic theory to study the electron and phonon transport properties of metals and insulators in the bulk form. The coupling between electrical current and heat flux due to electric field and temperature gradient will be studied

in the next section, followed by a discussion of the size effect on the electrical and thermal conductivities.

5.3.1 Electrical Conductivity

We start with the simple kinetic theory approach based on the Drude free-electron model, also known as the Drude–Lorentz theory. As shown in Fig. 5.9, the electrical resistance of a resistor is $R = r_e L/A_c = L/(\sigma A_c)$, where r_e is the resistivity; its inverse σ is the conductivity, L is the length, and A_c is the cross-sectional area. Ohm's law relates the voltage drop ΔV and the current I by $\Delta V = IR$, which can be rearranged as

$$\frac{I}{A_c} = \sigma \frac{\Delta V}{L} \tag{5.48}$$

Notice that $J = I/A_c$ is the *current density* (charge per unit cross-sectional area per unit time), and $E = \Delta V/L$ is the electric field (note that the electric field is in the direction of decreasing voltage). Rewriting it in the vector form, we have

$$\mathbf{J} = \sigma \mathbf{E} \tag{5.49}$$

The above equation may be considered as the microscopic Ohm's law. An electron of charge $-e$ is accelerated in an electric field according to Newton's law as

$$\mathbf{F} = -e\mathbf{E} = m_e \frac{\mathrm{d}\mathbf{v}}{\mathrm{d}t} \tag{5.50}$$

Due to collisions, electrons cannot move completely freely. The velocity change of an electron during a relaxation time τ (the average traveling time between collisions) due to an external field is called the *drift velocity* $\mathbf{u}_d$. The probability that a traveling particle will collide with another particle or a defect during an infinitesimal time $\mathrm{d}t$ is given by $\mathrm{d}t/\tau$. The acceleration term in Eq. (5.50) can then be approximated by

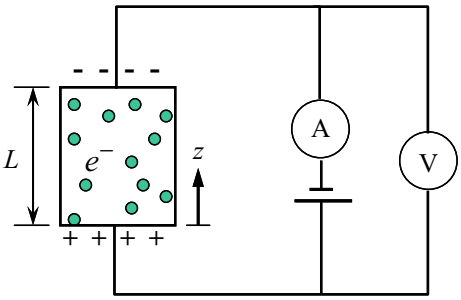

Fig. 5.9 Illustration of electrical conduction

$\mathbf{u}_\mathrm{d}/\tau$. Alternatively, one can also consider a damping force that is proportional to the drift velocity given as $m_\mathrm{e}\gamma\mathbf{u}_\mathrm{d}$, where the damping coefficient γ happens to be the electron scattering rate $1/\tau$. At steady state, the damping force must balance the external electrical force, i.e., $-e\mathbf{E} = m_\mathrm{e}\mathbf{u}_\mathrm{d}/\tau$ [28]. The current density is related to the drift velocity by $\mathbf{J} = -en_\mathrm{e}\mathbf{u}_\mathrm{d}$, hence,

$$\mathbf{J} = \frac{n_\mathrm{e}e^2\tau}{m_\mathrm{e}}\mathbf{E} \tag{5.51}$$

Comparing the above equation with Eq. (5.49), we obtain the Drude–Lorentz expression:

$$\sigma = \frac{n_\mathrm{e}e^2}{m_\mathrm{e}}\tau \tag{5.52}$$

The preceding equation is often used to obtain the relaxation time τ from the measured electrical conductivity σ. At moderate temperatures, it can be assumed that the characteristic velocity of electrons is the Fermi velocity v_F, and the mean free path of electrons can be written as

$$\Lambda_\mathrm{e} = v_\mathrm{F}\tau \tag{5.53}$$

The electron scattering mechanisms are illustrated in Fig. 5.10. Electron–electron scattering is inelastic and usually negligible compared with electron–phonon scattering, which is also inelastic. Because lattice vibrations are enhanced as temperature increases, electron–phonon scattering is expected to be dominant at high temperatures. Defect or impurity scattering, on the other hand, is important at low temperatures. For bulk materials that are large enough, boundary scattering is negligible. According to Matthiessen's rule, the scattering rate of independent scattering events can be added to yield the total scattering rate. For a bulk material, we have

$$\frac{1}{\tau} = \frac{1}{\tau_\mathrm{e-e}} + \frac{1}{\tau_\mathrm{e-ph}} + \frac{1}{\tau_\mathrm{e-d}} \approx \frac{1}{\tau_\mathrm{e-ph}} + \frac{1}{\tau_\mathrm{e-d}} \tag{5.54}$$

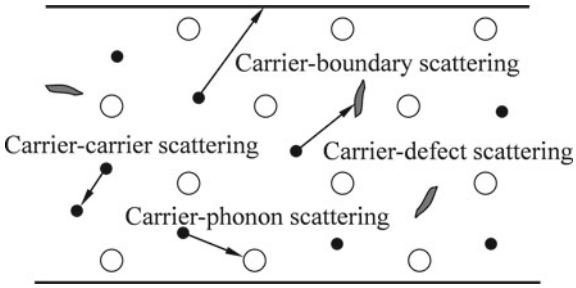

Fig. 5.10 Schematic of various carrier scattering mechanisms

where the subscripts e–e, e–ph, and e–d are for electron–electron, electron–phonon, and electron–defect scattering. It should be noted that the free-electron description is often applied to model the electrical conductivity of (doped) semiconductors, in which both electrons and holes (positive charges) can carry currents. For some metals, as to be explained in Chap. 6, the charge carriers are actually holes rather than electrons. Using Eq. (5.53), we can write Eq. (5.54) in terms of the mean free path as follows:

$$\frac{1}{\Lambda_{\mathrm{e}}} = \frac{1}{\Lambda_{\mathrm{e-ph}}} + \frac{1}{\Lambda_{\mathrm{e-d}}} \tag{5.55}$$

Different scattering mechanisms can be considered separately. Boundary scattering becomes important when the characteristic dimension L_{c} is comparable to the mean free path of the bulk material Λ_{e}. Here, L_{c} can be the thickness of a thin film or the diameter of a thin wire. An effective mean free path can be defined for the evaluation of the scattering rate and the conductivity:

$$\frac{1}{\Lambda_{\mathrm{e,eff}}} = \frac{1}{\Lambda_{\mathrm{e}}} + \frac{1}{\Lambda_{\mathrm{e-b}}} \tag{5.56}$$

where the subscript e–b is for electron–boundary scattering. It can be seen that when boundary scattering is important, the effective mean free path will be suppressed, or the scattering rate will increase. The electrical conductivity will be reduced, and the reduction is size dependent. This is similar to the molecular heat transfer discussed in Chap. 4 when the *Kn* number, i.e., the ratio of the mean free path to the characteristic length (Λ/L_{c}), is comparable or greater than 1. Further discussion of the size effect on the conductivities of solids will be given in Sect. 5.5.

The Bloch formula for electrical resistivity due to electron–phonon scattering gives

$$r_{\mathrm{e-ph}} = 4r_0\left(\frac{T}{\Theta}\right)^5 \int_0^{\Theta/T} \frac{x^5 \mathrm{e}^x}{(\mathrm{e}^x - 1)^2}\mathrm{d}x \tag{5.57}$$

where r_0 is a constant, and Θ is a characteristic temperature that is very close to the Debye temperature [29]. The derivation of the above equation requires a careful treatment of the electron–phonon interaction within the framework of the electron band theory considering both the *N* process and the *U* process, which will be discussed in Chap. 6. The Bloch formula predicts that the electrical resistivity approaches zero as the temperature approaches absolute zero for a pure metal. When $T \ll \Theta$, the low-temperature approximation of the lattice resistivity can be written as

$$r_{\mathrm{e-ph}} \approx 498 r_0 T^5/\Theta^5 \tag{5.58}$$

Because of impurities, electron–defect scattering gives a residual resistivity r_{e-d} that is important at low temperatures, and its value is independent of temperature. Adding the scattering rates using Matthiessen's rule, the electrical resistivity is obtained as [29]

$$r_e = r_{e-ph} + r_{e-d} \tag{5.59}$$

Figure 5.11 compares the model with the electrical resistivity data recommended for high-purity bulk metals after annealing [30]. Taking the electrical resistivity of gold as an example, it can be seen that phonon scattering dominates the electrical resistivity at high temperatures and results in $r_{e-ph} \approx r_0 T/\Theta$, which is proportional to T. It should be noted that Θ_D listed in Table 5.1 can be used to approximate Θ in most cases. The constant r_0 can be determined using the resistivity values at 22 °C, or 295 K, given in Table 5.2. At very low temperatures, $r_e \approx r_{e-d}$, which is independent of temperature but depends strongly on the impurity concentration.

Example 5.5 Consider a large copper specimen of high purity with a very small defect scattering rate of $\tau_{e-d}^{-1} = 5 \times 10^8$ rad/s at the liquid helium temperature of 4.2 K. Find the electrical resistivity, the electron relaxation time,, and the mean free path of this specimen at 1, 295, and 590 K.

Solution We first use Eq. (5.52) to evaluate the residual resistivity at 1 K by assuming that the scattering rate is the same at 4.2 and 1 K. This yields an electrical resistivity $r_e \approx r_{e-d} = \frac{m_e}{n_e e^2}\frac{1}{\tau_{e-d}} = 2.1 \times 10^{-5}\,\mu\Omega\,\text{cm}$ or conductivity $\sigma = 4.76 \times 10^{12}\,(\Omega\,\text{m})^{-1}$. The electrical resistivity at 295 K is given in Table 5.2 to be $r_{e-ph} \approx r_e = 1.7\,\mu\Omega\,\text{cm}$. Because the Debye temperature for Cu is 340 K, we can approximate the resistivity

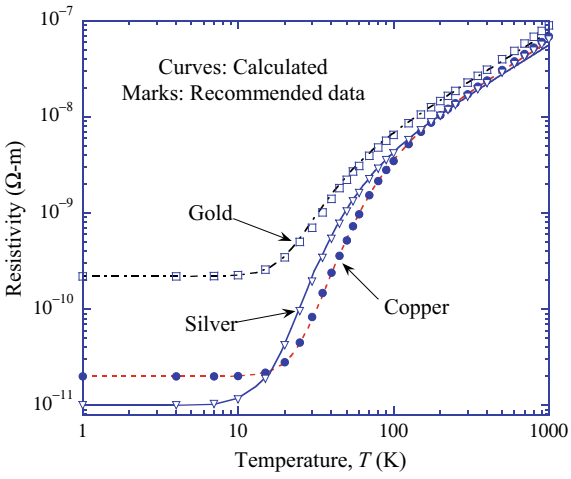

Fig. 5.11 Comparison of the measured electrical resistivity data [30] of 99.999% pure copper, gold, and silver with the model considering electron–phonon scattering and electron–defect scattering using Eq. (5.59)

at 590 K to be twice that of the resistivity at 295 K, or 3.4 μΩ cm. The relaxation time is approximately 2×10^{-9} s at 1 K, 2.47×10^{-14} s at 295 K, and 1.24×10^{-14} s at 590 K since the number density is assumed to be temperature independent. Using Eq. (5.53) and the Fermi velocity of $v_F = 1.57 \times 10^6$ m/s from Example 5.2, we have the mean free path $\Lambda_e = 3.14$, 38.8, and 19.4 nm at 1, 295, and 590 K, respectively. The conductivity of a copper film with a thickness of less than 100 nm may be affected by boundary scattering. At low temperatures, however, boundary scattering may be dominant for low-dimensional structures even at the micrometer length scale.

For metals, electrons are also responsible for thermal transport. Knowledge of the electrical transport is critical to the understanding of thermal properties. The effect of boundary scattering on transport properties is called the classical size effect [1, 2]. Quantum size effect can modify the DOS of electrons and hence the electrical and thermal properties, as will be discussed in Sect. 5.6.

5.3.2 *Thermal Conductivity of Metals*

In metals, free electrons are the main thermal energy carriers. As discussed in Chap. 4, kinetic theory predicts that the thermal conductivity is

$$\kappa = \frac{1}{3}\rho c_{v,e} v_F \Lambda_e \tag{5.60}$$

where $\rho = n_e m_e$ is the mass of electrons per unit volume and $c_{v,e}$ is the mass specific heat of the electrons. Note that $\rho c_{v,e}$ is the volumetric specific heat of electrons and can be expressed as $\rho c_{v,e} = \frac{n_e \pi^2 k_B^2 T}{2\mu_F}$ using the electron specific heat formula given in Eq. (5.24). Substituting the expression for $\rho c_{v,e}$ and $v_F \Lambda_e = v_F^2 \tau \approx 2\mu_F \tau / m_e$ into Eq. (5.60), we obtain the thermal conductivity of a given metal as follows:

$$\kappa = \frac{n_e \pi^2 k_B^2 T}{3 m_e} \tau \tag{5.61}$$

which is proportional to τT. The Wiedemann–Franz law can be obtained by comparing this equation with the expression for the electrical conductivity given in Eq. (5.52), viz.,

$$Lz \equiv \frac{\kappa}{\sigma T} = \frac{1}{3}\left(\frac{\pi k_B}{e}\right)^2 = 2.44 \times 10^{-8}\,\mathrm{W\,\Omega/K^2} \tag{5.62}$$

where Lz is called *the Lorentz number*. The measured Lz value for most conductors is between 2.2 and $2.7 \times 10^{-8}\,\mathrm{W\,\Omega/K^2}$ at room temperature. The derivations given above were based on the simple kinetic theory, which is consistent with the solution of the BTE under the assumptions of local equilibrium and the relaxation

time approximation. The actual scattering process may result in some differences in the effectiveness of transferring momentum and energy during electron–phonon scattering. More detailed theories and experiments have shown that the thermal conductivity of metals is independent of temperature at moderate and high temperatures [29]. The Wiedemann–Franz law is therefore valid near and above room temperature for most metals. As the temperature is lowered, electron–phonon scattering yields a thermal resistance (or $1/\kappa$) that is proportional to T^2, not T^4 as one would obtain by combining Eqs. (5.57) and (5.62). Recall that in the intermediate region, approximately between 10 and 100 K, the Wiedemann–Franz law is not valid. At very low temperatures, defect scattering dominates and, because defect scattering is elastic, the Wiedemann–Franz law is valid again so that $\kappa \propto T$. Therefore, the thermal conductivity at cryogenic temperatures can be expressed as

$$\frac{1}{\kappa(T)} = \frac{A}{T} + BT^2 \tag{5.63}$$

where A and B are positive constants. The first term on the right-hand side dominates at very low temperatures, when the thermal conductivity is proportional to T. As the temperature increases, the thermal conductivity reaches a peak and then falls down proportional to T^{-2}. As the temperature approaches the room temperature, the thermal conductivity changes little with temperature until the melting point is reached. Figure 5.12 plots the measured thermal conductivity of copper with different impurity concentrations [31]. The highest purity annealed copper has a residual resistivity of $5.79 \times 10^{-12}\ \Omega$ m. Oxygen-free high conductivity (OFHC) copper is commonly used in absolute cryogenic radiometers to build the cavity receiver. Even 0.5% impurity concentration will make the conductivity to dramatically decrease at lower temperatures. On the other hand, the thermal conductivity is less sensitive to impurity at temperatures above 100 K and changes little until the melting temperature

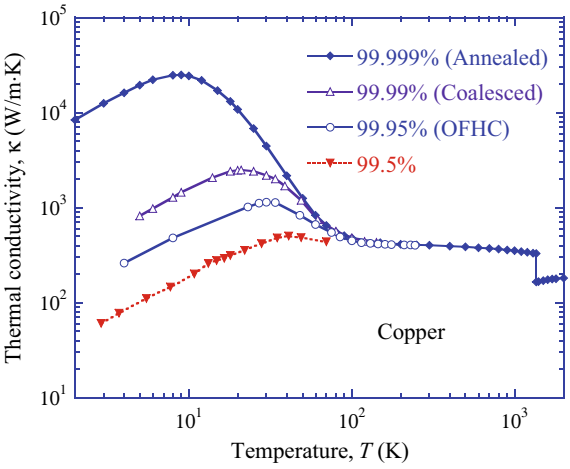

Fig. 5.12 Thermal conductivity of copper with different purity levels [31]

of 1358 K. Beyond the melting temperature, the thermal conductivity values are for liquid copper.

5.3.3 *Derivation of Conductivities from the BTE*

So far, we have used simple kinetic theory to discuss the electrical and thermal conductivities of metals. It is hoped that these discussions have provided some insights into basic phenomena. To understand the detailed mechanisms, we now present the approaches based on the BTE under two assumptions: local equilibrium and relaxation time approximation. Recall from Chap. 4 that the distribution function can be expressed in terms of $f(\mathbf{r}, \mathbf{v}, t)$ or $f(\mathbf{r}, \mathbf{p}, t)$, where $\mathbf{p} = m_e\mathbf{v}$ for electrons. In describing the phonon specific heat, we have extensively used the phonon wavevector $\mathbf{k}$ as well as the k-space. The advanced theory based on the electronic band structure, to be discussed in Chap. 6, is also based on the k-space. Using the magnitude relations, $p = h/\lambda$ and $k = 2\pi/\lambda$, we have $\mathbf{k} = \mathbf{p}/\hbar$. Therefore, the distribution function can be written in terms of $\mathbf{k}$ or $f(\mathbf{r}, \mathbf{k}, t)$. The energy of an electron is related to its wavevector by $\varepsilon = \frac{\hbar\mathbf{k}\cdot\hbar\mathbf{k}}{2m_e} = \frac{\hbar^2k^2}{2m_e}$. Under the local-equilibrium condition, the distribution function can be written in terms of temperature $T(\mathbf{r}, t)$ and energy ε such that

$$f(\mathbf{r}, \mathbf{k}, t)\mathrm{d}\mathbf{k} = f_1(\varepsilon, T)\frac{\mathrm{d}\mathbf{k}}{\mathrm{d}\varepsilon}\mathrm{d}\varepsilon = f_1(\varepsilon, T)D(\varepsilon)\mathrm{d}\varepsilon \tag{5.64}$$

where $D(\varepsilon) = \mathrm{d}\mathbf{k}\big/\mathrm{d}\varepsilon$ is the DOS, and $f_1(\varepsilon, T)$ is such that $n(\mathbf{r}, t) = \int_0^\infty f_1(\varepsilon, T)D(\varepsilon)\mathrm{d}\varepsilon$ and $\bar{\varepsilon}(\mathbf{r}, t) = \int_0^\infty \varepsilon f_1(\varepsilon, T)D(\varepsilon)\mathrm{d}\varepsilon$. For the equilibrium distribution of free electrons, $f_1(\varepsilon, T)$ is nothing but the Fermi–Dirac function given in Eq. (5.15). When the distribution function is isotropic in the k-space, the DOS is given in Eq. (5.18) since $\mathrm{d}\mathbf{k} = \mathrm{d}k_x\mathrm{d}k_y\mathrm{d}k_z = 4\pi k^2\mathrm{d}k$ and $\mathrm{d}\varepsilon = \hbar^2k\mathrm{d}k/m_e$. As discussed earlier, free electrons will occupy all the quantum states below the Fermi level. The Fermi level corresponds to a maximum k in all directions in the k-space, which is a spherical surface. All the electron quantum states are included in this *Fermi sphere*. The argument is similar to the Debye model of phonons, where there is an upper bound of the wavevector and the distribution is assumed to be isotropic. We will see in Chap. 6 that the Fermi surface even for monatomic solids with the simplest crystalline structures is not exactly spherical. This is because the electrons in solids are not really independent particles. For simplicity, a spherical Fermi surface is assumed in this section.

Suppose there is a constant electric field E along with a temperature gradient in the z-direction. The function $f_1(\varepsilon, T)$ is a nonequilibrium distribution that depends on z. At steady state under the relaxation time approximation, we can rewrite Eq. (4.54) as follows:

$$f_1(\varepsilon, T) = f_0(\varepsilon, T) + \tau(\varepsilon)\left(\frac{eE}{m_e}\frac{\partial f_1}{\partial \varepsilon}\frac{\partial \varepsilon}{\partial v_z} - v_z\frac{\partial f_1}{\partial T}\frac{\mathrm{d}T}{\mathrm{d}z}\right) \tag{5.65}$$

where $f_0(\varepsilon, T)$ corresponds to the equilibrium distribution, which for electrons is the Fermi–Dirac function f_{FD}. The relaxation time is not taken as a constant; rather, it is assumed to be dependent on the wavevector or the energy. Note that $\frac{\partial \varepsilon}{\partial v_z} = \frac{\partial \varepsilon}{\partial v}\frac{\partial v}{\partial v_z} = m_e v\frac{v_z}{v} = m_e v_z$. As discussed in Chap. 4, under local equilibrium, we also assume that

$$\frac{\partial f_1}{\partial \varepsilon} \approx \frac{\partial f_0}{\partial \varepsilon} \quad \text{and} \quad \frac{\partial f_1}{\partial T} \approx \frac{\partial f_0}{\partial T} \tag{5.66}$$

Note that this should be viewed as a simplified notation that is valid only when the partial derivatives are substituted into the integration over the k-space. We will consider the effect of applied field and temperature gradient separately. When there is no temperature gradient, the current density can be written as

$$J_e = -eJ_N = -e\int_0^\infty v_z\left(f_{\mathrm{FD}} + \tau v_z eE\frac{\partial f_{\mathrm{FD}}}{\partial \varepsilon}\right)D(\varepsilon)\mathrm{d}\varepsilon \tag{5.67a}$$

The first term $-\int_0^\infty ev_z f_{\mathrm{FD}}(\varepsilon, T)D(\varepsilon)\mathrm{d}\varepsilon$ is zero; and therefore,

$$J_e = -e^2E\int_0^\infty \tau(\varepsilon)v_z^2\frac{\partial f_{\mathrm{FD}}}{\partial \varepsilon}D(\varepsilon)\mathrm{d}\varepsilon \tag{5.67b}$$

Because the integration is over the equilibrium distribution, it is one-third of the integration if v_z^2 is replaced by $v^2 = 2\varepsilon/m_e$. The electrical conductivity can be expressed as

$$\sigma = -\frac{2e^2}{3m_e}\int_0^\infty \frac{\partial f_{\mathrm{FD}}}{\partial \varepsilon}\tau(\varepsilon)\varepsilon D(\varepsilon)\mathrm{d}\varepsilon \tag{5.68}$$

Note that $\partial f_{\mathrm{FD}}/\partial\varepsilon \approx -\delta(\varepsilon - \mu)$, where $\delta(\varepsilon - \mu)$ is the Dirac delta function with a sharp peak at $\varepsilon = \mu$ and essentially zero when $\varepsilon \neq \mu$. Furthermore, $\int_\infty^\infty f(x)\delta(x-a)\mathrm{d}x = f(a)$. Consequently, the only active electrons are those around the Fermi level. This small fraction of electrons, however, is responsible for the conduction of electricity and heat in metals. We have by assuming $\mu(T) \approx \mu_F$ that

$$\sigma = \frac{2e^2}{3m_e}\tau_F\mu_F D(\mu_F) \tag{5.69}$$

which is the same as Eq. (5.52) since $D(\mu_F) = 3n_e/(2\mu_F)$ according to Eqs. (5.18) and (5.20). The relaxation time is not the average of all electrons but the average of only those electrons near the Fermi surface.

To evaluate the thermal conductivity, we set the applied field to be zero. Note that for an open system of fixed volume, $dU = \delta Q - \mu dN$, i.e., the heat flux is equal to the energy flux *minus* the product of the chemical potential and the particle flux. Hence,

$$q_z'' = J_E - \mu J_N = \int_0^\infty v_z(\varepsilon - \mu)\left(f_{FD}(\varepsilon, T) - \tau(\varepsilon)v_z\frac{\partial f_{FD}}{\partial T}\frac{dT}{dz}\right)D(\varepsilon)d\varepsilon \quad (5.70)$$

Note again that the integration of the equilibrium distribution function in Eq. (5.70) is zero. Furthermore, the integration for v_z^2 can be converted into the integration for $v^2 = 2\varepsilon/(3m_e)$. After some manipulations, it can be shown that the thermal conductivity is

$$\kappa = \frac{2}{3m_e}\int_0^\infty \tau(\varepsilon)(\varepsilon - \mu)\varepsilon\frac{\partial f_{FD}}{\partial T}D(\varepsilon)d\varepsilon \quad (5.71a)$$

Using Eq. (B.82) from Appendix B.8, i.e., $\frac{\partial f_{FD}}{\partial T} = -\frac{\partial f_{FD}}{\partial \varepsilon}\left(\frac{\varepsilon-\mu}{T}\right)$, we obtain after applying Eq. (B.80) that

$$\begin{aligned}\kappa &= -\frac{2}{3m_eT}\int_0^\infty \tau(\varepsilon)(\varepsilon - \mu)^2\varepsilon\frac{\partial f_{FD}}{\partial \varepsilon}D(\varepsilon)d\varepsilon \\ &= \frac{2}{3m_eT}\tau(\mu_F)\mu_F D(\mu_F)\frac{\pi^2(k_BT)^2}{3}\end{aligned} \quad (5.71b)$$

This is essentially the same expression as in Eq. (5.61) for the electron thermal conductivity obtained from simple kinetic theory. The discussion above based on the Fermi–Dirac distribution not only confirms the simple kinetic theory but also explains why v_F should be used in Eqs. (5.53) and (5.60) rather than the rms velocity of electrons. A familiarity with the BTE will help the study of the classical size effect due to boundary scattering and thermoelectricity phenomena to be discussed in subsequent sections.

The derivation above has confirmed the electrical conductivity and thermal conductivity expressions. This also explains that the scattering rate corresponds to electrons with energy equal to the Fermi energy. Therefore, the Wiedemann–Franz law is also confirmed since the scattering rates for the electron (momentum) transport and that for energy transport cancel each other. Electron–phonon scattering must satisfy the energy and momentum conservations. When the amount of energy change of

electrons before and after collision is comparable with $k_B T$, the scattering is inelastic, and thus the two scattering processes can differ significantly. This happens at intermediately lower temperatures since $k_B T$ is small. At very low temperatures, since electron–defect scattering is elastic, the transport of electron momentum is as effective as the transport of energy. As discussed earlier, the result in the intermediate low-temperature region for electron–phonon scattering is such that the electrical resistivity follows T^5, while $1/\kappa$ follows T^2. In order for Eqs. (5.60) and (5.61) to be valid, it is often thought as if the relaxation time for thermal conductivity is somewhat different from that for electrical conductivity. Actually, it is not because the relaxation times are different; it is because the relaxation time approximation is not valid. By using two relaxation times, one can simplify the scattering process. The relaxation time for momentum transfer retains its meaning of the relaxation time, as in Eq. (5.52) for the electrical conductivity. On the other hand, the relaxation time for thermal transport given in Eq. (5.61) is sometimes called the *energy relaxation time*, which is taken as a weighted average to approximate the difference in the scattering effectiveness for energy exchange [6, 29].

5.3.4 Thermal Conductivity of Insulators

Heat conduction in electrical insulators is dominated by lattice waves or phonons. This class of materials includes diamond, quartz, sapphire, and silicon carbide, as well as semiconductor materials like silicon, germanium, and gallium arsenide. Kinetic theory predicts the thermal conductivity of dielectric materials or electrical insulators as follows:

$$\kappa = \frac{1}{3} \rho c_v v_a \Lambda_{ph} \tag{5.72}$$

where ρc_v is the lattice volumetric specific heat, v_a is the average speed of corresponding acoustic waves or phonons, and Λ_{ph} is the phonon mean free path and is related to the scattering rate by $\Lambda_{ph} = v_a \tau$. When v_a is used, it is often assumed that the dispersion relation is linear, i.e., $v_g = v_p$. For crystalline solids, the acoustic speed is on the order of 5000 m/s and depends little on temperature; however, it may depend on the polarization. The density decreases slightly as temperature increases due to thermal expansion, but the change is negligibly small. The specific heat cv is a function of temperature as predicted by the Debye theory, and it is nearly constant at temperatures close to or higher than the Debye temperature. The mean free path can be evaluated based on phonon–phonon scattering and phonon–defect scattering.

The BTE for phonons was first derived by Rudolf E. Peierls in 1929. In some publications, it is referred to as the Boltzmann–Peierls or Peierls–Boltzmann equation. Here, we use a simplified model to derive Eq. (5.72) from the relaxation time approximation of the BTE, based on the Debye theory. The assumption is that the phonon velocity can be taken as a constant that is averaged over all three modes

according to Eq. (5.7), as described by the DOS. For phonons, the distribution function can be conveniently converted into the frequency ν domain. Suppose there is a temperature gradient in the z-direction; using the similar procedure as done in the previous section, the thermal conductivity can be expressed as

$$\kappa = \iiint\limits_{\nu,\phi,\theta} v_z h\nu\tau v_z \frac{\partial f_{\mathrm{BE}}}{\partial T} \frac{D(\nu)}{4\pi} \sin\theta \mathrm{d}\theta \mathrm{d}\phi \mathrm{d}\nu \tag{5.73}$$

where $D(\nu)/4\pi$ can be viewed as the density of states per unit solid angle. Noting that $v_z = v_\mathrm{a}\cos\theta$ and the distribution function is independent of the direction, we can integrate Eq. (5.73) over all angles first to get $\int_0^{2\pi}\int_0^{\pi}\cos^2\theta\sin\theta\mathrm{d}\theta\mathrm{d}\phi = 4\pi/3$. With the upper limit of frequency ν_m determined by Eq. (5.9), we can rewrite Eq. (5.73) in the following:

$$\kappa = \frac{1}{3}\int_0^{\nu_\mathrm{m}} \tau v_\mathrm{a}^2 h\nu \frac{\partial f_{\mathrm{BE}}}{\partial T} D(\nu)\mathrm{d}\nu \tag{5.74}$$

The integration over the spherical coordinates offers a different way for deriving the 1/3 term in the kinetic expression of thermal conductivity obtained earlier for a molecular gas and an electron gas. In addition to the assumption that the acoustic velocity is independent of the frequency, we further assume that the scattering rate is independent of the frequency. Hence, both τ and v_a can be taken out of the integrand. The remaining part is the specific heat per unit volume, defined in Eq. (5.31). It is clear that Eq. (5.72) can be obtained based on the assumption that phonon speed, relaxation time, and mean free path are independent of frequency.

Using Matthiessen's rule, the phonon mean free path can be expressed as

$$\frac{1}{\Lambda_{\mathrm{ph}}} = \frac{1}{\Lambda_{\mathrm{ph-ph}}} + \frac{1}{\Lambda_{\mathrm{ph-d}}} \tag{5.75}$$

where ph–ph and ph–d stand for phonon–phonon scattering and phonon–defect scattering, respectively. The inverse of the mean free path can be added because they are proportional to the number of collisions per unit time (or scattering rate). The scattering rate due to phonon–phonon scattering is inversely proportional to temperature at relatively high temperatures, i.e., $\Lambda_{\mathrm{ph-ph}}$ decreases as temperature increases. This causes a reduction in thermal conductivity as temperature goes up. Thus, in the high-temperature limit, the thermal conductivity can be modeled as inversely proportional to temperature in a first-order approximation.

At low temperatures, defect scattering dominates and the scattering rate is more or less constant. The thermal conductivity depends on the specific heat and should also vary with T^3. The size of the sample affects the mean free path and hence the thermal conductivity. Also, as the temperature is reduced, phonons with lower frequencies play an important role in the thermal transport and storage. Thus, boundary scattering

is expected to be more important at low temperatures. Similar to that for electron scattering, the effective mean free path including boundary scattering can be defined as

$$\frac{1}{\Lambda_{\mathrm{ph,eff}}} = \frac{1}{\Lambda_{\mathrm{ph}}} + \frac{1}{\Lambda_{\mathrm{ph-b}}} \tag{5.76}$$

Figure 5.13 shows the thermal conductivity of silicon with different impurity concentrations. For highly pure single-crystal silicon, the thermal conductivity is comparable with a good electrical conductor such as aluminum. As the impurity concentration increases, the scattering rate increases and the mean free path decreases, resulting in a reduction in the thermal conductivity. The contribution of free electrons or holes to the thermal conductivity of semiconductors is insignificant as compared to that of lattice vibration. Therefore, the temperature dependence of thermal conductivity for other crystalline insulators is similar to that of Si. At very low temperatures, $\kappa \propto T^3$ due to the temperature dependence of the specific heat; at high temperatures, $\kappa \propto T^{-1}$ due to the increased phonon–phonon scattering rate. Diamond has the highest thermal conductivity (as high as 2200 W/m K at room temperature) among all bulk materials, due to its large sound velocity and mean free path.

Example 5.6 Estimate the mean free path and the phonon scattering rate of pure silicon at 5, 10, 20, 100, 300, and 1000 K. Also, calculate the corresponding thermal diffusivity $\alpha = \kappa/\rho c_p$.

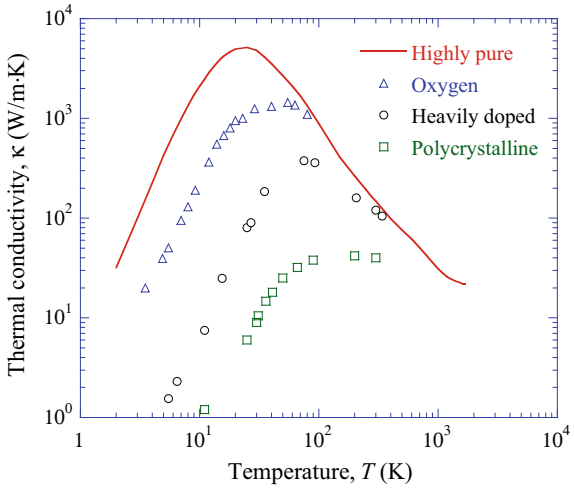

Fig. 5.13 Data of thermal conductivity of silicon taken from Touloukian et al. [31]. The fitted curve is for a highly pure silicon with a dopant concentration less than 10^{16} cm^{-3}; triangles are for a p-type single-crystal silicon with an oxygen concentration of 2×10^{17} cm^{-3}; circles are for a heavily doped n-type silicon with a phosphorus concentration of 2×10^{19} cm^{-3}; and squares are for a p-type polycrystalline silicon with a boron concentration of 3×10^{20} cm^{-3}

Solution The purpose of this example is to give some quantitative information about the mean free path and its temperature dependence. The calculation is straightforward using Eq. (5.74) by assuming that the density and the phonon velocity are independent of temperature. From Example 5.1, we have $v_a \approx 6000$ m/s, and the density is 2330 kg/m^3 (from Table 5.1). The specific heat can be calculated from the Debye model, and the thermal conductivity of intrinsic Si can be found from Fig. 5.13. The computed results are tabulated in the following table.

Temperature (K)	5	10	20	100	300	1000
Thermal conductivity κ (W/m K)	424	2110	4940	884	148	31.2
Specific heat c_p (J/kg K)	0.034	0.28	3.43	260	712	921
Mean free path Λ(m)	2.7×10^{-3}	1.6×10^{-3}	3.1×10^{-4}	7.3×10^{-7}	4.5×10^{-8}	7.3×10^{-9}
Scattering rate $1/\tau$ (rad/s)	2.2×10^{6}	3.7×10^{6}	1.9×10^{7}	8.2×10^{9}	1.3×10^{11}	8.3×10^{11}
Thermal diffusivity α(m^2/s)	5.4	3.3	0.62	1.5×10^{-3}	8.9×10^{-5}	1.5×10^{-6}

The mean free path and thermal diffusivity increase dramatically as the temperature is lowered. Because the crystal is highly pure, there is very little scattering at low temperatures. The decrease in conductivity is caused by the reduction in the specific heat. At high temperatures, the specific heat of Si does not change significantly. Hence, the decrease in thermal conductivity is due to the increase of the phonon–phonon scattering rate. It should be mentioned that at very high temperatures, thermally activated free electrons and holes will also increase the impurity scattering.

When the phonon mean free path is comparable with the smallest dimension so that $Kn \equiv \Lambda/L_c > 1$, boundary scattering or the classical size effect should be considered, as will be discussed in Sect. 5.5. When $Kn \gg 1$, ballistic or phonon–boundary scattering becomes dominant compared with phonon–phonon and phonon–defect scattering. As in the case of free molecule flow, Fourier's law is applicable only in the diffusion limit. When ballistic scattering is significant, the temperature at the boundary is discontinuous. The heat transfer process by phonons is more radiative than conductive, as in the case of thermal radiation through a transparent medium. Even at steady state, the 1D temperature distribution without heat generation is nonlinear. We will study the equation of phonon radiative transfer (EPRT) in Chap. 7 along with other equations that should be used for small timescales or length scales, where Fourier's law of heat conduction breaks down. This is especially important

at low temperatures, for small structures, and/or in rapid processes such as during a short laser pulse.

So far, we have studied the basics of phonon contributions to the thermal conductivity under the relaxation time approximation for a gray medium, i.e., by assuming that τ is independent of the vibration frequency. Furthermore, we have taken the average acoustic velocity and assumed that it is also independent of the vibration frequency. A further assumption is that the phonon dispersion relations are isotropic and linear up to a maximum frequency. Real crystals behave very differently from the simple pictures just presented. To understand this, we must study the phonon dispersion relations for all phonon branches, with different polarizations and along different crystal directions. While the study of crystalline structures and phonon dispersion relations will be deferred to Chap. 6, we can write the general expression for thermal conductivity under the local-equilibrium condition in two forms. The summation form reads as

$$\kappa(\hat{\mathbf{n}}) = \sum_P \sum_K \hbar\omega(\mathbf{k}) \frac{\partial f_{\mathrm{BE}}}{\partial T} \tau(\mathbf{k}) v_{\mathrm{g,n}}^2(\mathbf{k}) \tag{5.77}$$

where the summation is over the wavevector index K and the polarization index P. Note that $v_{\mathrm{g,n}}(\mathbf{k})$ is the phonon group velocity for the given polarization in the direction $\hat{\mathbf{n}}$ along which the thermal conductivity is to be evaluated. The integration form reads

$$\kappa(\hat{\mathbf{n}}) = k_{\mathrm{B}} \sum_P \int_0^\infty \tau(\omega) v_{\mathrm{g,n}}^2(\omega) \left(\frac{\hbar\omega}{k_{\mathrm{B}}T}\right)^2 \frac{\mathrm{e}^{\hbar\omega/k_{\mathrm{B}}T}}{(\mathrm{e}^{\hbar\omega/k_{\mathrm{B}}T} - 1)^2} D(\omega)\mathrm{d}\omega \tag{5.78}$$

where $D(\omega)$ is the DOS for an individual polarization. If the DOS is properly handled so that it contains information about a particular microstructure, Eq. (5.78) would be identical to Eq. (5.77). Otherwise, Eq. (5.78) is the approximation of Eq. (5.77) for large systems. For a large system with isotropic dispersion in the k-space, we have

$$D(\omega) = \frac{1}{(2\pi)^3} \frac{\mathrm{d}\mathbf{k}}{\mathrm{d}\omega} = \frac{1}{2\pi^2} \frac{k^2}{\mathrm{d}\omega/\mathrm{d}k} = \frac{\omega^2}{2\pi^2 v_{\mathrm{p}}^2 v_{\mathrm{g}}} \tag{5.79}$$

where $v_{\mathrm{p}} = \omega/k$ and $v_{\mathrm{g}} = \mathrm{d}\omega/\mathrm{d}k$ are the phase and group speeds for the corresponding polarization and can be calculated if the dispersion relation $\omega = \omega(\mathbf{k})$ is known.

Therefore,

$$\kappa = \frac{k_{\mathrm{B}}}{6\pi^2} \left(\frac{k_{\mathrm{B}}T}{\hbar}\right)^3 \sum_P \int_0^{x_{\mathrm{m}}} \tau(x) \frac{v_{\mathrm{g}}(x)}{v_{\mathrm{p}}^2(x)} \frac{x^4 \mathrm{e}^x}{(\mathrm{e}^x - 1)^2} \mathrm{d}x \tag{5.80}$$

where the upper limit corresponds to the maximum frequency of each phonon polarization or branch. Equation (5.79) helps us understand low-temperature behavior of thermal conductivity of insulators.

For the same frequency, while the energy of a phonon is the same as that of a photon $h\nu$, the acoustic wave has a much shorter wavelength than the electromagnetic wave because of the small propagation speed v_a compared to the speed of light. Thus, the momentum of a phonon is much greater than that of a photon of the same frequency. As an example, our ears sense sound waves in the frequency range from 20 to 20,000 Hz. Assume $v_a = 1000$ m/s; then, the wavelength range is 50 m to 5 cm. In solids, however, the most important frequencies for thermal energy transfer are much higher and temperature dependent. The smallest vibration wavelength is roughly $\lambda_{min} = 2L_0 \approx 0.5$ nm. With a typical velocity of $v_a = 5000$ m/s in crystalline solids, the highest frequency ν_m is on the order of 10 THz or 10^{13} Hz. Compared with the electromagnetic wave spectrum, this frequency falls in the mid-infrared spectral region. Therefore, electromagnetic radiation can interact with such phonons, and the resulted absorption is called lattice absorption or phonon absorption. High-frequency phonons are called *optical phonons*. On the other hand, the frequency of acoustic phonons ranges from 0 to 10 THz. By setting $k_B T = h\nu$, we find that the frequency corresponding to the thermal energy of translational motion of a particle is on the order of $\nu = k_B T/h = 6$ THz at 300 K (where $k_B T = 26$ meV). The thermal phonon wavelength λ_{th} is therefore on the order of 1 nm with $v_a \approx 5000$ m/s. On the other hand, low-frequency phonons are responsible for energy storage and transfer in crystalline solids at cryogenic temperatures. The shift in the dominant frequency for phonon transport resembles Wien's displacement law for blackbody radiation because phonons and photons are governed by the same statistics. The phonon wave effect and quantum size effect are expected to become important when the characteristic dimension is on the order of the thermal wavelength, as illustrated earlier in the study of specific heat of solids.

For amorphous and disordered solids that are poor electric conductors, periodic lattice structure does not exist and phonons if they exist cannot propagate very far. Cahill et al. [32] extended the work of Albert Einstein in 1911 by assuming that the mean free path for the ith phonon mode $\Lambda_i = \tau_i v_i$ is limited to half of the phonon wavelength. That is to say that the relaxation time is half of the period, $\tau_i = \pi/\omega$. Some earlier works used the lattice constant or the phonon wavelength as the minimum mean free path [32–34]. By substituting $\tau = \pi/\omega$ and $v_p = v_g = v_i$ into Eq. (5.80), the minimum thermal conductivity can be expressed as

$$\kappa_{min} = \frac{k_B}{6\pi}\left(\frac{k_B T}{\hbar}\right)^2 \sum_i \int_0^{x_i} \frac{1}{v_i} \frac{x^3 e^x}{(e^x - 1)^2} dx \tag{5.81a}$$

where $x_i = \Theta_i/T$ and Θ_i can be calculated from (5.10) by substituting v_i for v_a. Using Eq. (5.10), Eq. (5.81) may be expressed as follows according to Ref. [32]:

$$\kappa_{\min} = k_B \left(\frac{\pi}{6} n_a^2\right)^{1/3} \sum_i v_i \left(\frac{T}{\Theta_i}\right)^2 \int_0^{x_i} \frac{x^3 e^x}{(e^x - 1)^2} dx \tag{5.81b}$$

At room temperature, the thermal conductivity of most amorphous solids falls in the range 0.2–5 W/m K [34]. Note that there are no fitting parameters in Eq. (5.81b) as long as the number density of the atoms and the acoustic velocities for the transverse and longitudinal phonons are given. Overall, Eq. (5.81b) agrees well with the measured thermal conductivity for a large number of disordered solids, though some materials exhibit even lower thermal conductivities than predicted $\kappa_{\min}$. While Eq. (5.81a) or (5.81b) removes the relaxation time and mean free path, in disordered materials when some of the vibration eigenstates are localized, definition of phonon velocities and wavevectors is questionable.

Another approach was developed by Allen and Feldman [35] by extending the Kubo–Greenwood formulation, which is a quantum mechanical theory for electron transport based on the linear response theory, to the thermal conductivity of disordered solids. The key is to relate the conductivity to the heat current operator matrix, which under the harmonic assumption can be related to the mode diffusivity without defining the group velocity or scattering rate. The obtained conductivity formula is expected to be applicable to disordered media where the wavevectors of the carriers can hardly be defined [35–38]. The temperature-dependent thermal conductivity is thus expressed in terms of a summation [35]:

$$\kappa = \frac{1}{V} \sum_i C(\omega_i) D_{\text{dif}}(\omega_i) \tag{5.82a}$$

where $C(\omega)$ is the specific heat of the harmonic oscillator,

$$C(\omega) = \hbar\omega \frac{\partial f_{\text{BE}}}{\partial T} = \frac{k_B x^2 e^x}{(e^x - 1)^2}, \text{ with } x = \frac{\hbar\omega}{k_B T} \tag{5.82b}$$

and the mode diffusivity is expressed as

$$D_{\text{dif}}(\omega_i) = \frac{\pi V^2}{3\hbar^2 \omega_i^2} \sum_{j(\neq i)} \left|S_{ij}\right|^2 \delta(\omega_i - \omega_j) \tag{5.82c}$$

The heat current operator is a measure of the coupling strength between vibration mode i and j and can be calculated from harmonic lattice dynamic theory [35–37]. Some discussions on how to obtain semi-classical expressions of the diffusivity will be given later.

In a follow-up study of amorphous silicon, Allen et al. [36] divided the heat carriers in crystals (*vibrons*) into *propagons* that have a larger mean free path than the lattice constant and are propagating modes, *diffusons* that are most popular and largely responsible for heat transfer but are not propagating, and *locons* that are

localized modes that do not contribute to heat transport. It should be noted that when anharmonicity is considered, the locon's contribution to heat transfer cannot be neglected [39, 40]. Based on atomistic simulation of amorphous silicon, Allen et al. [36] assigned 4% of the modes to propagons with frequencies less than 3 THz. The region between propagons and diffusons is called the Ioffe–Regel crossover where the mean free path is about the same as the atomic distance. When the frequency is further increased, the mean free path and wavevector cannot be rigorously defined. Locons are at frequencies higher than 17 THz and comprise about 3% of the modes; this was determined by finding the decay lengths, inverse participation ratios, and coordination numbers of the participating atoms [36]. It was shown that propagons dominate the thermal transport at low temperatures, while diffusons contribute to about 2/3 of the thermal conductivity at ambient temperature. A recent theoretical study [41] of amorphous silicon based on lattice and molecular dynamics showed that the propagon–diffuson transition frequencies could be as high as 5–10 THz and propagons might consist of 24% of all modes, suggesting that most heat is carried by elastic waves in amorphous silicon at temperatures from 100 K to 500 K.

We may rewrite Eq. (5.82a) in an integral form using the density of states [38]:

$$\kappa = \int_0^\infty C(\omega) D_{\text{dif}}(\omega) D(\omega) \mathrm{d}\omega \tag{5.83}$$

For propagons, by comparing Eq. (5.74) with (5.83), we see that $D_{\text{dif}} = \tau v_{\text{a}}^2/3 = \Lambda v_{\text{a}}/3$ and the upper limit in Eq. (5.83) can be set as the high-frequency limit of propagons. For diffusion, if the frequency-dependent mode diffusivity is obtained, Eq. (5.83) can be applied to calculate the thermal conductivity. Allen et al. [36] found a temperature independent $D_{\text{dif}}(\omega) \sim \omega^{-2}$ for amorphous silicon in the intermediate temperature range and predicted a low-temperature plateau of thermal conductivity between 10 and 30 K by combining the contributions of propagons and diffusons. Assuming diffusons travel stepwise following a random walk with two steps per period of oscillation, Agne et al. [38] obtained an expression of the mode diffusivity as follows:

$$D_{\text{dif}} = \frac{\omega}{3\pi} n_{\text{a}}^{-2/3} p \tag{5.84}$$

where p is the probability of a successful jump that may be taken as 1 for diffusons. Plugging Eq. (5.84) into Eq. (5.83) and setting the integration maximum ω_{m} according to Eq. (5.9), they obtained a minimum thermal conductivity expression, which may be applicable near room temperatures. At lower temperatures, propagons are responsible for the heat transfer, and the minimum thermal conductivity may be predicted with Eq. (5.81b). It should be noted that the minimum thermal conductivity using the combination of Eqs. (5.83) and (5.84) depends on the upper integration limit that is a function of the sound velocity.

Most polymers are disordered due to their complex morphologies and long chains structures. Typically, they are also electrical insulators and have relatively low thermal conductivities [42]. Due to the advancement of flexible electronics, energy harvesting, and biophysics, thermal transport in polymeric materials has received growing attention lately [43–47]. At room temperature, the thermal conductivity of commonly used amorphous polymers is mostly around 0.1–0.5 W/m K, though it can be as low as 0.06 W/m K or as high as 0.67 W/m K [42–44]. Like inorganic amorphous materials, as the temperature goes down from room temperature, the thermal conductivity of amorphous polymers monotonically decreases with a plateau-like behavior. Choy [42] used the BTE and the Debye DOS, Eq. (5.74), to describe the thermal transport by assuming that the mean free path Λ (or the scattering rate) has an inverse frequency dependence ($\tau \sim \omega^{-1}$) at low frequencies, and $\Lambda = \Lambda_{\min} = L_0$ when the frequency exceeds a certain threshold value to describe the localized modes. Kommandur and Yee [43] used the Allen–Feldman model, given in Eq. (5.83) with the Debye DOS, and considered the mode diffusivity as frequency dependent according to

$$D_{\text{dif}}(\omega) = \frac{1}{3} a v_{\text{a}}^2 \omega^{-n} \tag{5.85}$$

where n is taken as an adjustable parameter approximately between 1 and 2. The parameters a and n for propagons and diffusons, as well as the crossover frequency, were taken as adjustable parameters to fit the thermal conductivity data, since the contribution of locons is negligibly small. Both the BTE approach and the Allen–Feldman model can fit the temperature dependency reasonably well [42, 43]. While the starting points of the BTE and Kubo's linear response theory are conceptually different, it appears that the final model relations are well correlated though with different interpretations of the physical significance of the parameters.

In general, the properties of polymeric materials depend on the morphology, crystallinity, and chain orientation and alignment [45–47]. Polymers can have skeletal structures, planar molecular structures, or 1D linear macromolecules; subsequently, the specific heat may follow the general cubic, quadratic, and linear temperature dependence [48]. Furthermore, there exist glass transitions and other phase transitions that can give spikes in the specific heat of polymeric materials at the transition temperatures [48]. Filling the polymer with highly conductive nanostructured materials can increase the thermal conductivity of the polymer composite significantly (by more than an order or magnitude) to 10–20 W/m K at room temperature [45–47]. Furthermore, aligned polymer chains and nanofibers are expected to have very high thermal conductivities. Molecular dynamics modeling of single polyethylene chains has shown a converging thermal conductivity up to 350 W/m K and a value over 100 W/m K for polyethylene nanofibers [45, 49].

5.4 Thermoelectricity

Solid-state energy conversion devices are very important, and it is hoped that nanotechnology may offer solutions for improving the efficiency of these devices, such as thermoelectric refrigerators and power generators. An understanding of thermoelectricity is useful for further development of these solid-state energy conversion devices. To illustrate the *thermoelectric effect,* assume an electric field $\mathbf{E}$ and a temperature gradient ∇T exist along the z-direction of a conductor. The right-hand side of Eqs. (5.69a) or (5.70) needs to be modified to consider the existence of both an electric field and a temperature gradient. This can be done by applying Eqs. (5.65) and (5.66). By dropping the integration for the equilibrium distribution and using Appendix B.8, we can write the 3D vector forms of the current density and the heat flux as

$$\mathbf{J}_\mathrm{e} = L_{11}\left(\mathbf{E} + \frac{\nabla\mu}{e}\right) - L_{12}\nabla T \tag{5.86}$$

and

$$\mathbf{q}'' = L_{21}\left(\mathbf{E} + \frac{\nabla\mu}{e}\right) - L_{22}\nabla T \tag{5.87}$$

where

$$L_{11} = -e^2\Psi_0 \quad L_{12} = \frac{e}{T}\Psi_1\, L_{21} = T L_{12} = e\Psi_1, \text{ and } L_{22} = -\frac{1}{T}\Psi_2 \tag{5.88}$$

Here, the function Ψ_n is defined as

$$\Psi_n = \frac{1}{3}\int_0^\infty (\varepsilon - \mu)^n \tau v^2 \frac{\partial f_\mathrm{FD}}{\partial \varepsilon} D(\varepsilon)\mathrm{d}\varepsilon \tag{5.89}$$

In writing this equation, we have used Eq. (B.81) and converted $(\mathrm{d}\mu/\mathrm{d}T)\nabla T = \nabla\mu$ in order to consider the spatial dependence of μ. The detailed derivation of the preceding equations is left as an exercise (Problem 5.21). Let

$$\mathbf{E} + \frac{\nabla\mu}{e} = -\nabla\Phi \tag{5.90}$$

where Φ is called the *electrochemical potential* because it is the combination of the electrostatic potential and the chemical potential. For metals at low or intermediate temperatures, the variation in μ is relatively small, and the terms involving $\nabla\mu$ in Eqs. (5.86) and (5.87) can be dropped out. For semiconductors, changing the dopant or impurity concentration as well as the temperature may cause a large gradient of μ, and thus $\nabla\mu$ cannot be neglected. When there is no temperature gradient, we can

easily find the electrical conductivity of metals to be

$$\sigma = L_{11} \tag{5.91}$$

The thermal conductivity is defined according to $\mathbf{q}'' = -\kappa \nabla T$ when no electric current flows. By setting $J_e = 0$ and combining Eqs. (5.86) and (5.87), we find that the thermal conductivity is related to the coefficients by

$$\kappa = L_{22} - L_{12}L_{21}/L_{11} \tag{5.92}$$

For metals, the second term on the right-hand side is much smaller than the first one, so that we can approximate $\kappa \approx L_{22}$, as already discussed in Eq. (5.71a).

5.4.1 The Seebeck Effect and Thermoelectric Power

If a temperature gradient exists, according to Eq. (5.86), there will be a current flow even in the absence of an external field. In the case of open circuit when the current flow is zero, there will be a voltage across the rod whose ends are held at different temperatures. The *Seebeck effect,* as it was first noticed by T. J. Seebeck in 1821, can be used to directly produce electric power from a temperature difference. The *Seebeck coefficient,* also called *thermopower* or *thermoelectric power,* is defined as the induced thermoelectric voltage across a material of unit length per unit temperature difference. Therefore,

$$\Gamma_S = \frac{-\nabla \Phi}{\nabla T} = \frac{L_{12}}{L_{11}} \tag{5.93}$$

which has units V/K. To calculate L_{12} for a metal, we can use Eq. (B.79) to evaluate Ψ_1 in Eq. (5.89). The simplest approach is to assume that τ does not change much near the Fermi surface. The result gives (see Problem 5.22)

$$\Gamma_S \approx -\frac{\pi^2 k_B}{2e} \frac{k_B T}{\mu_F} \tag{5.94}$$

For metals, the Seebeck coefficient is negative, and its magnitude will increase as temperature goes up. From Table 5.2, $\mu_F = 7\,\text{eV}$ for copper. We have from Eq. (5.94) that $\Gamma_S = -1.6\,\mu\text{V/K}$ at 300 K and $-3.2\,\mu\text{V/K}$ at 600 K. However, the experimental values are positive with $1.83\,\mu\text{V/K}$ at 300 K and $3.33\,\mu\text{V/K}$ at 600 K [50, 51]. This sign error is due to the simplification used to evaluate Ψ_1, and it is an indication that the nearly free-electron model may not capture all the fundamental physics of metals. A proper quantum mechanical evaluation based on the actual band structure is rather complicated but has been carried out in some studies [6, 52]. Higher values of the Seebeck coefficient can exist in some alloys and semiconductors.

Generally speaking, the Seebeck coefficient is positive for *p*-type semiconductors whose majority carriers are holes and negative for *n*-type semiconductors whose majority carriers are electrons.

For a wire whose ends are at different temperatures T_1 and T_2, as in the open circuit shown in Fig. 5.14a, there will be a voltage difference between 1 and 2 according to the relation $V_2 - V_1 = -\int_{T_1}^{T_2} \Gamma_S(T)\mathrm{d}T$. For *n*-type semiconductors, $\Gamma_S(T)$ is negative and electrons at the higher temperature end tend to diffuse toward the lower temperature end. An electrostatic potential will be built up to balance the diffusion process. Hence, the voltage is higher at the higher temperature end. Thermoelectric voltage cannot be measured with the same type of wires because the electrostatic potentials would cancel out each other. To measure the thermoelectric power, a junction is formed with two types of wires having different Seebeck coefficients, type I (+) and type II (−), as shown in Fig. 5.14b. The leads can be a third type of wire or the same as one of the thermocouple wires. This is of course the familiar thermocouple arrangement for temperature measurement. A reference temperature (T_1) is needed because a thermocouple can only measure the temperature difference. The voltage output can be expressed as

$$\Delta V = \int_{T_1}^{T_2} \left[\Gamma_{S,I}(T) - \Gamma_{S,II}(T)\right]\mathrm{d}T = \Gamma_{I,II}\Delta T \tag{5.95}$$

In thermocouple practice, the difference $\Gamma_{I,II}$ is called the Seebeck coefficient or thermopower, and the potential difference ΔV is called the electromotive force (emf). Because the Seebeck coefficient is zero when a material becomes superconducting ($\sigma \to \infty$), superconductors have been used to establish an absolute scale of thermoelectric power [51]. In thermometry, a wire with a positive Seebeck coefficient and another with a negative Seebeck coefficient are combined to form a thermocouple junction. For example, a type-E thermocouple is made of a nickel–chromium alloy (chromel) and a copper–nickel alloy (constantan); on the other hand, a type-J thermocouple is made of copper and constantan. Historically, galvanometers were used

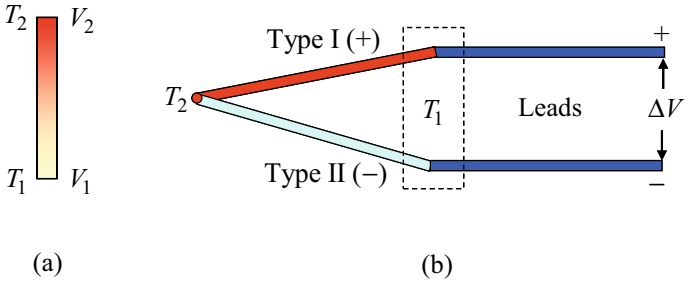

Fig. 5.14 Illustration of the Seebeck effect. **a** Single wire with a temperature difference between the two ends. **b** A thermocouple made of two different materials

to accurately measure the electric current in a potentiometer. The DC voltage can now be measured quickly and very accurately with a digital voltmeter/multimeter (DVM). Detailed discussions about the fundamentals and practice of thermoelectric thermometry based on metallic and alloy wires can be found from Bentley [50].

5.4.2 The Peltier Effect and the Thomson Effect

Equations (5.86) and (5.87) can be combined to eliminate the potential term so that

$$\mathbf{q}'' = \frac{L_{21}}{\sigma}\mathbf{J}_e - \kappa \nabla T \tag{5.96}$$

This equation suggests that there will be a heat flux in a material due to an external electric current, even without any temperature difference. This phenomenon, first discovered by Jean Peltier in 1834, is called the *Peltier effect,* which can be used for refrigeration (known as *thermoelectric cooling*) by passing through an electric current through a material. The coefficient L_{21}/σ is called the *Peltier coefficient*. It can be seen from Eqs. (5.88), (5.91), and (5.93) that

$$\Pi = L_{21}/\sigma = T\Gamma_S \tag{5.97}$$

This quantitative relationship between the Seebeck coefficient and the Peltier coefficient was revealed by William Thomson (Lord Kelvin) in the 1850s. Thomson's thermodynamic derivation led him to discover a third thermoelectric effect, known as the *Thomson effect,* which states that heat can be *released* or *absorbed* when current flows in a material with a temperature gradient. The energy received by a volume element for prescribed $\mathbf{J}_e$ and ∇T can be expressed as follows:

$$\mathbf{J}_e \cdot (-\nabla \Phi) - \nabla \cdot \mathbf{q}'' = \frac{J_e^2}{\sigma} + \nabla \cdot (\kappa \nabla T) - \left(T\frac{\mathrm{d}\Gamma_S}{\mathrm{d}T}\right)\mathbf{J}_e \cdot \nabla T \tag{5.98}$$

Notice that the common term $\Gamma_S \mathbf{J}_e \cdot \nabla T$ in both $\mathbf{J}_e \cdot (-\nabla \Phi)$ and $\nabla \cdot \mathbf{q}''$ cancels out. In Eq. (5.98), the first term is the heat generated by the Joule heating, the second term is the heat transferred into the control volume due to the temperature gradient, and the third term is caused by the Thomson effect. The last term on the right-hand side is nonzero when there is a current flow with a temperature gradient, unless the Seebeck coefficient is independent of temperature. It should be noted that, like the Seebeck effect and the Peltier effect, the Thomson effect is also a reversible process per se. The *Thomson coefficient K* is defined as the rate of the absorbed heat divided by the product of the current density and the temperature gradient. Thus,

$$K = T\frac{\mathrm{d}\Gamma_S}{\mathrm{d}T} \tag{5.99}$$

Equation (5.98) has provided a way to determine $d\Gamma_S/dT$, after σ and κ are measured at different temperatures. This allows for the absolute thermopower to be determined for certain materials at higher temperatures, since superconductivity can only occur at very low temperatures. A systematic study has resulted in the determination of absolute thermoelectric power for lead and platinum, which can then be used as reference materials to determine the absolute thermoelectric power for other materials [51]. It should be noted that, before the discovery of high-temperature superconductors, the highest temperature that a material could be made superconducting was 23 K in an alloy. Superconductivity at temperatures above 35 K was discovered in a ceramic material in 1986 and, shortly afterward, superconductivity above the boiling temperature of liquid nitrogen (78 K) was made possible.

Example 5.7 Consider a p-type semiconductor rod of diameter $d = 1$ mm and length $L = 2$ mm. One end of the rod is in contact with a heat sink at $T_L = 300$ K, and the other end is in contact with a heat source at $T_H = 350$ K. What is the open-circuit voltage? If a current $I = 0.8$ A is allowed to flow from the cold end to the hot end, what is the heat transfer rate to the heat sink? Neglect the temperature dependence of the thermal conductivity, the electrical resistivity, and the Seebeck coefficient by using $\kappa = 1.1$ W/m K, $r_e = 19\,\mu\Omega$ m, and $\Gamma_S = 220\,\mu$V/K, respectively.

Solution Assume there is no heat transfer via the side of the rod. For an open circuit, the electric potential is higher at the cold end, and the voltage across the rod is $V_{open} = \Gamma_S(T_H - T_L) = 11$ mV. The rate of heat transfer to the heat sink by conduction from the heat source is $q_C = (\pi d^2/4)\kappa(T_2 - T_1)/L = 21.6$ mW.

When an electric current is running from the cold end to the hot end, the Joule heating is generated uniformly inside the rod. The dissipated heat must reach both ends equally by conduction. The additional heat transfer to the heat sink is $q_J = I^2R/2 = 15.5$ mW, where $R = 48.4\,\text{m}\Omega$ is the resistance of the rod. On the other hand, the Peltier effect results in cooling, or heat removal from the heat sink. From Eq. (5.84), we have $q_P = -T_1\Gamma_S I = -52.8$ mW. The combination of the three terms gives the heat transfer rate as $q = q_C + q_J + q_P = -15.7$ mW. The negative sign indicates that heat is removed from the heat sink.

This example demonstrates the Peltier effect for thermoelectric refrigeration. It can be seen that a smaller thermal conductivity will decrease the heat transfer between the two ends: a smaller electrical resistivity will reduce the Joule heating,, and a larger Seebeck or Peltier coefficient will enhance the heat removal. For most metals, the thermal conductivity is too high, and the Seebeck coefficient is too small for refrigeration application. Some insulators can have a large Seebeck coefficient but their electrical resistivity is too high for them to be used in thermoelectric devices.

5.4.3 Thermoelectric Generation and Refrigeration

The study of thermoelectric generation and refrigeration has become an active research area since the 1950s, along with the development of semiconductor materials

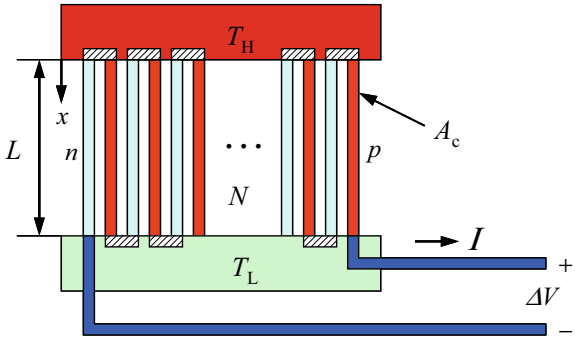

Fig. 5.15 Illustration of a thermoelectric generator or refrigerator

or *p*-*n* junctions. Heavily doped semiconductors exhibit large Seebeck coefficients. Alternative *n*-type or *p*-type semiconductors (or semimetals) are used as thermoelectric materials or *thermoelectric elements.* These include antimony tellurium (SbTe), bismuth tellurium (BiTe), and silicon germanium (SiGe) compounds. More recently, nanostructured materials are investigated as candidates to increase the performance of thermoelectric devices [53].

With the understanding of the Seebeck effect, the Peltier effect, and the Thomson effect, we are ready to perform a thermodynamic analysis of thermoelectric generators or refrigerators as illustrated in Fig. 5.15. There are N pairs of junctions that are connected electrically in series by metallic interconnects and thermally in parallel between the two heat sinks. To simplify the analysis, contact resistances are neglected, and it is assumed that all the thermoelectric elements have the same length L and the same cross-sectional area A_c. Furthermore, heat transfer by other modes is neglected except conduction by thermoelectric elements. Because contact electrical resistance is neglected, heat generation by the Joule heating happens due to resistance of the thermoelectric elements only. A load resistance R_L is used to evaluate the electric power output of the generator. A further assumption is that the thermal and electrical conductivities, as well as the Seebeck coefficient, are independent of temperature. This assumption is reasonable when the temperature difference between the two heat reservoirs is very small.

Consider a thermoelectric generator. In this case, heat is taken from the high-temperature reservoir T_H at the rate q_H, and some heat is released to the low-temperature reservoir T_L at the rate q_L. The generated thermoelectric power is

$$P = I\Delta V = q_H - q_L \tag{5.100}$$

The temperature distribution along the thermoelectric element is not linear, i.e., the temperature gradient is not constant. The steady-state temperature distribution along a single thermoelectric element can be solved by setting Eq. (5.98) to zero. Because of the assumption of constant values of I, κ, σ, and Γ_S, the Thomson coefficient also becomes zero. Therefore, we obtain

$$T(x) = \frac{J_e^2}{2\sigma\kappa}(L - x)x - \frac{x}{L}(T_H - T_L) + T_H \tag{5.101}$$

The resulting heat transfer rates due to temperature gradient are

$$-\kappa A_c \frac{dT}{dx}\bigg|_{x=0} = \kappa A_c \frac{T_H - T_L}{L} - \frac{I^2 L}{2\sigma A_c} \tag{5.102a}$$

and

$$-\kappa A_c \frac{dT}{dx}\bigg|_{x=L} = \kappa A_c \frac{T_H - T_L}{L} + \frac{I^2 L}{2\sigma A_c} \tag{5.102b}$$

Clearly, half of the Joule heating goes to the heat source, and the other half goes to the heat sink, as noticed in Example 5.7. Substituting Eq. (5.102) into Eq. (5.96) and using the subscripts n and p for different thermoelectric elements, we have

$$q_H = NI\Gamma_{np}T_H + NA_c\kappa_{np}\frac{\Delta T}{L} - N\frac{I^2 L}{2A_c\sigma_{np}} \tag{5.103a}$$

$$q_L = NI\Gamma_{np}T_L + NA_c\kappa_{np}\frac{\Delta T}{L} + N\frac{I^2 L}{2A_c\sigma_{np}} \tag{5.103b}$$

where $\Gamma_{np} = \Gamma_{S,p} - \Gamma_{S,n}$, $\kappa_{np} = \kappa_n + \kappa_p$, $\Delta T = T_H - T_L$, and $\sigma_{np} = \left(1/\sigma_n + 1/\sigma_p\right)^{-1}$. The output power is therefore

$$P = I\Delta V = q_H - q_L = NI\Gamma_{np}\Delta T - I^2 R_0 \tag{5.104}$$

where $R_0 = NL/(A_c\sigma_{np})$ is the resistance of all thermoelectric elements. The voltage is solely caused by the Seebeck effect, i.e., $\Delta V = N\Gamma_{np}\Delta T$. Assuming the load resistance is R_L, we have

$$I = \frac{\Delta V}{R_0 + R_L} = \frac{N\Gamma_{np}\Delta T}{R_0 + R_L} \tag{5.105}$$

Substituting Eq. (5.105) into Eq. (5.104), we see that the electric power is indeed $P = I^2 R_L$. The thermal efficiency can be calculated as follows:

$$\eta = \frac{P}{q_H} = \frac{\frac{R_L}{R_0}\frac{\Delta T}{T_H}}{\frac{1}{Z^* T_H}\left(1 + \frac{R_L}{R_0}\right)^2 + \left(1 + \frac{R_L}{R_0}\right) - \frac{\Delta T}{2T_H}} \tag{5.106}$$

where

$$Z^* = \frac{NL}{A_c \kappa_{np}} \frac{\Gamma_{np}^2}{R_0} = \frac{\sigma_{np} \Gamma_{np}^2}{\kappa_{np}} \tag{5.107}$$

is independent of the geometry [54]. When $1/Z^* T_H \ll 1$ and $R_0/R_L \ll 1$, we have $\eta \to 1 - T_L/T_H$, which is exactly the Carnot efficiency. Increasing Z^* will improve the efficiency. Hence, minimizing the thermal conduction, reducing the electrical resistance, and increasing the Seebeck coefficient of the thermoelectric elements are essential to improve the performance. A similar analysis can be done for thermoelectric cooling, which is left as an exercise (see Problem 5.25). In general, the *figure of merit* of thermoelectricity is defined as

$$Z = \frac{\sigma \Gamma_S^2}{\kappa} \tag{5.108}$$

which has units of K^{-1} and can be nondimensionalized by multiplying the temperature T. The resulting dimensionless parameter ZT (zee-tee) is often quoted as the figure of merit for thermoelectric materials or devices. This applies to both thermoelectric generation and refrigeration (see Problems 5.23 and 5.25).

Because of the compromise between a large electrical conductivity and a small thermal conductivity, along with the requirement of a large Seebeck coefficient, it has turned out that semiconductors are the best choice for thermoelectric applications. After an extensive pursuit in the 1950s, materials with ZT values between 0.5 and 1 near room temperature have been developed using $Bi_xSb_{2-x}Te_3$ and $Bi_2Se_yTe_{3-y}$. These materials are essentially doped V-VI semiconductors Sb_2Te_3 or Bi_2Te_3. In the past 25 years, intensive theoretical and experimental research has been conducted to increase the thermoelectric device performance by using nanostructured materials. Mildred Dresselhaus and coworkers predicted that multiple quantum wells or superlattices may enhance ZT values due to quantum confinement as well as a reduction in the phonon thermal conductivity; the idea has also been extended to PbTe/PbSe superlattice nanowires [55]. Superlattices made of SiGe/Si and GaAs/AlAs have also been considered. Since 2001, several groups have demonstrated ZT values exceeding 2 [53, 56]. Gang Chen's group has performed extensive investigations on the phonon and electron transport in nanostructured materials related to low-dimensional thermoelectricity, as discussed in a recent review [57]. The reduction in thermal conductivity may come from a combination of a number of factors including the mean-free-path reduction by boundary scattering, thermal resistance associated with acoustic mismatch or phonon scattering at the interface of dissimilar materials, and/or quantum confinement of the phonon DOS.

Before moving to the discussion of size effects on thermal conductivity, let us give an overview of irreversible thermodynamics and a brief introduction to nonequilibrium thermodynamics.

5.4.4 Onsager's Theorem and Irreversible Thermodynamics

The set of coupled equations given in Eqs. (5.86) and (5.87) is an example of *irreversible thermodynamics,* pioneered by Lars Onsager in the 1930s, alternatively known as the thermodynamics of irreversible processes or Onsager's theorem. Onsager described the phenomenological relations of interrelated or coupled transport processes using the following equation [58]:

$$\mathbf{J}_i = \sum_j \alpha_{ij} \mathbf{F}_j \tag{5.109}$$

where $\mathbf{J}_i$ is the flux of a physical quantity X_i with $J_i = \mathrm{d}X_i/\mathrm{d}t$, α_{ij} is called the *Onsager kinetic coefficient,* and $\mathbf{F}_i$ is the ith generalized driving force or *affinity.* In an equilibrium state, all $\mathbf{F}_i$'s are zero. Furthermore, the entropy of a system can be expressed as [59]

$$\mathrm{d}s = \sum_i f_i \mathrm{d}X_i \tag{5.110}$$

where f_i is a property that is related to $\mathbf{F}_i$ such that $\mathbf{F}_i$ is proportional to the gradient of f_i. The entropy flux is thus

$$\mathbf{s}'' = \sum_i f_i \mathbf{J}_i \tag{5.111}$$

If an infinitesimal control volume is chosen, the continuity equation can be written as

$$\frac{\partial X_i}{\partial t} + \nabla \cdot \mathbf{J}_i = 0 \tag{5.112}$$

The entropy balance becomes

$$\frac{\partial s}{\partial t} = \dot{s}_{\mathrm{gen}} - \nabla \cdot \mathbf{s}'' \tag{5.113}$$

where $\frac{\partial s}{\partial t} = \sum_i f_i \frac{\partial X_i}{\partial t}$ and $\nabla \cdot \mathbf{s}'' = \sum_i \nabla f_i \cdot \mathbf{J}_i + \sum_i f_i \nabla \cdot \mathbf{J}_i$. Using the continuity equation, we obtain the *volumetric entropy generation rate*:

$$\dot{s}_{\mathrm{gen}} = \sum_i \nabla f_i \cdot \mathbf{J}_i \tag{5.114}$$

Furthermore, the *Onsager reciprocity* is expressed as follows [58, 59]:

$$\alpha_{ij} = \alpha_{ji} \tag{5.115}$$

Lars Onsager (1903–1976) received the Nobel Prize in Chemistry in 1968 "for the discovery of the reciprocal relations bearing his name, which are fundamental for the thermodynamics of irreversible processes." The Onsager reciprocity was even considered by some researchers as the *fourth law of thermodynamics.*

Example 5.8 Determine the Onsager kinetic coefficients and the volumetric entropy generation rate for a conductor with constant current and temperature gradient.

Solution It should be noted that in thermoelectricity, $\mathbf{J}_1 = \mathbf{J}_e$, $\mathbf{J}_2 = \mathbf{q}''$, $\mathbf{F}_1 = -(1/T)\nabla\Phi$, and $\mathbf{F}_2 = \nabla(1/T) = -(1/T^2)\nabla T$. Thus, the Onsager relations are expressed as

$$\mathbf{J}_e = \alpha_{11}\frac{-\nabla\Phi}{T} - \alpha_{12}\frac{\nabla T}{T^2} \tag{5.116}$$

$$\mathbf{q}'' = \alpha_{21}\frac{-\nabla\Phi}{T} - \alpha_{22}\frac{\nabla T}{T^2} \tag{5.117}$$

Comparing the above expressions with Eqs. (5.86) and (5.87), we find that

$$\alpha_{11} = TL_{11}\ \alpha_{12} = \alpha_{21} = T^2L_{12}\ \text{and}\ \alpha_{22} = T^2L_{22} \tag{5.118}$$

The entropy generation rate can be calculated by using Eq. (5.99). Note that

$$\mathrm{d}s = \frac{\delta Q - \mu \mathrm{d}N}{TV} = \mathbf{q}'' \cdot \nabla\left(\frac{1}{T}\right) + \mathbf{J}_e \cdot \left(-\frac{\nabla\Phi}{T}\right) \tag{5.119}$$

In the steady state, the energy equation, Eq. (5.98), becomes

$$\mathbf{J}_e \cdot (-\nabla\Phi) - \nabla \cdot \mathbf{q}'' = 0 \tag{5.120}$$

Therefore, the volumetric entropy generation rates for 3D and 1D cases, respectively, are

$$\dot{s}_{\text{gen}} = \mathbf{q}'' \cdot \nabla\left(\frac{1}{T}\right) + \frac{1}{T}\nabla \cdot \mathbf{q}''\ \text{and}\ \dot{s}_{\text{gen}} = \frac{q''}{T^2}\frac{\mathrm{d}T}{\mathrm{d}x} + \frac{1}{T}\frac{\mathrm{d}q''}{\mathrm{d}x} \tag{5.121}$$

These results are consistent with the analysis in Chap. 2 (see Example 2.5 and Problem 2.29). Furthermore, Eq. (5.121) suggests that the Thomson effect is a reversible process that does not cause any entropy generation. The same can be said for both the Seebeck effect and the Peltier effect, which are reversible thermoelectric effects. In addition to thermoelectricity, irreversible thermodynamics has found applications in multicomponent diffusion, nonisothermal diffusion (when both a temperature gradient and a concentration gradient exist), and some magnetic processes [59]. A further advancement in nonequilibrium thermodynamics was made by Ilya Prigogine (1917–2003) who was awarded the Nobel Prize in Chemistry in 1977.

Prigogine's study extended irreversible thermodynamics to systems that are far from equilibrium and are allowed to exchange energy, mass, and entropy with their surroundings. Prigogine and colleagues demonstrated that ordered dissipative systems can be formed from disordered systems, when the systems are far from equilibrium, and dubbed this theory *dissipative structure,* which led to pioneering research in self-organization or self-assembly. The formation of ordered structures from disordered structures has diverse applications in chemical, biological, and social systems [60, 61]. It is beyond the scope of this book to go into the details of this theory.

5.5 Classical Size Effect on Conductivities

When the characteristic length, such as the thickness of a film, the diameter of a wire, or the size of a grain (for polycrystalline solids), is comparable to the mechanistic length, i.e., the mean free path, boundary or interface scattering becomes important. Subsequently, the thermal conductivity (as well as other transport coefficients) becomes size dependent and can also be anisotropic [62, 63]. Because the mean free paths of electrons and phonons tend to increase as temperature goes down, size effects are usually more important at low temperatures. The criteria are also different for different materials due to the different carrier types and scattering mechanisms. In the following section, we will study the effect of boundary scattering on electrical and thermal conductivities based on simple geometric considerations as well as derivations using the BTE.

5.5.1 Simple Geometric Considerations

The simple expression of thermal conductivity based on the kinetic theory is $\kappa = \frac{1}{3}(\rho c_v) v \Lambda_b$ for either electrons or phonons. Here, Λ_b is called the *bulk mean free path,* which is the mean free path when the material is infinitely extended. While the specific heat and the velocity are also size dependent, especially for phonons, let us focus on the size dependence of the mean free path. The main objective of this section is to illustrate how boundary scattering affects the thermal conductivity by reducing the mean free path. The argument is also applicable to the electrical conductivity, since it is also proportional to the mean free path. Shown in Fig. 5.16 are two geometric configurations to be considered: (*a*) and (*b*) for a thin film and (*c*) for a thin wire or rod.

In the ballistic transport limit when $d \ll \Lambda_b$, we assume that the mean free path in the film is the same as the thickness d, $\Lambda_f = d$. Thus, the conductivity ratio can be obtained as

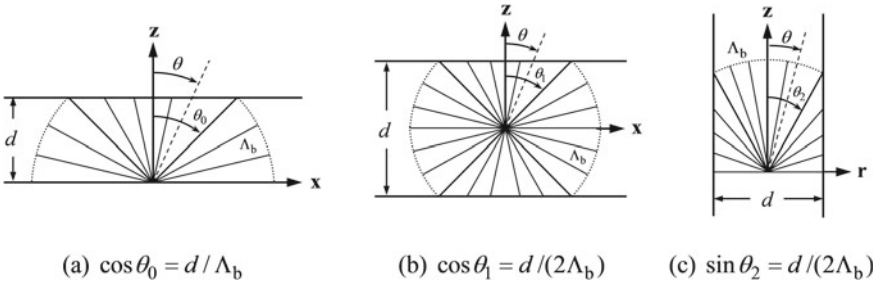

Fig. 5.16 Illustration of free-path reduction due to boundary scattering. **a** A thin film for paths originated from the surface. **b** A thin film for paths originated from the center. **c** A thin wire for paths originated from the center

$$\frac{\kappa_f}{\kappa_b} = \frac{\Lambda_f}{\Lambda_b} = \frac{1}{Kn} \tag{5.122}$$

where $Kn = \Lambda_b/d$ is the Knudsen number for electrons or phonons, borrowed from the definition used in rarefied gas dynamics. In the intermediate region, we can apply Matthiessen's rule as suggested in Eqs. (5.56) and (5.76) such that

$$\frac{1}{\Lambda_{eff}} = \frac{1}{\Lambda_b} + \frac{1}{\Lambda_f} \tag{5.123}$$

Accordingly,

$$\frac{\kappa_{eff}}{\kappa_b} = \frac{\Lambda_{eff}}{\Lambda_b} = \frac{1}{1 + Kn} \tag{5.124}$$

The result calculated from Eq. (5.124) is plotted in Fig. 5.17 to illustrate the size dependence of the effective thermal conductivity. It appears that this simple formula overpredicts the reduction in thermal conductivity, as compared with the more realistic models to be discussed next.

As early as 1901, J. J. Thomson first considered the size effect on the electrical conductivity of thin films. His argument was extended by K. Fuchs in 1938 based on the BTE. The geometric argument assumes that boundary scattering is diffuse and inelastic, i.e., the electrons are fully accommodated after scattering by a boundary. The concept of accommodation is the same as that used for ideal gas particles in the free molecule flow regime discussed in Sect. 4.4. However, for simplicity, the distribution of free paths is not taken into consideration. In other words, all paths are assumed to be the same as the bulk mean free path. When $d \ll \Lambda_b$, we may assume that all energy carriers originate from the boundary. From Fig. 5.16a, we see that

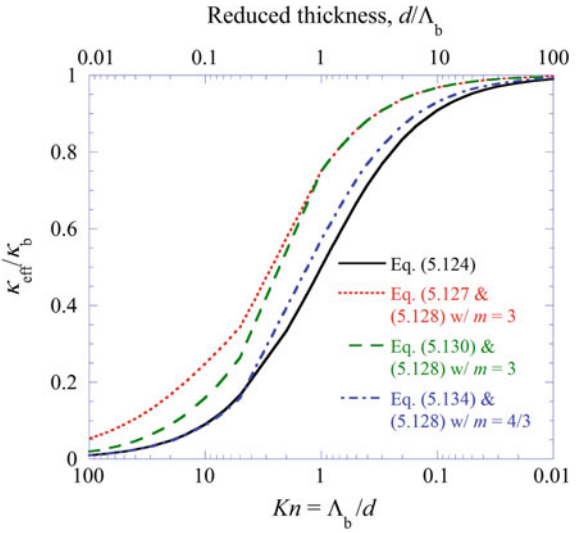

Fig. 5.17 Reduction in thermal conductivity due to boundary scattering. Note that Eq. (5.128) was used with different m values for $Kn < 1$, and interpolation was used for $1 < Kn < 5$

$$\Lambda(\theta) = \begin{cases} d/\cos\theta, & 0 < \theta < \theta_0 \\ \Lambda_b, & \theta_0 < \theta < \pi/2 \end{cases} \tag{5.125}$$

The free paths should be averaged over the hemisphere, and the weighted average can be written and evaluated as follows:

$$\frac{\Lambda_f}{\Lambda_b} = \frac{\int_0^{2\pi}\int_0^{\pi/2} \Lambda(\theta)\sin\theta \mathrm{d}\theta\mathrm{d}\phi}{\int_0^{2\pi}\int_0^{\pi/2} \Lambda_b \sin\theta \mathrm{d}\theta\mathrm{d}\phi} = \frac{\ln(Kn)+1}{Kn} \tag{5.126}$$

Applying Matthiessen's rule again, we have

$$\frac{\kappa_{eff}}{\kappa_b} = \frac{\Lambda_{eff}}{\Lambda_b} = \left(1 + \frac{Kn}{\ln(Kn)+1}\right)^{-1} \tag{5.127}$$

This equation, however, cannot be applied for small values of Kn since $\ln(Kn)$ becomes negative. Let us assume Eq. (5.127) is applicable for $Kn > 5$. When $Kn < 1$, we may use

$$\frac{\kappa_{eff}}{\kappa_b} = \frac{\Lambda_{eff}}{\Lambda_b} = \left(1 + \frac{Kn}{m}\right)^{-1} \tag{5.128}$$

where $m \approx 3$ for thin films [62, 63]. Equation (5.124) can be considered as a special case of Eq. (5.128) with $m = 1$. The results based on Eqs. (5.127) and (5.128) are plotted in Fig. 5.17 for comparison. The thermal conductivity in the intermediate region for $1 < Kn < 5$ is linearly interpolated based on the values at $Kn = 1$ and 5.

Equations (5.126) and (5.127) do not consider the direction of transport and cannot capture the anisotropic feature due to the size effect. Flik and Tien [63] employed a weighted average of the free-path components in the parallel and normal directions of thin films. Their work was extended to different geometries by Richardson and Nori [64]. For the z-direction, the projected mean free path is $\Lambda_z = \Lambda(\theta)\cos\theta$; hence, the weighted average becomes

$$\frac{\Lambda_z}{\Lambda_{\mathrm{b},z}} = \frac{\int_0^{2\pi}\int_0^{\pi/2}\Lambda(\theta)\cos\theta\sin\theta\mathrm{d}\theta\mathrm{d}\phi}{\int_0^{2\pi}\int_0^{\pi/2}\Lambda_\mathrm{b}\cos\theta\sin\theta\mathrm{d}\theta\mathrm{d}\phi} = \frac{2}{Kn} - \frac{1}{Kn^2} \tag{5.129}$$

The use of Matthiessen's rule allows us to obtain

$$\frac{\kappa_{\mathrm{eff},z}}{\kappa_\mathrm{b}} = \left(1 + \frac{Kn}{2 - Kn^{-1}}\right)^{-1} \text{ for } Kn > 5 \tag{5.130}$$

For $Kn < 1$, Eq. (5.128) should be used with $m = 3$, which can be obtained by integrating over the film when $Kn \ll 1$ [63]. The result from Eq. (5.130) is also shown in Fig. 5.17. For transport along the x-direction, one may assume that all the electrons originate from the center of the film for simplicity. The component of the free path is $\Lambda_x = \Lambda(\theta)\sin\theta\cos\phi$, where ϕ is the azimuthal angle. Due to symmetry, the integration can be carried out in a single octant only. It can be seen from Fig. 5.16b that $\Lambda(\theta) = d/(2\cos\theta)$ for $0 \le \theta < \theta_1$, and $\Lambda(\theta) = \Lambda_\mathrm{b}$ for $\theta_1 \le \theta < \pi/2$, where $\theta_1 = \cos^{-1}(d/2\Lambda_\mathrm{b})$. Subsequently,

$$\frac{\Lambda_x}{\Lambda_{\mathrm{b},x}} = \frac{\int_0^{\pi/2}\int_0^{\pi/2}\Lambda(\theta)\sin^2\theta\cos\phi\mathrm{d}\theta\mathrm{d}\phi}{\int_0^{\pi/2}\int_0^{\pi/2}\Lambda_\mathrm{b}\sin^2\theta\cos\phi\mathrm{d}\theta\mathrm{d}\phi} \tag{5.131}$$

After evaluation of the above integral, we obtain

$$\frac{\kappa_{\mathrm{eff},x}}{\kappa_\mathrm{b}} = \frac{2}{\pi Kn}\ln[2Kn(1+\sin\theta_1)] + 1 - \frac{2\theta_1}{\pi} - \frac{\sin\theta_1}{\pi Kn} \tag{5.132}$$

In the ballistic limit, i.e., $Kn \gg 1$, Eq. (5.132) reduces to $\kappa_{\mathrm{eff},x}/\kappa_\mathrm{b} \approx (2/\pi)\ln(4Kn)/Kn$. If the free paths were to originate from the boundary, the result could be obtained by replacing Kn with $Kn/2$ in Eq. (5.132). While it is perfectly logical to assume that all the carriers originate from the surface for the z-component in the ballistic limit. For thermal transport along a film with a temperature gradient in the x-direction, carriers must originate from a cross section or y-z plane inside the film. The transport process along the film is essentially diffusion-like with significant boundary scattering contributions. Anisotropy may arise between $\kappa_{\mathrm{eff},x}$ and $\kappa_{\mathrm{eff},z}$ due to boundary scattering. A simple argument is that paths with large polar angles are more important for parallel conduction, whereas paths with smaller polar angles are more important for normal conduction. Based on the geometry, it can be seen that paths with smaller polar angles are more likely to be scattered by the

boundary. Another reason that causes $\kappa_{\text{eff},x}$ to be greater than $\kappa_{\text{eff},z}$ is that scattering tends to be more specular for larger incidence angles. Specular reflection or elastic scattering does not reduce the conductivity because the incident particles only change the direction without any exchange of energy with the surface. Crystal anisotropy is another major reason for anisotropic conduction, sometimes the dominant reason, as in high-temperature superconducting $YBa_2Cu_3O_7$ films [63]. Grain boundaries can strongly influence the thermal conductivity in polycrystalline films [62]. For chemical–vapor-deposited polycrystalline diamond films, depending on the crystal orientation, κ_x may be greater or smaller than κ_z [65].

For circular wires, considering the conduction along a thin wire as shown in Fig. 5.16c, we have $\Lambda_z(\theta) = \Lambda_\text{b} \cos\theta$ for $0 < \theta < \theta_2$, and $\Lambda_z(\theta) = d\cot\theta/2$ for $\theta_2 < \theta < \pi/2$, where $\theta_2 = \sin^{-1}(d/2\Lambda_\text{b})$. Thus,

$$\frac{\Lambda_{\text{w},z}}{\Lambda_{\text{b},z}} = \frac{\int_0^{2\pi}\int_0^{\pi/2}\Lambda_z(\theta)\sin\theta\,\text{d}\theta\,\text{d}\phi}{\int_0^{2\pi}\int_0^{\pi/2}\Lambda_b\cos\theta\sin\theta\,\text{d}\theta\,\text{d}\phi} = \frac{1}{Kn} - \frac{1}{4Kn^2} \tag{5.133}$$

Applying Matthiessen's rule yields

$$\frac{\kappa_{\text{eff,w}}}{\kappa_\text{b}} = \frac{4Kn - 1}{4Kn^2 + 4Kn - 1} \tag{5.134}$$

which can be applied for $Kn > 5$ and approaches to Eq. (5.124) at large Kn. For $Kn < 1$, studies have shown that Eq. (5.128) is a good approximation with $m = 4/3$ [66, 67]. The reduction in thermal conductivity for thin wires is also indicated in Fig. 5.17, where values for $1 < Kn < 5$ are again based on a simple interpolation between the two expressions. Due to geometric confinement, the reduction in the mean free path is more severe for thin wires than for thin films. The geometric argument is easy to understand and may help gain a physical intuition of the size effect due to boundary scattering. In consideration of the classical size effect, it is assumed that Fourier's law is still applicable with a modified thermal conductivity. The size effect on the electron or phonon transport properties can also be formulated using the BTE for thin films and wires, as presented in the following.

5.5.2 *Conductivity Along a Thin Film Based on the BTE*

In Sect. 5.3.3, we derived electrical and thermal conductivities based on the BTE for bulk materials. The relaxation time approximation was adopted, and the distribution function was assumed to be not too far away from equilibrium, i.e., under the local-equilibrium conditions. To determine the size effect on the conductivities along thin films, the same assumptions will be applied. Consider the geometry shown in Fig. 5.16a, with a temperature gradient and an electric field in the x-direction only. Because of the finite thickness in the z-direction, the distribution function should

also be an explicit function of z, viz.,

$$f_1(\varepsilon, T, z) \approx f_0(\varepsilon, T) + \tau(\varepsilon)\left(\frac{eE}{m_e}\frac{\partial f_0}{\partial \varepsilon}\frac{\partial \varepsilon}{\partial v_x} - v_x\frac{\partial f_0}{\partial T}\frac{\mathrm{d}T}{\mathrm{d}x} - v_z\frac{\partial f_1}{\partial z}\right) \tag{5.135a}$$

Compared with Eq. (5.65), the last term was added because f_1 depends also on z. Here, the electric field and the temperature gradient are along the x-direction. In Eq. (5.135a), we have already replaced $\partial f_1/\partial \varepsilon$ with $\partial f_0/\partial \varepsilon$ and $\partial f_1/\partial T$ with $\partial f_0/\partial T$. We can rearrange Eq. (5.135a) as follows:

$$-\frac{eE}{m_e}\frac{\partial f_0}{\partial \varepsilon}\frac{\partial \varepsilon}{\partial v_x} + v_x\frac{\partial f_0}{\partial T}\frac{\mathrm{d}T}{\mathrm{d}x} + v_z\frac{\partial f_1}{\partial z} = -\frac{f_1 - f_0}{\tau(\varepsilon)} \tag{5.135b}$$

which is nothing but the steady-state BTE under the relaxation time approximation. The general solution can be expressed as

$$f_1 = f_0 + \tau v_x\left(eE\frac{\partial f_0}{\partial \varepsilon} - \frac{\partial f_0}{\partial T}\frac{\mathrm{d}T}{\mathrm{d}x}\right)\left[1 - \psi(\mathbf{v})\exp\left(-\frac{z}{\tau v_z}\right)\right],\ v_z > 0 \tag{5.136a}$$

and

$$f_1 = f_0 + \tau v_x\left(eE\frac{\partial f_0}{\partial \varepsilon} - \frac{\partial f_0}{\partial T}\frac{\mathrm{d}T}{\mathrm{d}x}\right)\left[1 - \psi(\mathbf{v})\exp\left(-\frac{d-z}{\tau v_z}\right)\right],\ v_z < 0 \tag{5.136b}$$

where $\psi(\mathbf{v})$ is an arbitrary function that accounts for the accommodation and scattering characteristics. If perfect accommodation is assumed with inelastic and diffuse scattering, then $\psi(\mathbf{v}) = 1$. Let us consider electrical conduction without any temperature gradient. For diffuse scattering only with $\psi(\mathbf{v}) = 1$, it can be shown that

$$f_1 = f_0 + \tau v_x eE\frac{\partial f_0}{\partial \varepsilon}\left[1 - \exp\left(-\frac{z}{\tau v_z}\right)\right],\quad v_z > 0 \tag{5.137a}$$

and

$$f_1 = f_0 + \tau v_x eE\frac{\partial f_0}{\partial \varepsilon}\left[1 - \exp\left(-\frac{d-z}{\tau v_z}\right)\right],\quad v_z < 0 \tag{5.137b}$$

We must substitute the distribution function into Eq. (5.67a) and integrate over (v_x, v_y, v_z), or over (v, θ, ϕ) or $(\varepsilon, \theta, \phi)$, in spherical coordinates, to obtain $J_e(z) = -eJ_N(z)$ along the film. Therefore,

$$J_e(z) = -e^2E\int_0^\infty \tau\frac{\partial f_{FD}}{\partial \varepsilon}\mathrm{d}\varepsilon\int_0^{2\pi}\mathrm{d}\phi\left\{\int_0^{\pi/2} v_x^2\left[1 - \exp\left(-\frac{z}{\tau v\cos\theta}\right)\right]v^2\sin\theta\mathrm{d}\theta\right.$$

$$+\int_{\pi/2}^{\pi} v_x^2\left[1-\exp\left(-\frac{d-z}{\tau v\cos\theta}\right)\right]v^2\sin\theta\mathrm{d}\theta\Bigg\} \tag{5.138}$$

Putting $v_x = v\sin\theta\cos\phi$, the integration over ϕ can be carried out independently. The average current flux $J_{\mathrm{e,avg}} = (1/d)\int_0^d J_{\mathrm{e}}(z)\mathrm{d}z$ can also be obtained. The properties of the Fermi integral allow the integration over ε to be carried out and expressed in terms of the properties at the Fermi surface, i.e., $\tau(\mu_{\mathrm{F}})$ and v_{F}. Notice that $\Lambda_{\mathrm{b}} = \tau(\mu_{\mathrm{F}})v_{\mathrm{F}}$, and let $J_{\mathrm{e,avg}} = \sigma_{\mathrm{f}}E$, where σ_{f} is the effective electrical conductivity of the film. After normalization of the electrical current density based on Eqs. (5.67a) and (5.68), we obtain the following relation:

$$\frac{\sigma_{\mathrm{f}}}{\sigma_{\mathrm{b}}} = F(Kn) \tag{5.139a}$$

where

$$\begin{aligned}
F(Kn) &= \frac{3}{4d}\int_0^{\pi/2}\sin^3\theta\int_0^d\left[1-\exp\left(-\frac{z}{\Lambda_{\mathrm{b}}\cos\theta}\right)\right]\mathrm{d}z\mathrm{d}\theta \\
&\quad+\frac{3}{4d}\int_{\pi/2}^{\pi}\sin^3\theta\int_0^d\left[1-\exp\left(-\frac{d-z}{\Lambda_{\mathrm{b}}\cos\theta}\right)\right]\mathrm{d}z\mathrm{d}\theta \\
&= \frac{3}{2d}\int_0^{\pi/2}\sin^3\theta\left\{d-\Lambda_{\mathrm{b}}\cos\theta\left[1-\exp\left(-\frac{d}{\Lambda_b\cos\theta}\right)\right]\right\}\mathrm{d}\theta \\
&= 1-\frac{3Kn}{8}+\frac{3Kn}{2}\int_1^{\infty}\left(\frac{1}{t^3}-\frac{1}{t^5}\right)\exp\left(-\frac{t}{Kn}\right)\mathrm{d}t
\end{aligned} \tag{5.139b}$$

Note that the mth-order *exponential integral* is defined as $E_m(x) = \int_1^{\infty}\mathrm{e}^{-xt}t^{-m}\mathrm{d}t$ or $E_m(x) = \int_0^1\eta^{m-2}\mathrm{e}^{-x/\eta}\mathrm{d}\eta$, which has the relation $E_{m+1}(x) = m^{-1}\left[\mathrm{e}^{-x} - xE_m(x)\right]$. Equation (5.139b) can also be expressed as

$$F(Kn) = 1-\frac{3Kn}{8}+\frac{3Kn}{2}\left[E_3\left(\frac{1}{Kn}\right)-E_5\left(\frac{1}{Kn}\right)\right] \tag{5.139c}$$

The asymptotic relations are

$$\frac{\sigma_{\mathrm{f}}}{\sigma_{\mathrm{b}}} \approx 1-\frac{3Kn}{8}\ \text{for}\ Kn \ll 1 \tag{5.140a}$$

and

$$\frac{\sigma_f}{\sigma_b} \approx \frac{3\ln(Kn)}{4Kn} \text{ for } Kn \gg 1 \tag{5.140b}$$

which is close to Eq. (5.132) for $Kn \gg 1$. The derivation using the BTE presented here inherently assumes that the electrons are originated from the film rather than from the boundaries.

For thermal conductivity, we can substitute Eq. (5.136a, 5.136b) with $\psi(\mathbf{v}) = 1$ into Eq. (5.70) and follow a similar procedure to obtain $\kappa_f/\kappa_b = F(Kn)$, where $F(Kn)$ is given in Eq. (5.139b) or (5.139c). At very low temperatures or near room temperature, the Wiedemann–Franz law is applicable, and the reduction in electrical and thermal conductivities is essentially the same. In the intermediate region, one could use different scattering rates or mean free paths for the bulk thermal and electrical conductivities to determine the size effect individually based on Eq. (5.139a). Another way to obtain κ_f/κ_b is to calculate the heat flux using Eq. (5.136a, 5.136b) with a finite temperature gradient as done by Kumar and Vradis [68]. They obtained complicated expressions and showed that the results are similar to σ_f/σ_b in a large range.

According to the discussion of thermoelectricity in Sect. 5.4, we could in principle quantify the size effect on other coefficients. If the same assumptions are used, to the first-order approximation, L_{12} and L_{21} are subject to boundary scattering and will also be reduced according to Eq. (5.139a). Because the thermoelectric power is the ratio of the two coefficients, the Seebeck coefficient along the film should be expected to remain the same regardless of boundary scattering. One should be cautious about this conclusion because the assumption of a spherical Fermi surface and the free-electron model are questionable when modeling thermoelectricity, as mentioned previously.

The above discussion can be extended to scattering with a specular component. Let parameter p, which is called *specularity,* represent the probability of scattering being elastic and specular. For specular and elastic scattering, carriers will continue to exchange energy and momentum inside the film after reflection by the boundary. Therefore, these scattering events do not cause any reduction in the effective mean free paths or conductivities along the film. If p is assumed to be independent of the incident direction, the function $\psi(\mathbf{v})$ in Eq. (5.136a, 5.136b) becomes

$$\psi(\mathbf{v}) = \frac{1-p}{1-p\exp(-d/\tau v_z)} \tag{5.141}$$

The function given in Eq. (5.139b) may be modified after some tedious derivations as follows:

$$F(Kn, p) = 1 - \frac{3(1-p)Kn}{2}\int_1^\infty \left(\frac{1}{t^3} - \frac{1}{t^5}\right)\frac{1-\exp(-t/Kn)}{1-p\exp(-t/Kn)}\mathrm{d}t \tag{5.142}$$

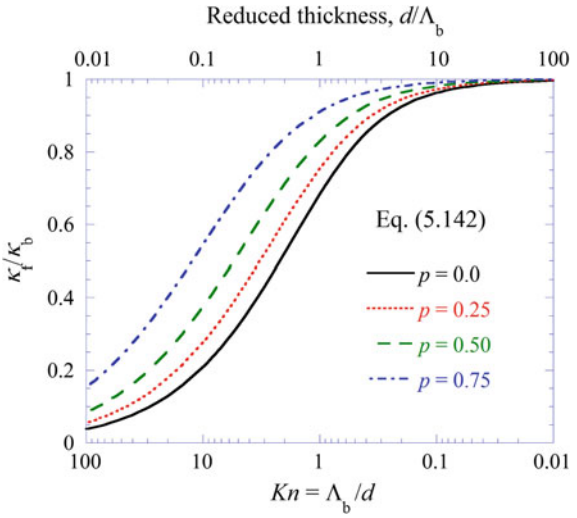

Fig. 5.18 Size effect on thermal conductivity along the film of thickness d, as predicted by the BTE with different specularities.

The effects of p and Kn on the effective conductivity are shown in Fig. 5.18. The trends with respect to Kn are very similar to those in Fig. 5.17 obtained from simple geometric considerations. For electron transport, since the de Broglie wavelength of electrons is less than 1 nm, boundary scattering can usually be considered diffuse, i.e., $p = 0$. For phonons, the wavelength may vary from the atomistic scale up to the size of the crystal. Therefore, the size effect needs to be considered for different phonon frequencies. The parameter p can be estimated based on the rms surface roughness σ_{rms} and the wavelength λ of the carrier by

$$p = \exp\left(-\frac{16\pi^2\sigma_{\text{rms}}^2\cos^2\theta_{\text{i}}}{\lambda^2}\right) \tag{5.143}$$

where θ_{i} is the angle of incidence. This equation can be derived from the wave scattering theory [69]. Generally speaking, $p \ll 1$ when $\lambda \leq \sigma_{\text{rms}}$. When $\lambda > 10\sigma_{\text{rms}}$, the specular reflection cannot be neglected. Furthermore, the specularity p increases with the incidence angle. The actual scattering distribution often consists of a broad specular lobe, and the nonspecular component is not perfectly diffuse. This is similar to light scattering by rough surfaces for which an in-depth discussion will be given in Chap. 9. Feng et al. [70] studied the effect of specularity and grain boundary scattering on the thermal conductivity of thin metal films. Their model for the reduction of thermal conductivity of copper and gold films agrees well with experimental values over a large temperature range.

As can be seen from Figs. 5.17 and 5.18, when $Kn = \Lambda_{\text{b}}/d > 0.1$, i.e., when $d < 10\Lambda_{\text{b}}$, the size effect may be significant, and boundary scattering dominates when $d < 0.1\Lambda_{\text{b}}$. Note that Examples 5.5 and 5.6 provide typical numerical values of the bulk mean free paths of electrons in a noble metal and of phonons in silicon. At room temperature, the electron mean free path of a metal is on the order of tens of

nanometers, and thus one would expect some size effect when d is less than 300 nm. For a highly pure metal at very low temperatures, however, the electron mean free path could be on the order of millimeters. In this case, even when d of the film is on the order of micrometers, boundary scattering would dominate the scattering process. Note that the method presented in this section is only for heat conduction along a film. For phonon conduction across a film, the BTE may be simplified using the equation of phonon radiative transfer to be discussed in Chap. 7.

5.5.3 Conductivity Along a Thin Wire Based on the BTE

The above discussion can be extended to conduction along a thin wire. For wires with circular cross sections, the effective conductivity can be expressed as [66, 67]

$$\frac{\kappa_w}{\kappa_b} \text{ or } \frac{\sigma_w}{\sigma_b} = 1 - \frac{12}{\pi} \int_0^1 \sqrt{1-\xi^2} \int_1^\infty \exp\left(-\frac{\xi t}{Kn}\right) \frac{\sqrt{t^2-1}}{t^4} \mathrm{d}t \, \mathrm{d}\xi \tag{5.144}$$

In particular, the asymptotic approximations with ≈1% accuracy are

$$\frac{\kappa_w}{\kappa_b} \text{ or } \frac{\sigma_w}{\sigma_b} \approx 1 - \frac{3}{4}Kn + \frac{3}{8}Kn^3 \text{ for } Kn < 0.6 \tag{5.145a}$$

and

$$\frac{\kappa_w}{\kappa_b} \text{ or } \frac{\sigma_w}{\sigma_b} \approx \frac{1}{Kn} - \frac{3(\ln Kn + 1)}{8Kn^2} - \frac{2}{15Kn^3} \text{ for } Kn > 1 \tag{5.145b}$$

If the scattering is not completely diffuse, a specularity parameter p similar to that for thin films can be introduced, and the expression becomes

$$\frac{\kappa_w}{\kappa_b} \text{ or } \frac{\sigma_w}{\sigma_b} = 1 - \frac{12(1-p)^2}{\pi} \sum_{m=1}^{\infty} m p^{m-1} G(Kn, m) \tag{5.146a}$$

where

$$G(Kn, m) = \int_0^1 \sqrt{1-\xi^2} \int_1^\infty \exp\left(-\frac{m\xi t}{Kn}\right) \frac{\sqrt{t^2-1}}{t^4} \mathrm{d}t \, \mathrm{d}\xi \tag{5.146b}$$

Again, different mean free paths and Kn numbers should be used for thermal and electrical conductivities in the region where the Wiedemann–Franz law is not applicable.

5.5.4 Size Effects on Crystalline Insulators

For crystalline solids, phonons are the principal heat carriers. Simple geometric arguments can also be applied to give qualitative results of the size effect using the phonon mean free path. The BTE or Boltzmann–Peierls equation can be used to more rigorously predict the thermal conductivity of bulk solids as well as the size effect on the thermal conductivity. The distribution function of phonons depends on the frequency or the wavevector, which are related by the dispersion relation. The group velocity can be calculated from the dispersion curve for a given phonon mode or branch. In general, the scattering rate is frequency dependent. The Boltzmann–Peierls equation at a given frequency under the relaxation time approximation for steady-state 1D conduction can be expressed as follows:

$$v_x \frac{\partial f_{\mathrm{BE}}}{\partial T} \frac{\mathrm{d}T}{\mathrm{d}x} + v_z \frac{\partial f_1}{\partial z} = -\frac{f_1 - f_{\mathrm{BE}}}{\tau(\omega)} \tag{5.147}$$

where v_x and v_z are the components of the group velocity that depend on the frequency. The solution is similar to Eq. (5.136a, 5.136b), especially for the z-dependence. Following the discussions in Sect. 5.3.4 on phonon thermal conductivity, in conjunction with the average heat flux along the film, we can rewrite Eq. (5.80) as follows:

$$\kappa_{\mathrm{f}} = \frac{k_{\mathrm{B}}^4 T^3}{6\pi^2 \hbar^3} \sum_P \int_0^{x_{\mathrm{m}}} \frac{\tau(x) v_{\mathrm{g}}(x)}{v_{\mathrm{p}}^2(x)} \frac{x^4 \mathrm{e}^x}{(\mathrm{e}^x - 1)^2} F(Kn_x, p)\mathrm{d}x \tag{5.148}$$

where $x = \hbar\omega/k_{\mathrm{B}}T$ is a reduced frequency and the Knudsen number, $Kn_x = \tau(x)v_{\mathrm{g}}(x)/d = \Lambda(x)/d$, is thus a function of the frequency ω. In this equation, the summation index P accounts for all phonon polarizations, the upper bound of the integration is the cutoff frequency for each polarization, and the function $F(\xi, p)$ can be calculated from Eq. (5.142). If an average Kn that is independent of the frequency can be used, combining Eqs. (5.148) with (5.80) gives $\kappa_{\mathrm{f}}/\kappa_{\mathrm{b}} = F(Kn, p)$ as expected. A similar equation can be developed for thin wires [67, 71].

For semiconductors, such as silicon, the phonon mean free path is on the order of tens of nanometers at room temperature. Therefore, the size effect can be neglected for a 1-μm-thick silicon film above room temperature. However, as temperature is lowered, the size effect becomes more and more significant. Numerical calculations dealing with the conductivity reduction are left as exercises. Kenneth Goodson's group has experimentally demonstrated the size effect on the thermal conductivity of both intrinsic and doped silicon films with thicknesses from a few micrometers down to 20 nm [72]. The thermal transport properties of silicon nanowires and other semiconductor nanowires have been extensively studied both experimentally and theoretically for thermoelectric applications [4, 53, 73–79].

5.5.5 Mean-Free-Path Distribution

As previously discussed, the scattering rate and the mean free path both depend on the frequency. If all modes are combined, the thermal conductivity can be expressed as an integration with respect to frequency $\kappa = \int_0^\infty \kappa_\omega(\omega)\mathrm{d}\omega$. The integrand is the distribution function of thermal conductivity in terms of frequency (i.e., a frequency spectrum). To facilitate understanding and analysis of the experimental data, it has been proposed to use the mean free path (MFP) as the independent variable such that the bulk thermal conductivity can be expressed as follows [80, 81]:

$$\kappa_{\mathrm{bulk}} = \int_0^\infty \kappa_\Lambda(\Lambda)\mathrm{d}\Lambda \tag{5.149a}$$

where

$$\kappa_\Lambda(\Lambda) = \kappa_\omega(\omega)\left(\frac{\mathrm{d}\Lambda}{\mathrm{d}\omega}\right)^{-1} = -\sum_P \int_0^\infty \frac{1}{3}C(\omega)v\Lambda\left(\frac{\mathrm{d}\Lambda}{\mathrm{d}\omega}\right)^{-1} \tag{5.149b}$$

Here, $C(\omega)$ is the volumetric specific heat as given in Eq. (5.82b). The group velocity v and mean free path Λ for each phonon branch are also functions of frequency. We can interpret Eq. (5.149b) as the thermal conductivity per unit MFP, i.e., the thermal conductivity distribution function in terms of the mean free path. It is simply referred to as the *MFP distribution* or *MFP spectrum* [81], unless noted otherwise, Λ refers to the bulk mean free path.

With nanostructures, due to boundary scattering, the $\kappa_\Lambda(\Lambda)$ at a given bulk MFP is reduced by a factor that depends on the Knudsen number. Therefore, we can write

$$\kappa_{\Lambda,\mathrm{nano}}(\Lambda) = \kappa_\Lambda(\Lambda)F_{\mathrm{nano}}(Kn, p) \tag{5.150}$$

where F_{nano} is a structure-dependent function of Kn and the specularity p. It may be thought as the ratio of the MFP in the nanostructure to that of the bulk, i.e., $F_{\mathrm{nano}} = \Lambda_{\mathrm{nano}}/\Lambda$. The Knudsen number depends on the characteristic length and varies with the bulk MFP. Thus, the thermal conductivity of the nanostructure can be written as

$$\kappa_{\mathrm{nano}} = \int_0^\infty \kappa_{\Lambda,\mathrm{nano}}(\Lambda)\mathrm{d}\Lambda = \int_0^\infty \kappa_\Lambda(\Lambda)F_{\mathrm{nano}}(Kn, p)\mathrm{d}\Lambda \tag{5.151}$$

The cumulative distribution function (CDF) can also be defined for thermal conductivity in terms of the mean free path as follows:

$$K_\Lambda(\Lambda) = \frac{1}{\kappa_{\text{nano}}} \int_0^\Lambda \kappa_\Lambda(\xi) F_{\text{nano}}(Kn, p) \mathrm{d}\xi \tag{5.152}$$

For bulk materials, simply set $\kappa_{\text{nano}} = \kappa$ and $F_{\text{nano}} = 1$ in Eq. (5.152). This equation is called the (normalized) thermal conductivity accumulation function.

The mean-free-path spectrum and the thermal conductivity accumulation function have been experimentally and theoretically investigated for both bulk and nanostructured materials [78–82]. These studies have significantly improved our understanding of heat conduction in bulk and nanostructured solid materials and devices. Further discussion is postponed to Chap. 7.

5.6 Quantum Conductance and the Landauer Formalism

In the above discussion, the Fourier law was assumed to hold under the local-equilibrium approximation, with reduced thermal conductivities to include the effect of boundary scattering. Many works have employed ab initio techniques, lattice dynamics, and equilibrium or nonequilibrium molecular dynamics to study thermal transport at the nanoscale [4, 82–84]. In heterogeneous structures, such as superlattices, when thermal transport across the multiple layers is considered, the local-equilibrium assumption breaks down in the ballistic regime. Further discussion of non-Fourier conduction, especially for transient processes, will be deferred to Chap. 7. For superlattice nanowires, both lateral and longitudinal confinements exist, so each element is like a quantum dot confined in all three dimensions. When the quantum confinement becomes significant, the relaxation time approximation used to solve the BTE is not applicable. Landauer's formalism is presented here for modeling certain nonequilibrium and ballistic transport phenomena. This section also introduces the quantum size effect on electrical and thermal transport processes, with an emphasis on the concept of quantum conductance and its implications.

Quantum size effect on the lattice specific heat was discussed in Sect. 5.2. Attention is now paid to the electrical conductance of metallic materials and thermal conductance of dielectric materials. For bulk solids, the DOS for electrons $D(\varepsilon)$ is proportional to $\sqrt{\varepsilon}$, as given in Eq. (5.18) and illustrated in Fig. 5.5b. Note that for phonons or photons, the energy $\varepsilon = \hbar\omega$ is proportional to the frequency and $D(\omega)$ is proportional to ω^2 when the dispersion is linear; see Eq. (5.35) and Fig. 5.4. For electrons or holes, $\varepsilon = \frac{p^2}{2m^*} = \frac{\hbar^2 k^2}{2m^*}$, where k is the wavevector and m^* is the effective mass. For the electron gas in a 2D solid, the density of states becomes $D(\varepsilon) = 2 \times \frac{k}{2\pi}\frac{\mathrm{d}k}{\mathrm{d}\varepsilon} = \frac{m^*}{\pi\hbar^2}$, which can be derived using Eq. (5.37) considering the spin degeneracy. In a quantum well of thickness L, the energy levels are quantized in the normal or z-direction according to Eq. (3.80), i.e., $\frac{n^2h^2}{8m^*L^2}$, where n is a positive integer. The combined energies can be expressed as

$$\varepsilon_n(k) = \frac{n^2\hbar^2}{2m^*L} + \frac{\hbar^2(k_x^2 + k_y^2)}{2m^*} \tag{5.153}$$

and the resulting DOS is given by

$$D(\varepsilon) = \frac{nm^*}{\pi\hbar^2}, \quad \text{for } \varepsilon_n \le \varepsilon < \varepsilon_{n+1} \text{ and } n = 1, 2, \ldots \tag{5.154}$$

which is a staircase function, as depicted in Fig. 5.19a, along with the bulk DOS. The reason that the DOS for the nth subband is multiplied by n is because $k_{z,n} = n\pi/L$, where $k_{\min} = \pi/L$. Before applying Eqs. (5.36) and (5.37), we must multiply the total number of modes N by $k_{z,n}L/\pi$. For 1D quantum wires confined in both y- and z-directions (assuming a rectangular shape of $L_y \times L_z$), the energy levels are given by

$$\varepsilon_{l,n} = \frac{l^2\hbar^2}{2m^*L_y} + \frac{n^2\hbar^2}{2m^*L_z} \tag{5.155}$$

For each subband (l, n), the DOS becomes

$$D(\varepsilon) = \frac{nl}{\pi\hbar}\sqrt{\frac{2m^*}{\varepsilon - \varepsilon_{l,n}}} \tag{5.156}$$

which has an inverse square-root dependence of energy and a singularity at $\varepsilon_{l,n}$, as shown in Fig. 5.19b. For 3D confined quantum dots, the energy levels are completely discrete; subsequently, the DOS becomes isolated delta functions (not shown in Fig. 5.19).

The quantization of electron energy levels or phonon frequencies in small structures suggests that the resulting transport properties may also be quantized. For example, the electrical conductance may depend on the applied current or force for the nanocontact in a stepwise manner. The thermal conductance of insulators can also be quantized due to limited available phonon modes in small structures and

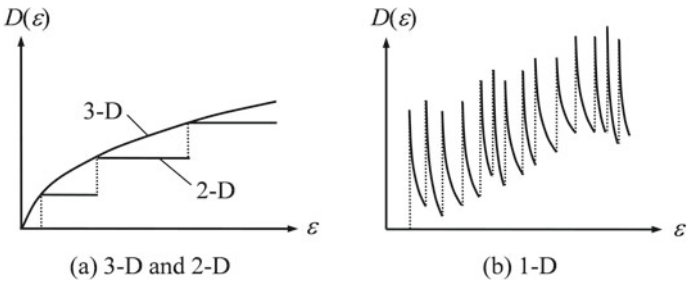

Fig. 5.19 Electron density of states due to quantum confinement. **a** 2D quantum wells versus 3D bulk solids. **b** 1D quantum wires.

at low temperatures. In this section, we use conductance rather than conductivity for reasons to be explained soon. Long before the quantization of conductance was experimentally observed, physicists had formulated different theories to understand the transport phenomena in the quantum or ballistic regimes. Landauer and collaborators [85] have developed a formalism to treat electrical current flow as a transmission probability when carriers are scattered coherently and the resulting ballistic transport behaves quantum mechanically. Landauer's formalism can easily be applied to the 1D case for conductance through a narrow channel, as illustrated in Fig. 5.20a. Suppose ballistic transmission exists in the channel connecting two reservoirs of different electrochemical potentials; there will be a current flow from 1 to 2 and reversely from 2 to 1. In the absence of losses by scattering and reflection, the net current flow can be expressed as

$$J_e = J_{1\to 2} - J_{2\to 1} = -ev_F(\mu_1 - \mu_2)D(\varepsilon) \tag{5.157}$$

where μ is the chemical potential. The derivation can be easily generalized to include the electrostatic potential. Note that the DOS in the 1D case is $D(\varepsilon) = (\pi\hbar v_F)^{-1}$ considering the electronic spin degeneracy. Because the voltage drop is $V_1 - V_2 = -(\mu_1 - \mu_2)/e$, the electrical conductance for complete transmission becomes

$$g_{e0} = \frac{J_e}{V_1 - V_2} = \frac{e^2}{\pi\hbar} \text{ or } \frac{2e^2}{h} \tag{5.158}$$

which gives a universal constant with a value of $7.75 \times 10^{-5}\ \Omega^{-1}$ or a resistance value of 12.91 kΩ. This is the quantum conductance for an ideal 1D conductor, in which there is no resistance or voltage drop associated with the channel itself. Instead, the voltage drop is associated with the perturbation at each end of the channel as it interacts with the reservoir [85]. In the above derivation, we assumed that the Fermi distribution function can be approximated as a step function (i.e., at absolute zero temperature). By introducing a transmission coefficient ξ_{12} and using the actual

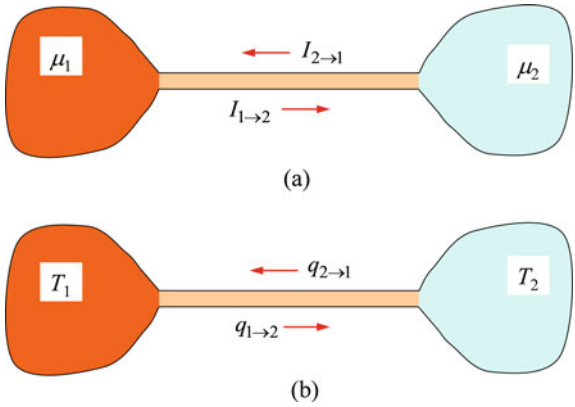

Fig. 5.20 Illustration of quantum conductance. **a** Electrical current flow through a narrow metallic channel due to different electrochemical potentials. **b** Heat transfer between two heat reservoirs through a narrow dielectric channel

distribution function, one can modify Eq. (5.157) to the following [85, 86]:

$$J_e = \int_0^\infty (-ev_F)\xi_{12}(\varepsilon)[f_{FD}(\varepsilon, \mu_1) - f_{FD}(\varepsilon, \mu_2)]D(\varepsilon)d\varepsilon \tag{5.159}$$

For small potential differences, using the following approximation,

$$\frac{f_{FD}(\varepsilon, \mu_1) - f_{FD}(\varepsilon, \mu_2)}{\mu_2 - \mu_1} = -\frac{\partial f_{FD}(\varepsilon, \mu)}{\partial \mu} = \frac{\partial f_{FD}(\varepsilon, \mu)}{\partial \varepsilon}$$

we obtain the expression of the electrical conductance:

$$g_e = -\frac{2e^2}{h}\int_0^\infty \xi_{12}(\varepsilon)\frac{\partial f_{FD}}{\partial \varepsilon}d\varepsilon \tag{5.160}$$

which reduces to Eq. (5.158) at absolute zero temperature when $\xi_{12}(0)$ is taken to be 1. The transmission coefficient or probability is given by a scattering matrix (the S-matrix) based on a solution of Schrödinger's equation. The solution is in the form of eigenvalues called eigenchannels, each with a transmission coefficient τ_i between 0 and 1. Thus, the expression of conductance is reduced to

$$g_e = \frac{2e^2}{h}\sum_i \tau_i \tag{5.161}$$

Depending on how many propagation modes at the Fermi level are excited, the conductance varies in a discontinuous manner. Conductance quantization has been realized in metallic nanocontacts, nanowires, and carbon nanotubes [86–89], even at room temperature, and has also been predicted by molecular dynamics simulations [90, 91]. These discoveries are very important for the development of single-electron transistors, nanoelectromechanical systems, nanotribology, and quantum computing.

The ballistic thermal transport process resembles electromagnetic radiation between two blackbodies separated by a vacuum. For a 1D photon gas, the Stefan–Boltzmann law reads $q'' \propto T^2$ rather than $q'' \propto T^4$. In a solid nanostructure (channel) that links two heat reservoirs, as illustrated in Fig. 5.20b, the ballistic heat conduction can be treated in a similar way so that

$$q_{1\to 2} = \frac{1}{2\pi}\sum_P \int_{\omega_P}^{\omega_D} \xi_P(\omega)\hbar\omega f_{BE}(\omega, T_1)d\omega \tag{5.162a}$$

and

$$q_{2\to 1} = \frac{1}{2\pi}\sum_P \int_{\omega_P}^{\omega_D} \xi_P(\omega)\hbar\omega f_{BE}(\omega, T_2)\mathrm{d}\omega \tag{5.162b}$$

where $\xi_P(\omega)$ is the transmission coefficient (or probability) of the polarization branch P, which accounts for both scattering in the channel and reflection from the junctions. Here, the upper bound ω_D approaches infinity at very low temperatures, and the lower bound is the cutoff frequency for the phonon mode P. This cutoff frequency is determined by the width of the channel and the order of propagating phonon modes, like in a waveguide. More specifically, if a rectangular cross section is considered whose dimensions are L_x and L_y, the cutoff frequency for the (m,n) mode is given by

$$k_{mn} = \frac{\omega_{mn}}{v_s} = \sqrt{\left(\frac{m\pi}{L_x}\right)^2 + \left(\frac{n\pi}{L_y}\right)^2} \tag{5.163}$$

Apparently, a narrow channel enables a large cutoff wavenumber. Note that the zeroth-order mode always exists because it has a zero cutoff frequency. If the integration in Eq. (5.162) is expressed in terms of the wavevector, there will be a group velocity v_g term. In writing Eq. (5.162), we have assumed $v_g = v_p$ for a linear dispersion relation. The net heat transfer is calculated by $q_{12} = q_{1\to 2} - q_{2\to 1}$, which is commonly done in radiation heat transfer. Assuming that the temperature difference is small, we obtain the thermal conductance as

$$g_T = \frac{q_{12}}{T_1 - T_2} = \frac{1}{2\pi}\sum_P \int_{\omega_P}^{\omega_D} \xi_P(\omega)\hbar\omega \frac{\partial f_{BE}(\omega, T)}{\partial T}\mathrm{d}\omega \tag{5.164a}$$

or

$$g_T = \frac{k_B^2 \bar{T}}{h}\sum_P \int_{x_P}^{x_D} \xi_P(x)\frac{x^2 e^x}{(e^x - 1)^2}\mathrm{d}x \tag{5.164b}$$

Note that $\bar{T}$ represents the average temperature. At sufficiently low temperatures, only the lowest phonon branches, whose cutoff frequency equals zero, may contribute to the conductance. If the transmission coefficient is assumed to be unity, each of the lowest phonon modes will contribute to the thermal conductance by

$$g_{T0} = \frac{\pi k_B^2 T}{6\hbar} \quad \text{or} \quad \frac{\pi^2 k_B^2 T}{3h} \tag{5.165}$$

which has a value $g_{T0}/T = 0.947\,\mathrm{pW/K^2}$ and is another universal constant that can be viewed as the Stefan–Boltzmann constant in 1D space for each mode. If the above derivation is repeated to obtain electron thermal conductance, we will end

up with $2g_{T0}$ due to the electronic spin degeneracy. Therefore, the Lorentz number $Lz = \frac{\kappa}{\sigma T} = \frac{g_T}{g_e T}$ in the ballistic regime remains the same as given in Eq. (5.62) for the diffusive regime [92]. Roukes and collaborators [93] have experimentally demonstrated quantum thermal conductance using a 60-nm-thick silicon nitride membrane. They reported a $16g_{T0}$ behavior at temperatures below 0.6 K since the structure was suspended by four narrow bridges (channels). Each bridge or channel acts like a wire with four phonon modes (two transversal, one longitudinal, and one torsional). Murphy and Moore [74] used Landauer's formalism to study phonon transport in silicon nanowires considering temperature dependence and the effect of diffusive and localized modes on the frequency-dependent transmission coefficient.

Carbon nanotubes (CNTs) have been known for a while, especially for its associated large thermal conductivities [94–98]. Single-walled carbon nanotubes can be made essentially free from defect scattering and boundary scattering due to atomistic smoothness. Their diameters can be made as small as a few nanometers, while their lengths can be several micrometers. Thermal conductivities of single-walled and multi-walled nanotubes have been measured with suspended MEMS bridges and are found to exceed that of diamond at room temperature [97]. The thermal conductivity was calculated from the measured thermal conductance based on an effective cross-sectional area. Above room temperature, phonon–phonon anharmonic interactions may provide a means for diffusive conduction behavior. Nanotube bundles, on the other hand, are subject to various scattering mechanisms and possess a lower thermal conductivity; yet they may still behave like good thermal conductors (κ values from 50–300 W/m K). Furthermore, the contact may be attributed to the reduction in conductance. Contact resistance due to interface scattering needs to be further addressed in order to realize the potential of nanotubes for use in heat transfer enhancement [99]. Mingo and Broido calculated the thermal conductance of carbon nanotubes in the ballistic limit [100]; for semiconductor nanotubes at sufficiently low temperatures, the thermal conductance becomes $4g_{T0}T$ due to the four lowest phonon modes regardless of the length and the cross-sectional area. In this regime, the thermal conductivity of CNTs increases with length. As the temperature increases from cryogenic temperatures, the thermal conductivity of CNTs first increases due to the increased specific heat and reaches a peak around 300–400 K, and then decreases due to phonon–phonon scattering. In the diffusion limit, the conductivity is independent of the length and diminishes as temperature further increases. For nanotubes whose band structures are metal-like, such as with (6,0) and (18,0) chiral numbers, electron ballistic transport may be important; however, electron–phonon scattering will dominate at sufficiently high temperatures.

5.7 Summary

This chapter began with lattice vibrations (i.e., phonons) in solids and discussed the dimensionality and the quantum size effect on the lattice specific heat. Free-electron theory was applied, assuming a spherical Fermi surface, to predict the electronic specific heat, as well as electrical and thermal conductivities of solids. The Boltzmann transport equation under the relaxation time approximation and the local-equilibrium assumption was used to derive the electrical and thermal conductivities as well as the thermoelectric coefficients within the framework of irreversible thermodynamics. A brief discussion of the efficiency of thermoelectric power and refrigeration systems was then provided. The classical size effect on electrical and thermal conductivities was presented using both geometric arguments and the BTE, followed by a discussion on the mean-free-path distribution and the thermal conductivity accumulation function. Finally, the concept of conductance quantization for both electrical current and heat flow was introduced using Landauer's formalism. The properties were discussed with examples of representative materials, such as noble metals, semiconductors, quantum wells, superlattices, nanowires, and carbon nanotubes. In the next chapter, the band theory for electrons and phonons will be introduced as an advanced topic of the transport theory of solids.

Problems

5.1 Calculate the specific heat of lead, using both the Einstein model and the Debye model, for temperatures equal to 2, 10, 20, 50, 100, 200, 300, 600, and 800 K. Use $\Theta_D = 88$ K and $\Theta_E = 65$ K since the specific heats calculated with these values agree with the data well for the whole temperature range. Compare your answer with the values from Touloukian and Buyco [7]. Explain the low-temperature and high-temperature behavior.

5.2 In the first stage of designing a refrigeration system that will cool 1 kg of Pb from 300 to 2 K. Assume the Debye model can be used to calculate the temperature-dependent specific heat of lead (with $\Theta_D = 88$ K). Answer the following questions:

(a) How much energy must be removed from Pb?
(b) How much entropy must be transferred out from Pb?
(c) Assuming that the environment is at 300 K, what is the least amount of work necessary to perform this refrigeration task?
(d) Consider the refrigeration in three temperature ranges: (1) from 300 to 100 K; (2) from 100 to 20 K; and (3) from 20 to 2. What is the least amount of work needed in each temperature range?

5.3 Plot the Fermi function f_{FD} versus ε for $T = 0$, 500, and 5000 K. Plot the distribution function of free electrons in metal $f(\varepsilon)$ as a function of ε. Discuss the main features of these plots. [Use eV as the unit for energy.]

5.4 The Fermi energy (at 0 K) of copper is $\mu_{\mathrm{F}} = 7.07$ eV. What is $\mu(T)$ of Cu at 1000 and 10,000 K? Determine the maximum and root-mean-square free-electron speeds in copper at 0 K. Plot the electron distribution functions in terms of the speed and the kinetic energy for $T = 0$, 300, and 4000 K.

5.5 The Fermi energy of silver is $\mu_{\mathrm{F}} = 5.51$ eV. Calculate $\mu(T)$ of Ag at $T = 400$ and 4000 K. What is the rms speed of electrons at 0 K? What is the Fermi velocity? Plot the Fermi function at 0 and 4000 K in one graph and discuss the differences.

5.6 For $k_{\mathrm{B}}T \ll \mu_{\mathrm{F}}$, the specific heat of free-electron gas in metal may be expressed as $\bar{c}_{v,\mathrm{e}} = \frac{\bar{R}}{n_e k_{\mathrm{B}}} \int_0^\infty \frac{\partial f_{\mathrm{FD}}}{\partial T} D(\varepsilon)\varepsilon \mathrm{d}\varepsilon$. Evaluate this integration to obtain Eq. (5.24) by referring Appendix B.8.

5.7 Calculate the Fermi energy of silver using the molecular weight and density. Estimate the spacing between the adjacent atoms of Ag. Calculate and plot the electron specific heat and the lattice specific heat of Ag at temperatures from 0 to 1000 K. Show in a separate graph the low-temperature behavior. How do your calculated values agree with experimental data found in a heat transfer text?

5.8 Calculate the Fermi energy μ_{F} for copper based on the molecular weight and density. What is the rms speed of free electrons in Cu at 0 and 300 K? Find the electronic specific heat and the lattice specific heat in J/kg K of Cu at 0.1, 1, 10, 30, and 500 K. When can you apply the T^3 law, and when can you use the Delong–Petit law?

5.9 Calculate the electronic specific heat and the lattice specific heat of gold at 1, 10, 100, 300, and 1000 K. Sketch their temperature dependence. At what temperature is the electronic and lattice contributions the same? How does your calculated result compare with the value given in a heat transfer text?

5.10 The Mayer relation for the specific heat can be written as $c_p - c_v = \frac{T\beta_P^2}{\rho\kappa_T}$, where $\beta_P = \frac{1}{v}\left(\frac{\partial v}{\partial T}\right)_P$ is the isobaric volume expansion coefficient, $\kappa_T = -\frac{1}{v}\left(\frac{\partial v}{\partial P}\right)_T$ is the isothermal compressibility, and ρ is the density. Noting that the sound speed v_{a} is defined according to $v_{\mathrm{a}}^2 = \left(\frac{\partial P}{\partial \rho}\right)_s = \frac{c_p}{c_v \rho \kappa_T}$, we can write $\frac{c_p - c_v}{c_v} = \frac{T\beta_P^2 v_{\mathrm{a}}^2}{c_p}$. A simple estimate of the relative difference between the specific heats is readily obtained by assuming that v_{a} is independent of temperature, c_p on the right-hand side is approximately $3R$, and $\beta_P = 3\alpha$, where α is the linear thermal expansion coefficient. For silicon, $\alpha \approx 4.6 \times 10^{-6}\,\mathrm{K}^{-1}$ at 1000 K and $v_{\mathrm{a}} \approx 5000$ m/s. For copper, $\alpha \approx 2.2 \times 10^{-5}\,\mathrm{K}^{-1}$ and $v_{\mathrm{a}} \approx 2500$ m/s. Estimate the relative difference between c_p and c_v at 1000 K for silicon and copper.

5.11 Graphene is a single sheet of carbon atoms arranged in hexagonal pattern. The phonon mode with the lowest speed is the out-of-plane transverse acoustic mode, when the atoms vibrate perpendicular to the plane. It has a dispersion relation $\omega(k) = ak^2$, with $a = 6 \times 10^{-7}\,\mathrm{m^2 s}$. It is expected that this mode

is the dominate mode for the lattice specific heat at low temperatures (below 100 K). Using the 2D solid model with the quadratic dispersion to show that $c_v(T) \propto T$ at low temperatures, i.e., $T \ll \Theta_D$.

5.12 Evaluate the specific heat of a thin GaAs film of two different thicknesses: $L = 2$ and 10 nm. Plot the calculated specific heat with and without planar modes. Compare your results with that predicted by the Debye model for the bulk GaAs at $T \ll \Theta_D$.

5.13 Develop a computer program to calculate the lattice specific heat of CdS or ZnO_2 cubic nanocrystals with different sizes: $L = 2$, 10, and 20 nm. Discuss the low-temperature behavior in terms of Eqs. (5.43) and (5.44).

5.14 For a nanowire of diameter $d = 5$ nm, show that $c_v(T) \propto T$ at low temperatures for a linear dispersion. If the length of the nanowire is $L = 10d$, what is the lowest temperature asymptote of the specific heat due to the second quantum size effect?

5.15 Calculate the electron scattering rate and the mean free path of copper at 295 K. Use the linear relations for the electrical resistivity and the Wiedemann–Franz law to calculate the thermal conductivity at 200, 400, 600, and 800 K. Compare the calculated results with data from a heat transfer textbook.

5.16 Calculate the electron scattering rate $1/\tau$, the mean free path Λ, the electrical conductivity σ, and the thermal conductivity κ of aluminum near room temperature. If the temperature is increased by 5%, how will $1/\tau$, Λ, σ, and κ change? Express the scattering rate in both rad/s and Hz. Discuss why one should divide it by 2π to express $1/\tau$ in Hz.

5.17 Sketch the thermal conductivity versus temperature from 0 to 1000 K for silver. What is the dependence of κ on T, as the temperature approaches absolute zero? How does the thermal conductivity change above 300 K?

5.18 Find the data for the electrical and thermal conductivities of a good conductor in a large temperature range, and evaluate when the Wiedemann–Franz law is valid. Show the low-temperature and high-temperature asymptotes for both σ and κ.

5.19 In the text, we stated that $\partial f_{FD}/\partial \varepsilon$ is a Dirac delta function and used it to obtain the electrical conductivity in Eq. (5.63). Prove that when $k_B T \ll \mu_F$, the integral $\int_0^\infty G(\varepsilon) \frac{\partial f_{FD}}{\partial \varepsilon} d\varepsilon \approx -G(\mu_F)$, where $G(x)$ is an analytical function of x. Then, derive Eq. (5.49) from Eq. (5.63).

5.20 Sketch the thermal conductivity of germanium (relatively pure) as a function of temperature [31]. Explain the trend of thermal conductivity at very low temperatures and at above room temperature. Can you assume that the thermal conductivity is independent of temperature near room temperature?

5.21 Derive Eqs. (5.74) through (5.80). Show that in Eq. (5.80), the second term is much smaller than the first term for metals.

5.22 Prove Eq. (5.82a, 5.82b, 5.82c), and calculate the Seebeck coefficient for Ag at 300 and 600 K. The measured Seebeck coefficient of Ag is 1.51 μV/K at 300 K and 3.72 μV/K at 600 K. On the other hand, the Seebeck coefficient for Pt is −5.28 μV/K at 300 K and −11.66 μV/K at 600 K. If an Ag-Pt thermocouple

is formed with a junction temperature $T_2 = 600$ K and a reference temperature $T_1 = 300$ K, find the output voltage (see Fig. 5.14b).

5.23 For given values of T_L, T_H, and Z^*, there exists an optimal ratio R_L/R_0 for achieving the maximum efficiency of the thermoelectric generator given in Eq. (5.94). Show that

$$\eta_{max} = \frac{\Delta T}{T_H} \frac{\sqrt{1 + Z^* T_M} - 1}{\sqrt{1 + Z^* T_M} + T_L/T_H},$$

where $T_M = (T_H + T_L)/2$. Calculate the maximum efficiency, normalized to the Carnot efficiency, for $T_L = 300$ K and $T_H = 800$ K as a function of the dimensionless parameter $Z^* T_M$. Plot it for $Z^* T_M$ from 0.3 to 3. Discuss the significance of ZT in thermoelectric devices.

5.24 Consider a thermoelectric generator made of two semiconductors working between $T_L = 300$ K and $T_H = 600$ K. The p-type material is made of $Bi_{0.5}Sb_{1.5}Te_3$, and the n-type material is made of $Bi_2Se_{0.75}Te_{2.25}$, with the following average properties: $\kappa_p = 1.2$ W/m K, $\kappa_n = 1.3$ W/m K, $r_{e,p} = 15\,\mu\Omega$ m, $r_{e,n} = 13\,\mu\Omega$ m, $\Gamma_p = 210\,\mu$V/K, and $\Gamma_n = -190\,\mu$V/K. Assume that the length $L = 0.8$ cm and the cross section $A_c = 0.3$ cm^2 for both materials. A generator with a diameter of 10 cm contains 100 pairs ($N = 100$). Find the power output at the maximum efficiency (see Problem 5.23).

5.25 Perform a thermodynamic analysis of the thermoelectric cooling using the same configuration as in Fig. 5.15. By noting that no load resistance is needed and the voltage supplied $\Delta V = N\Gamma_{np}\Delta T + IR_0$, show that the coefficient of performance of a thermoelectric refrigeration is

$$COP = \frac{|q_L|}{P} = \frac{I\Gamma_{np}A_c\sigma_{np}T_L - I^2L/2 - A_c^2\sigma_{np}\kappa_{np}\Delta T/L}{I\Gamma_{np}A_c\sigma_{np}\Delta T + I^2L}.$$

The maximum COP can be obtained by setting the derivative with respect to I equal to zero. Show that

$$COP_{max} = \frac{T_L}{\Delta T} \frac{\sqrt{1 + Z^* T_M} - T_H/T_L}{\sqrt{1 + Z^* T_M} + 1},$$

where $T_M = (T_H + T_L)/2$.

5.26 Estimate the thermal conductivity along a copper film with various thicknesses: $d = 400$, 100, and 50 nm at 300 K. What if the temperature is reduced to 1 K?

5.27 Estimate the thermal conductivity along a copper wire with various diameters: $d = 400$, 100, and 50 nm at 1 and 300 K, respectively. Compare simple geometric averaging of free paths with the BTE. What are the electron de Broglie wavelengths at these temperatures? If the surface roughness parameter $\sigma_{rms} = 2$ nm, will the scattering be mostly diffuse or specular at each temperature?

5.28 At 5 K, calculate the thermal conductivity, perpendicular ($\kappa_{\text{eff},z}$) and parallel ($\kappa_{\text{eff},x}$) to the plane, for a 200-nm-thick gold film. Calculate the effective thermal conductivity $\kappa_{\text{eff,w}}$ of a gold wire of 5-μm thickness. Hint: use the bulk resistivity value from Fig. 5.11.

5.29 In Example 5.6, we have calculated the properties of a single-crystal silicon at various temperatures. Use simple relations with $p = 0$ to estimate the thermal conductivities of silicon from 5 to 1000 K along a 50-nm-thick thin film and a 100-nm-thick thin wire. Assume the surface roughness $\sigma_{\text{rms}} = 2\,\text{nm}$. Will the diffuse model be a good assumption? For the thin film, redo the calculation using the specularity p estimated based on the thermal phonon wavelength λ_{th}.

5.30 The diameter of a carbon nanotube is determined by its chiral numbers (m, n) according to $d = 0.07834\sqrt{m^2 + mn + n^2}$. What is the diameter of (10,10) single-walled nanotubes? Assume that the wall thickness (unit atomic layer) is 0.34 nm. What is the cross-sectional area? Calculate the phonon thermal conductivity κ in the ballistic limit considering the four phonon modes at 100 K for (10,10) nanotubes with length $L = 100$ nm, 1 μm, and 10 μm. Will the ballistic limit of thermal conduction hold at room temperature and above?

References

1. M.I. Flik, B.I. Choi, K.E. Goodson, Heat transfer regimes in microstructures. J. Heat Transf. **114**, 666–674 (1992)
2. C.L. Tien, G. Chen, Challenges in microscale conductive and radiative heat transfer. J. Heat Transf. **116**, 799–807 (1994)
3. D.G. Cahill, K. Goodson, A. Majumdar, Thermometry and thermal transport in micro/nanoscale solid-state devices and structures. J. Heat Transf. **124**, 223–241 (2002)
4. D.G. Cahill, W.K. Ford, K.E. Goodson, G.D. Mahan, A. Majumdar, H.J. Maris, R. Merlin, S.R. Phillpot, Nanoscale thermal transport, J. Appl. Phys. **93**, 793–818 (2003); D.G. Cahill, P.V. Braun, G. Chen, D.R. Clarke, S. Fan, K. E. Goodson, P. Keblinski, W.P. King, G.D. Mahan, A. Majumdar, H.J. Maris, S.R. Phillpot, E. Pop, L. Shi, Nanoscale thermal transport. II. 2003–2012. Appl. Phys. Rev. **1**, 011305 (2014)
5. C. Kittel, *Introduction to Solid State Physics*, 7th edn. (Wiley, New York, 1996)
6. N.W. Ashcroft, N.D. Mermin, *Solid State Physics* (Harcourt College Publishers, Fort Worth, TX, 1976)
7. Y.S. Touloukian, E.H. Buyco (eds.), *Thermophysical Properties of Matter,* Vol. 4: Specific Heat – Metallic Elements and Alloys; Vol. 5: Specific Heat – Nonmetallic Solids (IFI/Plenum, New York, 1970)
8. G. Nilsson, S. Rolandson, Lattice dynamics of copper at 80 K. Phys. Rev. B **7**, 2393–2400 (1973)
9. A.J.E. Foreman, Anharmonic specific heat of solids. Proc. Phys. Soc. (London) **79**, 1124–1141 (1962)
10. R.A. MacDonald, W.M. MacDonald, Thermodynamic properties of fcc metals at high temperatures. Phys. Rev. B **24**, 1715–1724 (1981)
11. V. Novotny, P.P.M. Meincke, J.H.P. Watson, Effect of size and surface on the specific heat of small lead particles. Phys. Rev. Lett. **28**, 901–903 (1972); V. Novotny, P.P.M. Meincke, Thermodynamic lattice and electric properties of small particles. Phys. Rev. B **8**, 4186–4199 (1973)

12. W. Yi, L. Lu, D.-L. Zhang, Z.W. Pan, S.S. Xie, Linear specific heat of carbon nanotubes. Phys. Rev. B **59**, R9015–R9018 (1999)
13. C. Dames, B. Poudel, W.Z. Wang, J.Y. Huang, Z.F. Ren, Y. Sun, J.I. Oh, C. Opeil, M.J. Naughton, G. Chen, Low-dimensional phonon specific heat of titanium dioxide nanotubes. Appl. Phys. Lett. **87**, 031901 (2005)
14. A.A. Valladares, The Debye specific heat in *n* dimensions. Am. J. Phys. **43**, 308–311 (1975)
15. A.J. McNamara, B.J. Lee, Z.M. Zhang, Quantum size effect on the lattice specific heat of nanostructures. Nanoscale Microscale Thermophys. Eng. **14**, 1–20 (2010)
16. W. DeSorbo, W.W. Tyler, The specific heat of graphite from 13 to 300 K. J. Chem. Phys. **21**, 1660–1663 (1953)
17. R.S. Prasher, P.E. Phelan, Size effect on the thermodynamic properties of thin solid films. J. Heat Transf. **120**, 1078–1081 (1998); R.S. Prasher, P.E. Phelan, Non-dimensional size effects on the thermodynamic properties of solids. Int. J. Heat Mass Transf. **42**, 1991–2001 (1999)
18. Y. Zhang, J.X. Cao, Y. Xiao, X.H. Yan, Phonon spectrum and specific heat of silicon nanowires. J. Appl. Phys. **102**, 104303 (2007)
19. Y. Zhou, X. Zhang, M. Hu, Nonmonotonic diameter dependence of thermal conductivity of extremely thin Si nanowires: competition between hydrodynamic phonon flow and boundary scattering. Nano Lett. **17**, 1269–1276 (2017)
20. Z. Rashid, L. Zhu, W. Li, Effect of confinement on anharmonic phonon scattering and thermal conductivity in pristine silicon nanowires. Phys. Rev. B **97**, 075441 (2018)
21. H.P. Baltes, E.R. Hilf, Specific heat of lead grains. Solid State Commun. **12**, 369–373 (1973)
22. R. Lautenschlager, Improved theory of the vibrational specific heat of lead grains. Solid State Commun. **16**, 1331–1334 (1975)
23. M.S. Dresselhaus, P.C. Eklund, Phonons in carbon nanotubes. Adv. Phys. **49**, 705–814 (2000)
24. J. Hone, B. Batlogg, Z. Benes, A.T. Johnson, J.E. Fischer, Quantized phonon spectrum of single-wall carbon nanotubes. Science **289**, 1730–1733 (2000); W.A. de Heer, A question of dimensions. Science **289**, 1702–1703 (2000)
25. J. Zimmermann, P. Pavone, G. Cuniberti, Vibrational modes and low-temperature thermal properties of graphene and carbon nanotubes: minimal force-constant model. Phys. Rev. B **78**, 045410 (2008)
26. R. Denton, B. Muhlschlegel, D.J. Scalapino, Thermodynamic properties of electrons in small metal particles. Phys. Rev. B **7**, 3589–3607 (1973)
27. W.P. Halperin, Quantum size effects in metal particles. Rev. Mod. Phys. **58**, 533–606 (1986)
28. Z.M. Zhang, Clarification of the relation between drift velocity and relaxation time. J. Thermophys. Heat Transf. **26**, 189–191 (2012)
29. J.M. Ziman, *Electrons and Phonons* (Oxford University Press, Oxford, UK, 1960); reprinted in the Oxford Classics Series, 2001
30. R.A. Matula, Electrical resistivity of copper, gold, palladium, and silver. J. Phys. Chem. Ref. Data **8**, 1147–1298 (1979)
31. Y.S. Touloukian, R.W. Powell, C.Y. Ho, P.G. Klemens (eds.), *Thermophysical Properties of Matter,* Vol. 1: Thermal Conductivity – Metallic Elements and Alloys; Vol. 2: Thermal Conductivity – Nonmetallic Solids (IFI/Plenum, New York, 1970)
32. D.G. Cahill, S.K. Watson, R.O. Pohl, Lower limit to the thermal conductivity of disorderd crystals. Phys. Rev. B **46**, 6131–6140 (1992)
33. G.A. Slack, The thermal conductivity of nonmetallic crystals. Solid State Phys. **34**, 1–71 (1979)
34. M.C. Wingert, J. Zheng, S. Kwon, R. Chen, Thermal transport in amorphous materials: a review. Semicond. Sci. Technol. **31**, 113003 (2016)
35. P.B. Allen, J.L. Feldman, Thermal conductivity of disordered harmonic solids. Phys. Rev. B **48**, 12581–12588 (1993)
36. P.B. Allen, J.L. Feldman, J. Fabian, F. Wooten, Diffusons, locons and propagons: Character of atomic vibrations in amorphous Si. Philos. Mag. B **79**, 1715–1731 (1999)
37. J.M. Larkin, A.J.H. McGaughey, Thermal conductivity accumulation in amorphous silica and amorphous silicon. Phys. Rev. B **89**, 144303 (2014)

38. M.T. Agne, R. Hanus, G.J. Snyder, Minimum thermal conductivity in the context of diffuson-mediated thermal transport. Energy Environ. Sci. **11**, 609–616 (2018)
39. D.M. Leitner, Vibrational energy transfer and heat conduction in a one-dimensional glass. Phys. Rev. B **64**, 094201 (2001)
40. W. Lv, H. Asegun, Non-negligible contributions to thermal conductivity from localized modes in amorphous silicon dioxide. Sci. Rep. **6**, 35720 (2016)
41. J. Moon, B. Latour, A.J. Minnich, Propagating elastic vibrations dominate thermal conduction in amorphous silicon. Phys. Rev. B **97**, 024201 (2018)
42. C.L. Choy, Thermal conductivity of polymers. Polymer **18**, 984–1004 (1977)
43. S. Kommandur, S.K. Yee, An empirical model to predict temperature-dependent thermal conductivity of amorphous polymers. J. Polymer Sci. B: Polymer Phys. **55**, 1160–1170 (2017)
44. X. Xie, K. Yang, D. Li, T.-H. Tsai, J. Shin, P.V. Braun, D.G. Cahill, High and low thermal conductivity of amorphous macromolecules. Phys. Rev. B **95**, 035406 (2017)
45. A. Henry, Thermal transport in polymers. Ann. Rev. Heat Transf. **17**, 485–520 (2014)
46. H. Chen, V.V. Ginzburg, J. Yang, Y. Yang, W. Liu, Y. Huang, L. Du, B. Chen, Thermal conductivity of polymer-based composites: fundamentals and applications. Prog. Polymer Sci. **59**, 41–85 (2016)
47. X. Xu, J. Chen, J. Zhou, B. Li, Thermal conductivity of polymers and their nanocomposites. Adv. Mater. **30**, 1705544 (2018)
48. M. Pyda, A. Boller, J. Grebowicz, H. Chuah, B.V. Lebedev, B. Wunderlich, Heat Capacity of Poly(trimethylene terephthalate). J. Polymer Sci. B: Polymer Phys. **36**, 2499–2511 (1998)
49. S. Shen, A. Henry, J. Tong, R. Zheng, G. Chen, Polyethylene nanofibres with very high thermal conductivities. Nat. Nanotech. **5**, 251–255 (2010)
50. R.E. Bentley, *Theory and Practice of Thermoelectric Thermometry* (Springer, Singapore, 1998)
51. R.B. Roberts, The absolute scale of thermoelectricity II. Phil. Mag. B **43**, 1125–1135 (1981)
52. O. Dreirach, The electrical resistivity and thermopower of solid noble metals. J. Phys. F: Met. Phys. **3**, 577–584 (1973)
53. C.J. Vineis, A. Shakouri, A. Majumdar, M.G. Kanatzidis, Nanostructured thermoelectrics: big efficiency gains from small features. Adv. Mater. **22**, 3970–3980 (2010)
54. S.L. Soo, *Direct Energy Conversion* (Prentice-Hall, Englewood Cliffs, NJ, 1968)
55. L.D. Hicks, M.S. Dresselhaus, Effect of quantum-well structures on the thermoelectric figure of merit. Phys. Rev. B **47**, 12727–12731 (1993); M.S. Dresselhaus, Y.-M. Lin, O. Rabin, G. Dresselhaus, Bismuth nanowires for thermoelectric applications. Microscale Thermophys. Eng. **7**, 207–219 (2003); Y.-M. Lin, M. S. Dresselhaus, Thermoelectric properties of superlattice nanowires. Phys. Rev. B **68**, 075304 (2003)
56. J. He, T.M. Tritt, Advances in thermoelectric materials research: looking back and moving forward. Science **357**, eaak9997 (2017)
57. Z. Tian, S. Lee, G. Chen, Comprehensive review of heat transfer in thermoelectric materials and devices. Ann. Rev. Heat Transf. **17**, 425–483 (2014)
58. L. Onsager, Reciprocal relations in irreversible processes. I & II. Phys. Rev. **37**, 405–426; **38**, 2265–2279 (1931)
59. H.B. Callen, *Thermodynamics and an Introduction to Thermostatistics*, 2nd edn. (Wiley, New York, 1985)
60. D. Kondepudi, I. Prigogine, *Modern Thermodynamics: From Heat Engines to Dissipative Structures* (Wiley, New York, 1998)
61. D. Jou, G. Lebon, J. Casas-Vázquez, *Extended Irreversible Thermodynamics*, 4th edn. (Springer, Berlin, 2010)
62. C.R. Tellier, A.J. Tosser, *Size Effects in Thin Films* (Elsevier, Amsterdam, 1982)
63. M.I. Flik, C.L. Tien, Size effect on the thermal conductivity of high-T_c thin-film superconductors. J. Heat Transf. **112**, 872–881 (1990)
64. R.A. Richardson, F. Nori, Transport and boundary scattering in confined geometrics: analytical results. Phys. Rev. B **48**, 15209–15217 (1993)

65. J.E. Graebner, S. Jin, G.W. Kammlott, J.A. Herb, C.F. Gardinier, Large anisotropic thermal conductivity in synthetic diamond films. Nature **359**, 401–403 (1992)
66. D. Stewart, P.M. Norris, Size effect on the thermal conductivity of thin metallic wires: Microscale implications. Microscale Thermophys. Eng. **4**, 89–101 (2000)
67. S.G. Walkauskas, D.A. Broido, K. Kempa, T.L. Reinecke, Lattice thermal conductivity of wires. J. Appl. Phys. **85**, 2579–2582 (1999)
68. S. Kumar, G.C. Vradis, Thermal conductivity of thin metallic films. J. Heat Transfer **116**, 28–34 (1994)
69. P. Beckman, A. Spizzichino, *The Scattering of Electromagnetic Waves from Rough Surfaces* (Artech House Inc, Norwood, MA, 1987)
70. B. Feng, Z. Li, X. Zhang, Effect of grain-boundary scattering on the thermal conductivity of nanocrystalline metallic films. J. Phys. D Appl. Phys. **42**, 055311 (2009)
71. J. Zou, A. Balandin, Phonon heat conduction in a semiconductor nanowire. J. Appl. Phys. **89**, 2932–2938 (2001)
72. M. Asheghi, M.N. Touzelbaev, K.E. Goodson, Y.K. Leung, S.S. Wong, Temperature-dependent thermal conductivity of single-crystal silicon layers in SOI substrates. J. Heat Transf. **120**, 30–36 (1998); M. Asheghi, K. Kurabayashi, R. Kasnavi, K.E. Goodson, Thermal conduction in doped single-crystal silicon films. J. Appl. Phys. **91**, 5079–5088 (2002); W. Liu, M. Asheghi, Thermal conductivity measurements of ultra-thin single crystal silicon layers. J. Heat Transf. **128**, 75–83 (2006)
73. D. Li, Y. Wu, P. Kim, L. Shi, P. Yang, A. Majumdar, Thermal conductivity of individual silicon nanowires. Appl. Phys. Lett. **83**, 2934–2936 (2003)
74. P.G. Murphy, J.E. Moore, Coherent phonon scattering effects on thermal transport in thin semiconductor nanowires. Phys. Rev. B **76**, 155313 (2007)
75. A.I. Hochbaum, R. Chen, R.D. Delgado, W. Liang, E.C. Garnett, M. Najarian, A. Majumdar, P. Yang, Enhanced thermoelectric performance of rough silicon nanowires. Nature **451**, 163–167 (2008)
76. P. Martin, Z. Aksamija, E. Pop, U. Ravaioli, Impact of phonon-surface roughness scattering on thermal conductivity of thin Si nanowires. Phys. Rev. Lett. **102**, 125503 (2009)
77. H. Kim, I. Kim, H.-J. Choi, W. Kim, Thermal conductivities of $Si_{1-x}Ge_x$ nanowires with different germanium concentrations and diameters. Appl. Phys. Lett. **96**, 233106 (2010)
78. G. Xie, Y. Guo, X. Wei, K. Zhang, L. Sun, J. Zhong, G. Zhang, Y.-W. Zhang, Phonon mean free path spectrum and thermal conductivity for $Si_{1-x}Ge_x$ nanowires. Appl. Phys. Lett. **104**, 233901 (2014)
79. A. Malhotra1, M. Maldovan, Impact of phonon surface scattering on thermal energy distribution of Si and SiGe nanowires. Sci. Rep. **6**, 25818 (2016)
80. A.J. Minnich, J.A. Johnson, A.J. Schmidt, K. Esfarjani, M.S. Dresselhaus, K.A. Nelson, G. Chen, Thermal conductivity spectroscopy technique to measure phonon mean free paths. Phys. Rev. Lett. **107**, 095901 (2011)
81. F. Yang, C. Dames, Mean free path spectra as a tool to understand thermal conductivity in bulk and nanostructures. Phys. Rev. B **87**, 035437 (2013)
82. T. Shiga, D. Aketo, L. Feng, J. Shiomi, Harmonic phonon theory for calculating thermal conductivity spectrum from first-principles dispersion relations. Appl. Phys. Lett. **108**, 201903 (2016)
83. P.K. Schelling, S.R. Phillpot, P. Keblinski, Comparison of atomic-level simulation methods for computing thermal conductivity. Phys. Rev. B **65**, 144306 (1999)
84. A.J. Kulkarni, M. Zhou, Size-dependent thermal conductivity of zinc oxide nanobelts. Appl. Phys. Lett. **88**, 141921 (2006)
85. R. Landauer, Spatial variation of currents and fields due to localized scatters in metallic conduction. IBM J. Res. Develop. **1**, 223–231 (1957); R. Landauer, Conductance determined by transmission: probes and quantized constriction resistance. J. Phys.: Condens. Matter **1**, 8099–8110 (1989); Y. Imry, R. Landauer, Conductance viewed as transmission. Rev. Mod. Phys. **71**, S306–S312 (1999)

86. G. Rubio, N. Agraït, S. Vieira, Atomic-sized metallic contacts: mechanical properties and electronic transport. Phys. Rev. Lett. **76**, 2302–2305 (1996)
87. N. Agraït, A.L. Yeyati, J.M. van Ruitenbeek, Quantum properties of atomic-sized conductors. Phys. Rep. **377**, 81–279 (2003)
88. L. Chico, L.X. Benedict, S.G. Louie, M.L. Cohen, Quantum conductance of carbon nanotubes with defects. Phys. Rev. B **54**, 2600–2606 (1996)
89. S. Frank, P. Poncharal, Z.L. Wang, W.A. de Heer, Carbon nanotube quantum resistors. Science **280**, 1744–1746 (1998)
90. U. Landman, W.D. Luedtke, N.A. Burnham, R.J. Colton, Atomistic mechanisms and dynamics of adhesion, nanoindentation, and fraction. Science **248**, 454–461 (1990)
91. U. Landman, W.D. Leudtke, B.E. Salisbury, R.L. Whetten, Reversible manipulations of room temperature mechanical and quantum transport properties in nanowire junctions. Phys. Rev. Lett. **77**, 1362–1365 (1996)
92. A. Greiner, L. Reggiani, T. Kuhn, L. Varani, Thermal conductivity and Lorenz number for one-dimensional ballistic transport. Phys. Rev. Lett. **78**, 1114–1117 (1997)
93. K. Schwab, E.A. Henriksen, J.M. Worlock, M.L. Roukes, Measurement of the quantum of thermal conductance. Nature **404**, 974–977 (2000); K. Schwab, J.L. Arlett, J.M. Worlock, M.L. Roukes, Thermal conductance through discrete quantum channels. Physica E **9**, 60–68 (2001)
94. J. Hone, M. Whitney, C. Piskoti, A. Zettl, Thermal conductivity of single-walled carbon nanotubes. Phys. Rev. B **59**, 2514–2516 (1999)
95. S. Berber, Y.-K. Kwon, D. Tománek, Unusually high thermal conductivity of carbon nanotubes. Phys. Rev. Lett. **84**, 4613–4616 (2000)
96. S. Maruyama, A molecular dynamics simulation of heat conduction of a finite length single-walled carbon nanotube. Microscale Thermophys. Eng. **7**, 41–50 (2003)
97. P. Kim, L. Shi, A. Majumdar, P.L. McEuen, Thermal transport measurements of individual multiwalled nanotubes. Phys. Rev. Lett. **87**, 215502 (2001)
98. C. Yu, L. Shi, Z. Yao, D. Li, A. Majumdar, Thermal conductance and thermopower of an individual single-wall carbon nanotube. Nano Lett. **5**, 1842–1846 (2005)
99. A.J. McNamara, Y. Joshi, Z.M. Zhang, Characterization of nanostructured thermal interface materials – a review. Int. J. Thermal Sci. **62**, 2–11 (2012)
100. N. Mingo, D.A. Broido, Carbon nanotube ballistic thermal conductance and its limits. Phys. Rev. Lett. **95**, 096105 (2005); N. Mingo, D.A. Broido, Length dependence of carbon nanotube thermal conductivity and the problem of long waves. Nano Lett. **5**, 1221–1225 (2005)